

1 REVISION #3—06 July 2020—submitted to *American Mineralogist*

2  
3 **An evolutionary system of mineralogy, Part III:**  
4 **Primary chondrule mineralogy (4566 to 4561 Ma)**

5  
6 **ROBERT M. HAZEN<sup>1,\*</sup>, SHAUNNA M. MORRISON<sup>1</sup>, AND ANIRUDH PRABHU<sup>2</sup>**

7 <sup>1</sup>Earth and Planets Laboratory, Carnegie Institution for Science,  
8 5251 Broad Branch Road NW, Washington DC 20015, U. S. A.

9 <sup>2</sup>Tetherless World Constellation, Department of Earth and Environmental Sciences,  
10 Rensselaer Polytechnic Institute, Troy NY 12180, U. S. A.

11  
12 **ABSTRACT**

13 Information-rich attributes of minerals reveal their physical, chemical, and biological modes of  
14 origin in the context of planetary evolution, and thus they provide the basis for an evolutionary  
15 system of mineralogy. Part III of this system considers the formation of 43 different primary  
16 crystalline and amorphous phases in chondrules, which are diverse igneous droplets that formed  
17 in environments with high dust/gas ratios during an interval of planetesimal accretion and  
18 differentiation between 4566 and 4561 Ma. Chondrule mineralogy is complex, with several  
19 generations of initial droplet formation via a variety of proposed heating mechanisms, followed in  
20 many instances by multiple episodes of reheating and partial melting. Primary chondrule  
21 mineralogy thus reflects a dynamic stage of mineral evolution, when the diversity and distribution  
22 of natural condensed solids expanded significantly.

23 \*E-mail: [rhazen@carnegiescience.edu](mailto:rhazen@carnegiescience.edu)

24 **Keywords:** classification; mineral evolution; natural kinds; chondrules; chondrite meteorites;  
25 planetesimals

26

## INTRODUCTION

27 The “evolutionary system” of mineralogy focuses on the inexorable emergence of mineral  
28 diversity and distribution through billions of years of cosmic evolution. This data-driven approach  
29 emphasizes the numerous information-rich aspects of minerals – attributes that point to a variety  
30 of physical, chemical, and ultimately biological mineral-forming processes (Hazen et al. 2008;  
31 Hazen and Ferry 2010; Hazen 2019). The first three parts of this evolutionary system focus on  
32 relatively unaltered components of chondrite meteorites: presolar “stardust” grains (see Part I;  
33 Hazen and Morrison 2020); refractory inclusions (i.e., CAIs, AOAs, and URIs, as described in  
34 Part II; Morrison and Hazen 2020); and primary chondrule phases (Part III, this study), all of which  
35 preserve episodes of mineral evolution prior to their incorporation into planetesimals (the subject  
36 of Part IV of this series) and extensive alteration by planetesimal processing, as recorded, for  
37 example, in both highly altered chondrite and achondrite meteorites (to be reviewed in Part V).

38 This system builds on classification protocols of the International Mineralogical Association  
39 (IMA), as codified by the Commission on New Minerals, Nomenclature and Classification (e.g.,  
40 Burke 2006; Mills et al. 2009; Schertl et al. 2018). We attempt to amplify and modify the IMA  
41 approach, which distinguishes each mineral “species” based on unique combinations of end-  
42 member composition and idealized crystal structure, leading to >5500 approved mineral species  
43 ([rruff.info/ima](http://rruff.info/ima); accessed 7 April 2020).

44 The power and simplicity of the IMA classification system lies in its recognition of mineral  
45 species based on the minimum information (measured in bits; e.g., Krivovichev 2012, 2013)  
46 necessary to distinguish among species. By design, IMA protocols do not consider such revelatory  
47 aspects of minerals as trace and minor elements, fractionated isotopes, structural defects, varied  
48 electromagnetic properties, textures and morphologies, compositional zoning, or inclusions.

49 Neither does the IMA take into account mineral ages or petrologic contexts when classifying  
50 mineral species. However, these and many other characteristics of minerals and their assemblages  
51 collectively provide powerful testimony regarding each mineral's origins, as well as its subsequent  
52 deep-time interactions with changing chemical and physical environments. The evolutionary  
53 system, by distinguishing minerals formed in different paragenetic contexts from stars to nebulae  
54 to dynamic planetary surfaces and interiors, thus provides a framework for classifying minerals in  
55 their spatial and temporal context.

56 The evolutionary system employs IMA nomenclature for most natural condensed solids, but it  
57 deviates from those protocols in three important ways. In some instances, we split IMA species  
58 into two or more "natural kinds," based on diagnostic combinations of attributes that arise from  
59 distinct paragenetic modes. Thus, isotopically anomalous hibonite condensed in the expanding,  
60 cooling atmospheres of AGB stars (labelled "*AGB hibonite*") is measurably distinct from hibonite  
61 condensed from the solar nebula to form a primary phase in a calcium-aluminum-rich inclusion  
62 ("*CAI hibonite*"). Many of the most common rock-forming minerals display multiple paragenetic  
63 contexts, each of which tells a different story about stages of planetary evolution; these species are  
64 thus split into two or more "natural kinds" in our system (Hazen 2019). Note that we employ a  
65 binomial nomenclature, with the first name designating the paragenetic mode and the second name  
66 the mineral species, which in the great majority of cases is the same as the approved IMA species  
67 name.

68 In a number of cases, we lump two or more approved IMA species into one natural kind when  
69 those multiple species satisfy two criteria: (1) the species are part of a continuous phase region that  
70 may be bounded by several different idealized end-members; and (2) all examples form by the  
71 same paragenetic mode. For example, CAIs hold a variety of micron-scale refractory metal

72 “nuggets” that occur as alloys of Mo, Ir, Os, Ru, Rh, Re, Pt, and W (Weber and Bischoff 1997;  
73 Berg et al. 2009; MacPherson 2014). These alloys, which are among the earliest high-temperature  
74 condensates in the solar nebula, occur in a range of elemental proportions, with Os, Ru, Re, or Mo  
75 as the dominant element in some individual sub-micrometer-scale grains. IMA protocols thus  
76 would name coexisting nuggets as “osmium,” “ruthenium,” “rhenium,” or “molybdenum” (though  
77 the latter two native elements have not been approved as species by the IMA). By contrast, we  
78 lump all of these metal alloys together into platinum group element alloys (“*CAI PGE alloy*”).  
79 Similar lumping occurs in a number of oxide and silicate minerals in chondrules, including  
80 members of the oxide spinel, olivine, and clinopyroxene groups.

81 A third deviation from IMA protocols relates to non-crystalline condensed phases, notably a  
82 variety of low-temperature interstellar condensates (e.g., amorphous H<sub>2</sub>O), impact phases (e.g.,  
83 maskelynite), and rapidly quenched silicate glasses that are especially important in the context of  
84 chondrules. These materials, though not generally incorporated in the current IMA scheme (e.g.,  
85 Hazen et al. 2013, Table 3; Hazen 2019), are important in discussions of planetary evolution (e.g.,  
86 Bradley 1994a, 1994b; Abreu and Brearley 2011) and they represent distinct condensed solid  
87 phases that should be included in any comprehensive catalog of planetary materials.

88 Each of these considerations – splitting, lumping, and amorphous phases – comes into play  
89 when considering primary chondrule minerals, which provide the focus of Part III of this series.

90

91 **CHONDRULES AND CHONDRITES**

92 Chondrite meteorites, the oldest sedimentary rocks in the solar system, hold vivid clues to the  
93 origins and evolution of stars and planets. Here we review the nature and origin of chondrules, the  
94 classification of chondrite meteorites in which they are found, and a chronology of the earliest  
95 stages of mineral evolution. Chondrule types, properties, origins, and implications have been the  
96 subject of several comprehensive reviews (King 1983; Kerridge and Matthews 1988; Hewins et  
97 al. 1996; Brearley and Jones 1998; Hutchison 2004; Connolly and Desch 2004; Krot et al. 2014;  
98 Scott and Krot 2014; Rubin and Ma 2017, 2020; Russell et al. 2018). What follows, therefore, is a  
99 brief summary in the context of chondrule mineralogy.

100

101 *Classification of Chondrules*

102 Chondrules are igneous particles that were once partially to completely melted. Most  
103 chondrules range in size from tens of micrometers to ~10 millimeters in diameter, though extreme  
104 examples vary from submicron (Rubin et al. 1982) to several centimeters (Prinz et al. 1988) in  
105 diameter. Chondrules often occur as near-spherical solidified droplets (e.g., Weyrauch and  
106 Bischoff 2012; Charles et al. 2018), though other chondrules and their fragments are preserved in  
107 irregular shapes as a consequence of incomplete melting of precursor dust and grains, adhesion  
108 and sintering of conjoined objects, or sculpting by dynamic nebular processes (e.g., Rubin 2006).  
109 Most chondrules are dominated by silicates, commonly olivine, pyroxene, and feldspar, but many  
110 other phases, including metal alloys, sulfides, nitrides, phosphides, and several varieties of glass,  
111 occur in varying proportions that point to formation in diverse physical and chemical  
112 environments. Indeed, chondrules span the range from nearly pure silica to nearly pure metal, with  
113 textures from holocrystalline to glass. Given that chondrites account for as many as 80 percent of

114 observed meteorite falls, and that chondrules are the most abundant components of most  
115 chondrites, a significant fraction of the material that now comprises terrestrial planets and moons  
116 may have once been stored in the form of these small igneous droplets.

117 Chondrule classification is based on a combination of mineralogical, textural, and  
118 compositional attributes. From a petrographic perspective, most common chondrules (more than  
119 80 percent in ordinary chondrites) display porphyritic textures, including types designated PO  
120 (porphyritic olivine), POP (porphyritic olivine + pyroxene), and PP (porphyritic pyroxene) –  
121 conventions introduced by Gooding and Keil (1981). Other textural types include BO (barred  
122 olivine) with skeletal olivine plate-like crystals that were evidently quenched from a peak  
123 temperature close to the liquidus of the chondrule; GOP (granular olivine pyroxene) with small  
124 uniform grains; RP (radial pyroxene) with needle-like pyroxene crystals radiating from a point on  
125 the chondrule periphery; cryptocrystalline chondrules with crystallites less than 2 micrometers in  
126 diameter; and rare glassy chondrules. An important component of most chondrules is fine-grained  
127 or glassy mesostasis – solidified residual melt that surrounds phenocrysts (Connolly et al. 1998;  
128 Hewins et al. 2005).

129 Chondrules are also classified by their chemical characteristics (e.g., McSween 1977a). Type I  
130 chondrules, featuring Mg-rich olivine and pyroxene, are relatively reduced with most iron in the  
131 form of Fe metal rather than silicates. They are further divided into types IA (Si poorer; olivine  
132 dominant), IB (Si richer; pyroxene dominant), and IAB (intermediate, with both olivine and  
133 pyroxene) chondrules. Type II chondrules are more oxidized, typically with greater than 10  
134 molecular percent (mol %) of the Fe end-member in Mg silicates (Grossman and Brearley 2005).  
135 The A, B, and AB designations for olivine- and pyroxene-bearing chondrules apply to type II  
136 chondrules, as well.

137 In addition, a suite of aluminum-rich chondrules displays a range of compositions, between Ca-  
138 Al and Na-Al members, and Na-Al-Cr chondrules (Bischoff and Keil 1983, 1984), as well as  
139 plagioclase-olivine inclusions or “POIs” (Sheng et al. 1991a). These objects have mineralogical  
140 and compositional attributes intermediate between CAIs and chondrules. Unlike other chondrules,  
141 POIs contain a suite of relatively refractory primary minerals (e.g., spinel, fassaite, and perovskite),  
142 as well as several minerals not reported as primary phases from other types of chondrules (e.g.,  
143 armalcolite, rutile, sapphirine, and zirconolite). Additional chondrule-like objects range from  
144 silica-rich, with greater than 90 weight percent (wt %) SiO<sub>2</sub>, to sulfide-metal nodules, with < 10  
145 wt % silicates and oxides (e.g., Brearley and Jones 1998; Zhang and Hsu 2009; Scott and Krot  
146 2014; Wang et al. 2016).

147 At the smallest extreme, microchondrules no more than 40-micrometers in diameter have been  
148 recorded as decorating the rims of larger chondrules in the least altered ordinary chondrite  
149 meteorites (Mueller 1962; Rubin et al. 1982; Rubin 1989; Krot and Rubin 1996; Krot et al. 1997a).  
150 These tiny objects, which display a range of textures analogous to their larger counterparts, may  
151 form during rapid reheating events that melt the exterior portions of parent chondrules (Bigolski  
152 et al. 2016) or by splattering following random collisions (Dobriça and Brearley 2016).

153

#### 154 *Classification of chondrite meteorites*

155 Chondrules occur in chondritic meteorites, which contain the most refractory rock-forming  
156 elements in ratios close to those observed in the solar photosphere. They accreted initially as  
157 accumulations of nebular particles with four principal components (Brearley and Jones 1998,  
158 Table 3): (1) chondrules, typically the most abundant constituent, composing up to 80 volume  
159 percent (vol %) in many meteorites, though sometimes completely lacking; (2) refractory

160 inclusions, including CAIs, URIs, and AOAs, representing from 0 to ~10 vol %; (3) opaque  
161 assemblages of metallic Fe-Ni alloys and sulfides, which usually constitute less than 5 vol % but  
162 exceed 90 vol % in some examples; and (4) fine-grained (10-nanometer to 5-micrometer in  
163 diameter) matrix with some combination of oxide, silicate, sulfide, metal, and organic phases,  
164 often with a small fraction of presolar grains. While chondrules are often the dominant constituent  
165 of chondrites, the ratios of these four components vary widely. Note that in this contribution we  
166 consider primary chondrule mineralogy, whose formation (along with the refractory inclusions) is  
167 assumed to predate the incorporation of chondrules into chondritic meteorites. These primary  
168 phases are best identified and described from the most pristine chondrites, which have experienced  
169 relatively little alteration by thermal, aqueous, and/or impact processes on their parent asteroidal  
170 bodies. Note, however, that many chondrules experienced some degree of alteration prior to  
171 chondrite formation through reactions with nebular gas, secondary heating events, and/or high-  
172 velocity collisions with other particles (e.g., Ruzicka 2012; Ebel et al. 2018). Therefore, the  
173 distinction between primary and secondary processes is sometimes difficult to discern.

174 Chondrite meteorites have been classified under a variety of systems, based on the ratios of  
175 constituents, bulk composition, primary mineralogy, mineralogical textures, and isotopic  
176 characteristics. Additional chondrite subdivisions are based on degrees of aqueous, thermal, and/or  
177 shock alteration within their parent body (Van Schmus and Wood 1967; Stöffler et al. 1991;  
178 Weisberg et al. 2006; Krot et al. 2014), as well as through weathering at or near Earth's surface  
179 (Wlotzka 1993).

180 Traditional classification of tens of thousands of chondrite meteorite finds and falls divides  
181 more than 99.5 percent of specimens into 14 groups, each represented by multiple examples (e.g.,  
182 Scott and Krot 2014). Six of these groups, including those in the classes of ordinary, enstatite, and

183 R chondrites, collectively are termed non-carbonaceous chondrites (NC). The most abundant  
184 meteorites, comprising as many as 80 percent of falls, and more than 90 percent of chondrites (i.e.,  
185 excluding achondrite, iron, and stony-iron meteorites), are ordinary chondrites (OC), which occur  
186 in three broad groups – H, L, and LL. These three groups are generally similar in their high  
187 percentage of chondrules (typically ~0.3 to 0.6 millimeters in diameter, comprising 60 to 80 vol  
188 %; Friedrich et al. 2015), with 10 to 15 vol % matrix and few CAIs. However, they vary  
189 significantly in metal composition, as well as in the mineralogy of Fe-bearing metal and silicate  
190 phases. H stands for high total Fe, L for low total Fe, and LL for even lower total Fe and low metal.

191 Enstatite chondrites (EC), including EH and EL groups (for higher and lower total Fe-Ni metal  
192 alloy, respectively; Sears et al. 1982), are relatively rare, comprising fewer than 2 percent of falls  
193 (Weisberg and Kimura 2012). They are distinguished by an extremely reduced suite of minerals  
194 (Brearley and Jones 1998; Jacquet et al. 2018; Weyrauch et al. 2018; Rubin and Ma 2020), with  
195 almost all of their iron in the form of metal or sulfide, in association with near end-member  
196 enstatite ( $\text{MgSiO}_3$ ) and forsterite ( $\text{Mg}_2\text{SiO}_4$ ). These oxygen- and water-poor rocks feature such  
197 rare minerals as oldhamite ( $\text{CaS}$ ), niningerite ( $\text{MgS}$ ), alabandite ( $\text{MnS}$ ), daubréelite ( $\text{FeCr}_2\text{S}_4$ ),  
198 caswellsilverite ( $\text{NaCrS}_2$ ), and perryite  $[(\text{Ni},\text{Fe})_8(\text{Si},\text{P})_3]$ . EH and EL groups differ in the average  
199 size of chondrules and in the composition of Fe metal alloys, but for the most part they have similar  
200 mineralogy.

201 Eight chondrite groups, abbreviated CI, CM, CO, CV, CR, CH, CB, and CK, form the  
202 carbonaceous chondrite class (CC), which accounts for ~4 percent of falls. They share several  
203 compositional and isotopic characteristics, most notably: (1) suites of organic molecules; (2)  
204 relatively high volatile content; (3) enrichment relative to solar average in refractory lithophile

205 elements such as Ca, Al, and Ti; and (4) relatively low  $^{17}\text{O}/^{16}\text{O}$  compared to Earth – all  
206 characteristics that may be consistent with formation farther from the Sun than other chondrite  
207 groups. However, the several carbonaceous chondrite groups differ significantly from each other  
208 in their relative percentages of chondrules, refractory inclusions, metal, and matrix, as well as  
209 chondrule size, degree of oxidation, and extent of aqueous alteration and thermal metamorphism.  
210 Note that all known CI, CK, and CM carbonaceous chondrites display significant thermal and/or  
211 aqueous alteration (e.g., Brearley and Jones 1998; Scott and Krot 2014); consequently, their  
212 mineralogy will be considered in Part V of this series.

213 Chondrite classification is further complicated by additional rare grouped meteorites, as well as  
214 more than a dozen ungrouped chondrites that do not fit neatly into the above scheme. A few of  
215 these unusual meteorites are carbonaceous chondrites (e.g., Ivanova et al. 2008; Wang and Hsu  
216 2009; Kimura et al. 2014); others are distinguished by unusual combinations of chemical, isotopic,  
217 and/or matrix characteristics (e.g., Pratesi et al. 2019). For example, K chondrites (named for the  
218 Kakangari meteorite) combine aspects of both CC and NC groups, while R chondrites (for  
219 Rumuruti) are related to ordinary chondrites, though they are highly oxidized, unusually rich in  
220 matrix, and have an anomalously high  $^{17}\text{O}/^{16}\text{O}$  compared to other NC meteorites. It should be  
221 noted that chondrite classification is likely incomplete, as thousands of finds have yet to be fully  
222 characterized and hundreds of new specimens are recovered every year.

223 An important consideration when cataloguing “primary” chondrule minerals is the degree of  
224 alteration experienced in the chondrite meteorite’s parent body. A non-intuitive numbering system,  
225 first introduced by Van Schmus and Wood (1967) and now in general use, defines the least altered  
226 and therefore unequilibrated chondrites as “3.0.” Increasing numbers from 3 to 7 (with higher  
227 resolution between 3.0 and 3.9 for CO, L, LL, and H chondrites) designate increasing degrees of

228 thermal alteration, whereas decreasing numbers below 3.0 relate to increased degrees of aqueous  
229 alteration. Additional refinements by Grossman and Brearley (2005) subdivide OC and CO 3.0 to  
230 3.2 chondrites into an even higher resolution scale from 3.00 to 3.15.

231 Many primary chondrule minerals have been modified by progressive degrees of thermal  
232 metamorphism and metasomatism within their parent bodies. Common changes include gradual  
233 equilibration of silicate compositions through diffusion, as well as silicate glass devitrification,  
234 most commonly characterized by the nucleation of feldspar and possibly Ca-rich clinopyroxene  
235 (Sears and Hasan 1987; Scott et al. 1994). By the time a chondrule reaches type 3.9, corresponding  
236 to metamorphism close to 600 °C, olivine compositions have equilibrated among a meteorite's  
237 diverse chondrules, whereas pyroxene remains unequilibrated. Feldspar may occur in a high-  
238 temperature Al-Si disordered state (Sears et al. 1995) and display alteration effects, including Ca-  
239 Na zoning and textural changes (Lewis and Jones 2016, 2019). In this treatment we focus on  
240 minerals found in the least equilibrated chondrites (optimally those designated 3.0, though in some  
241 instances we consider minerals in more-altered chondrites, as some meteorite groups always  
242 display some degree of metamorphism).

243

#### 244 *Formation mechanisms of chondrules*

245 The diversity of chondrule types points to a variety of precursor materials and formation events  
246 at different heliocentric distances and with a range of paragenetic conditions (Krot et al. 2005;  
247 Rubin 2000, 2010; Desch et al. 2012; Scott and Krot 2014; Ebel et al. 2018; Hubbard and Ebel  
248 2018). Most chondrules are thought to have formed from presolar and protoplanetary disk dust  
249 aggregates, as well as from a combination of earlier generations of chondrules, chondrule  
250 fragments, refractory amoeboid olivine aggregates (AOAs) that formed as nebular condensates,

251 and possibly debris from differentiated planetesimals (Weinbruch et al. 2000; Libourel et al. 2006;  
252 Sanders and Scott 2012; Weyrauch and Bischoff 2012; Ebert and Bischoff 2016; Krot et al. 2018;  
253 Marrocchi et al. 2019).

254 The dominant chondrule formation hypothesis for the past several decades has been rapid  
255 heating (perhaps at rates  $>10^6$  °C/hour; Tachibana and Huss 2005) and melting of dust aggregates.  
256 Note that even to partially melt these droplets required energy comparable to the gravitational  
257 potential energy of the nebular disk, itself (King and Pringle 2010). Melting is thought to have  
258 occurred by any one of a number of processes (Boss 1996; Desch et al. 2012; Connolly and Jones  
259 2016): FU Orionis-type flares (Bertout 1989; Bell et al. 2000; Hubbard and Ebel 2014); direct  
260 illumination in proximity to the protosun (Shu et al. 1996; Morlok et al. 2012); solar shock waves  
261 induced by the in-fall of gas (Iida et al. 2001; Morris and Boley 2018); planetary embryo-produced  
262 bow shocks (Desch and Connolly 2002; Hood and Weidenschilling 2012; Morris and Boley 2018),  
263 as well as associated magnetic effects (Mann et al. 2016; Mai et al. 2018); shocks produced by  
264 density waves (Wood 1996a; Boss and Durisen 2005); current sheet heating in partly ionized disk  
265 regions (McNally et al. 2014; Hubbard and Ebel 2015; Zhdankin et al. 2017); and nebular lightning  
266 (Sorrell 1995; Desch and Cuzzi 2000). Given the range and frequency of these rapid heating events  
267 in the solar nebula, many chondrules may have experienced multiple secondary melting events  
268 (Baecker et al. 2017).

269 Isotope systematics from chondrules and matrix also support the dust origins hypothesis by  
270 pointing to chondrule formation through localized melting events of dust aggregates in the  
271 protoplanetary disk. Kleine et al. (2018) find that ages of CV and CR chondrites are tightly  
272 constrained at 4565.1 +/- 0.8 and 4563.7 +/- 0.6 Ma, respectively. These dates suggest that the

273 formation interval for each chondrite type is significantly less than 1 million years, and that  
274 chondrule formation and chondrite accretion were temporally linked.

275 Other researchers favor additional chondrule formation scenarios related to planetesimal  
276 impacts (e.g., Krot et al. 1993; Asphaug et al. 2011; Sanders and Scott 2012). Johnson et al. (2012,  
277 2014, 2018) argue for the role of impact jetting, by which high-velocity impacts on growing  
278 planetesimals generate jets of partially molten materials. Chondrules form from cooling droplets,  
279 which are rapidly accreted to planetesimal surfaces. Sanders and Scott (2012, 2018) posit a similar  
280 scenario for chondrule origins through impact splashing (as opposed to the higher velocity jetting),  
281 with chondrules contaminated by mineral dust and larger grains, thus generating a variety of relict  
282 grains and a range of chemical and isotopic compositions (however, see Baecker et al. 2017).

283 Finally, a small population of CB and CH group chondrules appears to have formed by direct  
284 condensation from a superheated silicate gas within an impact plume (Krot et al. 2001b; Campbell  
285 et al. 2002, 2005a, 2005b; Rubin et al. 2003; Campbell and Humayun 2004; Gounelle et al. 2007;  
286 Fedkin et al. 2015). Evidence for a different origin of these chondrules includes a complete lack  
287 of relict grains, fine-grained textures, and condensation calculations suggesting formation in a  
288 high-density impact plume environment.

289

### 290 Temperature, pressure, and cooling histories of chondrules

291 Numerous attributes of chondrules, including mineralogy, crystal growth textures,  
292 disequilibrium partition coefficients among phases, diffusion-controlled zoning, exsolution, the  
293 presence of glassy or cryptocrystalline phases, and olivine defect density, point to their complex  
294 and varied thermal histories (e.g., Jones et al. 2018). All chondrules experienced one or more  
295 episodes of rapid heating close to or above their liquidus (~1500 to 2100 K), followed by initial

296 cooling to solidus temperatures (~1300 to 1500 K) at rates from 100s to 1000s °C/h, with slower  
297 rates (10s to 100s °C/h) below the solidus (e.g., Miyamoto et al. 2009; Chaumard et al. 2018;  
298 Cuvillier et al. 2018; Ebel et al. 2018). Variations in mineralogy, texture, and other chondrule  
299 attributes point to significant variability in formation conditions, in some cases suggesting different  
300 modes of chondrule origin.

301 Adding to their complex thermal histories, many chondrules display evidence for rapid heating  
302 events after their initial crystallization (Krot et al. 1997a; 2004a, 2018; Rubin 2010; Ruzicka 2012;  
303 Baecker et al. 2017). At least four lines of evidence point to multiple subsequent heating events  
304 for many, if not most, chondrules: (1) many chondrule phenocrysts nucleate on earlier generations  
305 of olivine or pyroxene relict grains with different chemical properties (Marrocchi et al. 2019); (2)  
306 some chondrules appear to envelop others (Wasson et al. 1995; Hobart et al. 2015); (3) many  
307 chondrules display thin igneous rims of re-melted material (Rubin 1984); and (4) normal-sized  
308 chondrules are sometimes surrounded by “microchondrules” (Krot and Rubin 1996; Krot et al.  
309 1997a).

310 A significant unresolved question regards the pressures at which chondrules formed (Wood  
311 1996b; Hewins and Zanda 2012; Connolly and Jones 2016; Ebel et al. 2018). The presumed  
312 average pressure of the protoplanetary disk was  $< 10^{-3}$  atm. At such a low pressure and the  
313 maximum temperatures of chondrule formation (1700 to 2000 K), even with cooling rates as great  
314 as 1000 °C/h one would expect characteristic Rayleigh fractionation of volatile elements and their  
315 isotopes (Hashimoto 1983; Davis et al. 1990; Richter et al. 2011; see Ebel et al. 2018, and  
316 references therein). However, such fractionation is not generally observed in volatile elements  
317 such as S, Zn, Cd, or Cu (Luck et al. 2005; Tachibana and Huss 2005; Wombacher et al. 2008;  
318 Moynier et al. 2009). In addition, careful analyses of olivine phenocrysts indicate that Na was not

319 completely lost, suggesting an ambient vapor pressure significantly greater than  $10^{-3}$  atm  
320 (Alexander et al. 2008; Fedkin and Grossman 2013). One possible explanation was offered by  
321 Galy et al. (2000), who proposed that the partial pressure of hydrogen ( $H_2$ ) gas in chondrule-  
322 forming regions was  $\sim 1$  bar – conditions that would inhibit volatile element loss and promote the  
323 stability of silicate melts (Ebel 2006). However, astrophysical models of the protoplanetary nebula  
324 do not support such a high hydrogen gas concentration. Indeed, a maximum pressure of  $\sim 10^{-3}$  atm  
325 is suggested by models of disk processes (D’Alessio et al. 2005).

326 An alternative explanation for the lack of volatile element fractionation relates to “high solid  
327 densities” during chondrule formation, where solid density refers to the ratio of nebular dust to gas  
328 relative to the solar average. A number of investigators (Wood and Hashimoto 1993; Ebel and  
329 Grossman 2000; Alexander et al. 2008; Alexander and Ebel 2012; Bischoff et al. 2017; Ebel et al.  
330 2018) propose that chondrule-forming regions had a chondrule-to-gas ratio sufficiently high –  
331 perhaps  $10^3$  to  $10^4$  times that of the Sun – so that stable chondrule melts achieved equilibrium with  
332 the surrounding hot gas. High volatile partial pressures from evaporated dust thus reduced the  
333 evaporative loss of volatiles from large melt droplets in spite of the relatively low ambient gas  
334 pressure (Alexander et al. 2008), while leading to the observed significant fraction of compound  
335 chondrules (Wasson et al. 2003; Cuzzi and Alexander 2006). Note that clear evidence exists for  
336 significant chondrule-gas exchange, for example through the reaction of forsterite plus SiO gas to  
337 form enstatite rims (Krot et al. 2004b; Libourel et al. 2006; Friend et al. 2016; Hezel et al. 2018;  
338 though see Rubin 2018).

339

340 *A chronology of nebular mineralization*

341 The evolutionary system of mineralogy considers the diversity and distribution of minerals  
342 through deep time, as novel physical, chemical, and ultimately biological processes led to new  
343 mineral-forming environments. Developing a chronology of the earliest mineral-forming events in  
344 the evolving protoplanetary disk is thus important for setting the stage as planets and moons  
345 emerge from nebular dust and gas. Efforts to determine the ages of the most ancient minerals  
346 preserved in chondrites, both through direct radiometric or other measurements and by contextual  
347 inferences, have led to an emerging (though as yet incomplete and at times contentious)  
348 chronology of the first few million years of nebular history (Table 1). At least three complementary  
349 aspects of chondrite meteorites – (1) radiometric geochronology; (2) textural relationships; and (3)  
350 the distribution of their components among two major groups of meteorites – reveal aspects of the  
351 earliest evolution of the protoplanetary disk.

352

353 *Presolar grains:* The oldest solid objects from our solar system are refractory inclusions with  
354 radiometric ages close to 4567 Ma (Connelly et al. 2012; Krot 2019). Presolar grains, by definition,  
355 predate those first nebular condensates and are the most ancient known solid objects. Heck et al.  
356 (2020) employed cosmic ray exposure ages of presolar moissanite (SiC) grains to identify  
357 individual mineral grains as old as 7 billion years, though the majority of stardust preserved in  
358 chondrite meteorites is less than 5 billion years old and the youngest observed stellar SiC grain  
359 formed only 3.9 +/- 1.6 million years before CAIs (i.e., ~4571 million years ago). Estimates of  
360 when the first condensed solid phase formed in the universe must remain somewhat speculative.  
361 However, astrophysical calculations of stellar nucleosynthesis processes (e.g., Burbidge et al.  
362 1957; Cameron et al. 1957; Schatz 2010; Bertulani 2013), coupled with increasingly high-  
363 resolution imaging of the first generations of stars in galaxies at distances > 13 billion light years

364 (Abel et al. 2002; Bond et al. 2013; Howes et al. 2015; Robertson et al. 2015; Bowman et al. 2018),  
365 suggest that large carbon-forming stars occurred early in cosmic history. We conclude that carbon-  
366 rich phases, including diamond, graphite, and moissanite, formed within the first billion years of  
367 the Big Bang, perhaps > 13 Ga.

368  
369 Refractory inclusions: The formation of calcium-aluminum-rich inclusions at 4567.3 +/- 0.16  
370 Ma (Connelly et al. 2012; see also, Amelin et al. 2002, 2010; Connelly et al. 2008; Bouvier and  
371 Wadhwa 2010; Krot 2019), provides the benchmark date for nebular mineralogy. Radiometric  
372 dating of CAI components, including  $^{207}\text{Pb}$ - $^{206}\text{Pb}$  (Amelin et al. 2010; Connelly et al. 2012;),  
373  $^{182}\text{Hf}$ - $^{182}\text{W}$  (Holst et al. 2013; Budde et al. 2015), and  $^{26}\text{Al}$ - $^{26}\text{Mg}$  (Kita et al. 2013; Nagashima et  
374 al. 2018) systematics, establish that CAIs were the first solids to condense in the solar nebula (Krot  
375 2019). CAIs evidently were produced during an interval of less than 300,000 years (Kita et al.  
376 2013; Krot et al. 2018), with the great majority of CAIs forming within the first 200,000 years  
377 after ~4567.3 Ma (MacPherson et al. 2010, 2012; Kita et al. 2013).

378 That early interval of nebular evolution must have been a dynamic time. Recent studies of  
379 significant diversity in the size, mineralogy, textures, contexts, and chemical and isotopic  
380 fractionation of CAIs, URIs, and AOAs point to multiple generations of these refractory objects,  
381 perhaps arising from distinct nebular reservoirs and a range of processes, including episodic  
382 melting, evaporation, condensation, and aggregation (Krot et al. 2008; Kööp et al. 2016a, 2016b,  
383 2018; see Krot 2019, and references therein).

384 Ultra-refractory inclusions, usually lumped with CAIs, display extreme enrichments by factors  
385 up to 1000 in Sc, Zr, Y, Ti, and other high field strength elements (El Goresy et al. 2002; Rubin  
386 and Ma 2017). These unusual compositions result in distinctive URI mineralogy, including a

387 variety of rare, micron-scale oxide and silicate phases such as tistarite ( $\text{Ti}_2\text{O}_3$ ), kaitianite  
388 ( $\text{Ti}^{3+}_2\text{Ti}^{4+}\text{O}_5$ ), anosovite  $[(\text{Ti}^4, \text{Ti}^{3+}, \text{Mg}, \text{Sc}, \text{Al})_3\text{O}_5]$ , lakargiite ( $\text{CaZrO}_3$ ), kangite  
389  $[(\text{Sc}, \text{Ti}, \text{Al}, \text{Zr}, \text{Mg}, \text{Ca})_{1.8}\text{O}_3]$ , tazheranite  $[(\text{Zr}, \text{Sc}, \text{Ca}, \text{Y}, \text{Ti})\text{O}_{1.75}]$ , allendeite ( $\text{Sc}_4\text{Zr}_3\text{O}_{12}$ ), eringaite  
390  $[\text{Ca}_3(\text{Sc}, \text{Y}, \text{Ti})_2\text{Si}_3\text{O}_{12}]$ , davisite  $[\text{Ca}(\text{Sc}, \text{Ti}^{3+}, \text{Ti}^{4+}, \text{Mg}, \text{Zr})\text{AlSiO}_6]$ , warkite  
391  $[\text{Ca}_2(\text{Sc}, \text{Ti}, \text{Al}, \text{Mg}, \text{Zr})_6\text{Al}_6\text{O}_{20}]$ , and thortveitite ( $\text{Sc}_2\text{Si}_2\text{O}_7$ ) (Rubin and Ma 2017, 2020; Morrison  
392 and Hazen 2020). Such extreme elemental fractionation points to an early period of condensation  
393 of the most refractory elements in the protoplanetary disk.

394 Amoeboid olivine aggregates display isotopic and trace element compositions that indicate  
395 formation in a low-pressure, high-temperature environment with high gas-to-dust ratio –  
396 conditions that prevailed within the first 300,000 years of the protoplanetary nebula (Krot et al.  
397 2004a). However, the forsterite-dominated mineralogy of AOAs indicates a slightly lower  
398 condensation temperatures compared to CAIs (Ebel 2006; Ebel et al. 2012). Wasserburg et al.  
399 (2012) suggested that AOAs are younger than the first CAIs by up to 25,000 years, a model  
400 supported by the observation that many AOAs incorporate small spinel-pyroxene-anorthite CAIs  
401 (Krot et al. 2004a). Note, however, that at least one group of CAIs (forsterite-bearing type B CAIs)  
402 evidently formed by melting AOAs, and thus are younger (Krot et al. 2001a; Bullock et al. 2012).  
403 In any event, AOAs, like CAIs, formed during the earliest period of the protoplanetary disk, prior  
404 to 4567.0 Ma.

405  
406 *Formation of planetesimals and proto-Jupiter:* Recent models of the origin and early evolution  
407 of the solar system underscore the important links between nebular dynamics and mineral  
408 condensation (Warren 2011; Budde et al. 2016; Kruijjer et al. 2017; Desch et al. 2018; Burkhardt

409 et al. 2019). Nebular gas and dust within 2 AU of the protosun was exposed at an early stage  
410 (within 100,000 years of the protosun's formation) to temperatures high enough to vaporize almost  
411 all constituents (Pollack et al. 1996; Warren 2011; Davis and Richter 2014; Kruijjer et al. 2017),  
412 though a significant fraction of presolar grains, gas, and organic matter more remote from the Sun  
413 was not heated above a few hundred degrees Kelvin (Mendybaev et al. 2002; Cody et al. 2011).

414 Important constraints on the nature and timing of refractory inclusion formation are provided  
415 by a striking dichotomy in the isotopic characteristics of carbonaceous chondrites (CC) versus  
416 non-carbonaceous chondrites (NC) meteorites, notably isotopes of O, Cr, Ti, Ni, and Mo, which  
417 reveal two distinct genetic lineages (Trinquier et al. 2007, 2009; Burkhardt et al. 2011; Warren  
418 2011; Kruijjer et al. 2017). The bimodal compositional characteristics of CC versus NC meteorites  
419 is underscored by the distribution of CAIs, which occur much more frequently in CC meteorites.  
420 This concentration of CAIs beyond Jupiter's orbit contrasts to their rarity in NC meteorites,  
421 including ordinary chondrites and enstatite chondrites.

422 One model posits that CC parent bodies accreted beyond Jupiter's orbit – far from where CAIs  
423 are thought to have originated. NC parent bodies, by contrast, consolidated inside Jupiter's orbit  
424 (Warren 2011; Budde et al. 2016). According to this model, these two groups of planet-forming  
425 materials remained physically separated, most plausibly by the formation of embryonic Jupiter  
426 within the first 500,000 years of the protoplanetary disk (Lambrechts et al. 2014; Morbidelli et al.  
427 2016; Desch et al. 2018; Kruijjer et al. 2017). Jupiter's gravitational field created a barrier for  
428 exchange between NC meteorites of the inner solar system and CC meteorites beyond the ~3 AU  
429 orbit of Jupiter.

430 An early formation of embryonic Jupiter is consistent with other evidence for rapid planetesimal  
431 formation. Isotopic studies of iron meteorites suggest that their parent bodies must have reached

432 diameters of 10s to 100s of kilometers and differentiated within the first 300,000 years (Kruijer et  
433 al. 2014), with Mars-sized objects forming significantly earlier than 1 million years, and perhaps  
434 as early as 100,000 years after the oldest CAIs (Chambers 2004; Chiang and Youdin 2010;  
435 Johansen et al. 2014). Note that the occurrence of protoplanets at this early stage of solar system  
436 evolution has important implications for the possible origins of some chondrule groups through  
437 impact-generated jetting or splashing (Johnson et al. 2018; Sanders and Scott 2018; however, for  
438 an opposing view see Baecker et al. 2017).

439 In spite of the isotopic differences between two chondrite populations, both NC (with a greater  
440 percentage of chondrules) and CC meteorites (with the majority of CAIs and AOAs) hold  
441 populations of highly refractory minerals that are thought to have formed within 2 AU of the  
442 protosun. One model posits that CAIs represent the earliest condensates (by ~4567.2 Ma), most of  
443 which were transported within the solar nebula's first 100,000 years by strong disk winds to  
444 beyond what would become Jupiter's orbit (Shu et al. 1996; though see Desch et al. 2010). This  
445 postulated dispersal and sequestration of CAIs resulted in the distinctive chemical and isotopic  
446 fractionation of solar system material, with carbonaceous meteorites predominating beyond the  
447 orbit of Jupiter (e.g., Kruijer et al. 2017). Many chondrules, which represent a second generation  
448 of condensates perhaps 1 to 5 million years after CAIs, formed primarily near the protosun, and  
449 the majority of these objects did not migrate from the inner solar system (Warren 2011; Kruijer et  
450 al. 2017; Desch et al. 2018), though other chondrules, notably those in carbonaceous chondrites,  
451 may have formed beyond the orbit of Jupiter (Rubin 2010, 2011).

452

453 Chondrules: Most researchers conclude that chondrules formed significantly after CAIs,  
454 AOAs, and URIs, probably commencing ~4566 million years ago. Important evidence comes from

455 composite chondrule-CAI objects and bulk chondrule compositions, which suggest that refractory  
456 inclusions were already present when chondrules formed (Rubin and Wasson 1988; Kita and  
457 Ushikubo 2012; MacPherson et al. 2012; Kawasaki et al. 2015; Krot et al. 2017).

458 Pb-Pb, Hf-W, and Al-Mg radiometric dating indicate that chondrules formed over an interval  
459 of ~4 to 5 million years (Bizzarro et al. 2017; Johnson et al. 2018; Kleine et al. 2018; Connelly  
460 and Bizzarro 2018). This extended chronology of chondrule formation is complicated by multiple  
461 paragenetic modes – i.e., different mechanisms for rapid heating – spanning several million years.  
462 According to the canonical view (however, see Krot 2019), the oldest chondrules appear to have  
463 formed approximately 1.5 million years after CAIs (e.g., Nagashima et al. 2018), as revealed by  
464  $^{26}\text{Al}$ - $^{26}\text{Mg}$  isotope systematics. The rapid decay of short-lived  $^{26}\text{Al}$  to  $^{26}\text{Mg}$  (half-life ~0.71  
465 million years) results in measurable excess  $^{26}\text{Mg}$  in the most ancient Al-rich, Mg-poor minerals  
466 formed in the protoplanetary disk, with a systematic decrease in initial  $^{26}\text{Al}/^{27}\text{Al}$  through the first  
467 few million years of solar system history.

468 Different groups of unequilibrated chondrules appear to have formed over relatively narrow  
469 time windows (Table 1). For example, CO and CV chondrules have both been dated as originating  
470 at 4565.1 +/- 0.8 Ma (Kurahashi et al. 2008; Budde et al. 2015; Kleine et al. 2018), whereas CR  
471 chondrules formed more than a million years later at 4563.7 +/- 0.6 Ma (Schrader et al. 2017;  
472 Kleine et al. 2018).

473 The formation of CB chondrules, the youngest group identified thus far and likely representing  
474 late-stage droplets of impact melts, is even more tightly constrained at 4562.5 +/- 0.2 Ma (Krot et  
475 al. 2005; Gilmour et al. 2009; Bollard et al. 2015), suggesting a single origin event near the end of  
476 the era of chondrule formation.

477 The ages of chondrules in enstatite chondrites are poorly constrained, but they may have formed  
478 closer to the end of the interval of chondrule formation. Whitby et al. (2002) employed iodine-  
479 xenon dating to estimate ages of EH chondrules to between 4564 and 4561 Ma, whereas Trieloff  
480 et al. (2013) dated individual presumably primary sphalerite grains to 4562.7 +/- 0.5 Ma. Thus,  
481 chondrules in enstatite chondrites may be among the younger known groups.

482 In spite of the widespread agreement regarding a significant temporal gap of more than a million  
483 years between the end of CAI formation and the beginning of chondrule formation, an alternative  
484 hypothesis has recently emerged. Contrary to Al-Mg and Hf-W results, recent Pb-Pb ages suggest  
485 that the earliest chondrules formed contemporaneously with CAIs at ~4567.3 Ma (Connelly et al.  
486 2012; Bollard et al. 2017; Connelly and Bizzarro 2018; Krot 2019). If heterogeneities existed in  
487 the protoplanetary disk's initial  $^{26}\text{Al}/^{27}\text{Al}$ , then comparative  $^{26}\text{Al}/^{26}\text{Mg}$  dating of CAIs and  
488 chondrules might be invalid (Larsen et al. 2011; Krot et al. 2012; Luu et al. 2016). Indeed, a few  
489 chondrules from unequilibrated ordinary chondrites display  $^{206}\text{Pb}$ - $^{207}\text{Pb}$  ages that are equal to, if  
490 not slightly older than, 4567.3 Ma (Connelly and Bizzarro 2018; see Krot 2019 for a review). If  
491 this reinterpretation is correct, then some chondrules formed contemporaneously with CAIs (Kita  
492 et al. 2015; Schrader et al. 2017; Nagashima et al. 2018), with the majority of chondrules forming  
493 during the first 1 million years of the protoplanetary disk (Connelly and Bizzarro 2018). Resolution  
494 of these discrepancies remains an important challenge in chondrite chronology. However,  
495 whatever their ages relative to refractory inclusions, all primary chondrule minerals appear to have  
496 formed within the first 6 million years of solar system history and they are thus among the oldest  
497 known solid phases. In the following sections we consider the primary mineralogy of chondrules.

498

499

## PRIMARY MINERALOGY OF CHONDRULES

500 The evolutionary system of mineralogy focuses on mineral “natural kinds,” which we define as  
501 types of minerals that possess distinctive suites of chemical and physical attributes that arise from  
502 a well-defined formation process during a well-characterized interval of planetary evolution  
503 (Hazen 2019). The defining attributes of a mineral natural kind, in addition to its major element  
504 composition and atomic structure as employed by the IMA, can include any diagnostic  
505 combination of physical, chemical, and/or (in the case of terrestrial minerals younger than ~3.8  
506 billion years) biological features of the mineral grain or its petrologic and environmental context.  
507 Because minerals display numerous relevant attributes, including trace and minor elements, stable  
508 and radioactive isotopes, crystal size and morphology, exsolution, twinning, zoning, solid and fluid  
509 inclusions, age, petrologic context, and more, this approach to classification relies on large and  
510 robust databases of mineral properties. Thus, we embrace the development of findable, accessible,  
511 interoperable, and reusable (i.e., “FAIR”) mineral data resources, which provide the essential  
512 foundation for data-driven discovery in mineralogy (Ghiorso and Sack 1995; Holland and Powell  
513 1998; Lehnert et al. 2000, 2007; Ghiorso et al. 2002; Downs and Hall-Wallace 2003; Downs 2006;  
514 Hazen et al. 2011, 2019a, 2019b; Golden et al. 2013; Hazen 2014; Morrison et al. 2020; see also  
515 <http://mindat.org> and <https://rruff.info/ima>, accessed 7 April 2020).

516 Primary chondrule minerals fit the definition of distinct natural kinds, because: (1) all of these  
517 minerals formed in a protoplanetary disk context of high local dust-to-gas relative to solar average;  
518 (2) all of these minerals emerged within individual objects < 5 centimeters diameter as a  
519 consequence of discrete rapid heating, partial to complete melting, and rapid cooling events; and  
520 (3) all chondrules appear to have formed within a narrow time interval between ~4567 and ~4561  
521 million years ago. These minerals differ, therefore, from earlier stellar and nebular condensates  
522 (i.e., presolar grains and refractory inclusions) that apparently formed in regions of relatively low

523 dust-to-gas ratio under sustained high temperatures. They also differ from contemporaneous and  
524 subsequent minerals that formed in the contexts of accreting and differentiating protoplanetary  
525 bodies.

526 In this context, we recognize 43 primary chondrule minerals, including clinoenstatite,  
527 plagioclase, kamacite, and many other phases (Table 2), as distinct natural kinds (e.g., primary  
528 chondrule clinoenstatite, or “*PC clinoenstatite*”). Note that we have decided not to further  
529 subdivided according to types of chondrules, types of their host chondrite meteorites, distinct  
530 mineral morphotypes, or other criteria.

531 It is true that the majority of chondrules in any one chondrite group typically have similar  
532 properties – average size, textural type, and oxygen isotope ratios, for example – which suggest a  
533 local, common origin for most of the chondrules in any given meteorite group (Jones 2012; Kita  
534 and Ushikubo 2012). Nevertheless, there are also diverse chondritic components, including CAIs,  
535 AOAs, URIs, and atypical chondrules, which reveal a diversity of spatial and temporal sources.  
536 Furthermore, the uniformity in chondrule size distribution in any one chondrite group, coupled  
537 with the characteristic differences in average chondrule size from one chondrite group to the next,  
538 do not necessarily reflect a common origin for chondrules in a given group. Rather, these size  
539 characteristics may be at least in part the result of aerodynamic sorting, for example within nebular  
540 winds, during turbulent accretion at the surfaces of chondrule parent bodies, or in an asteroid’s  
541 loosely consolidated regolith during outgassing (Akridge and Sears 1999; Kuebler et al. 1999;  
542 Cuzzi et al. 2001; Teitler et al. 2010). In that case, size sorting of some chondrules could have  
543 occurred long after chondrule formation and subsequent mixing. However, aerodynamic sorting  
544 cannot account for all differences among chondrules in a given meteorite (Rubin 2010). Even if  
545 most chondrules formed in proximity to each other, and if they accreted with a matrix that was

546 formed more or less contemporaneously (e.g., see Hezel et al. 2018, and references therein), the  
547 emergence of chondrite bulk characteristics always postdates the origin of the primary chondrule  
548 minerals. Therefore, in this review we lump all primary chondrule mineral occurrences for each  
549 mineral species.

550 We suggest that any attempt to subdivide primary chondrule minerals by combinations of  
551 attributes at this time would be speculative and premature. An important advantage of the  
552 evolutionary system of mineralogy, but one that also adds an admitted degree of arbitrariness to  
553 its protocols, is that individual mineral experts can subdivide IMA species into natural kinds  
554 according to their specific needs. Experts in chondrule textures, stable isotopes, or  
555 cathodoluminescence may thus wish to add mineral subtypes based on unambiguous differences  
556 in mineral attributes. However, lacking sufficiently robust chondrule mineral data resources, we  
557 choose not to subdivide primary chondrule minerals at this time beyond IMA recognized species  
558 or well-defined types of amorphous phases.

559

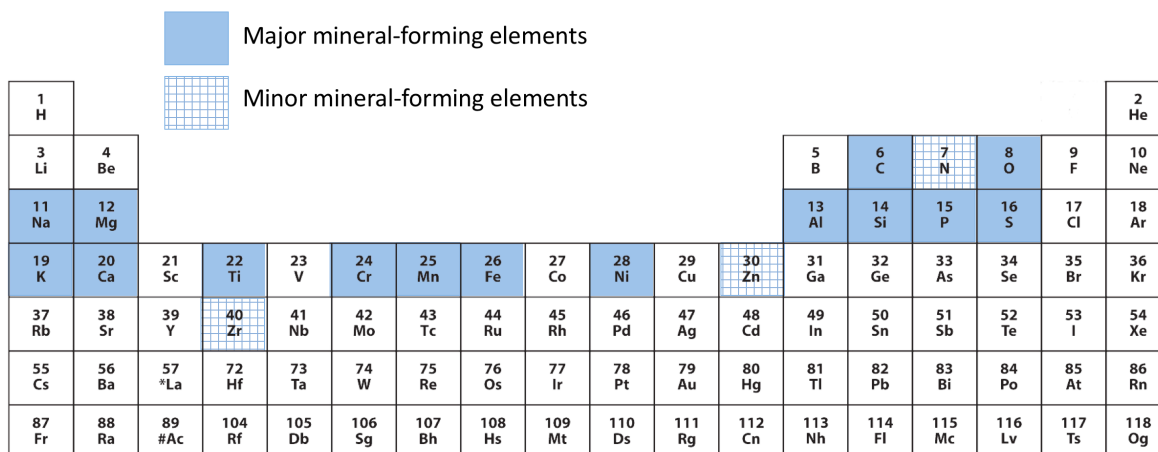
560 **SYSTEMATIC EVOLUTIONARY MINERALOGY – PART III:**

561 **PRIMARY CHONDRULE MINERALOGY**

562 In the following section we enumerate 43 primary chondrule minerals, which are defined as  
 563 solid condensed phases that formed during rapid heating and cooling of chondrule precursors to  
 564 temperatures close to the liquidus (at  $< 10^{-2}$  atm ambient pressure; i.e., not shock-induced phases),  
 565 as well as phases formed during subsequent chondrule cooling. Primary chondrule minerals must  
 566 have formed prior to sedimentation onto larger bodies and incorporation into chondrites. Most  
 567 primary chondrule minerals formed by melt crystallization in partially to fully molten droplets, but  
 568 we also include: (1) minerals formed by reactions between condensed phases and hot nebular gas  
 569 (Krot et al. 2004b; Libourel et al. 2006), and (2) varied solid-state reactions during initial cooling,  
 570 including silicate glass devitrification, polymorphic transformations, exsolution, and cation  
 571 ordering (e.g., Rubin and Ma 2020).

572 In **Table 2** we tabulate 43 primary chondrule minerals, encompassing 40 IMA-approved  
 573 species, the unapproved species ferropseudobrookite, and 2 amorphous phases. These primary  
 574 chondrule minerals incorporate 15 structurally essential chemical elements, as well as 3 significant  
 575 minor elements (**Figure 1**).

**PRIMARY MINERAL-FORMING ELEMENTS IN CHONDRULES**



577 **Figure 1.** Primary chondrule minerals form principally from 15 structurally essential elements, with important  
578 additional contributions from 3 additional minor elements.

579  
580  
581 Each mineral natural kind is given a binomial designation: the first name, in this case “*PC*” for  
582 all examples, indicates primary chondrule minerals, whereas the second name for the most part  
583 conforms to the name of an approved IMA mineral species. However, in several instances we  
584 deviate from IMA nomenclature:

- 585 • *Schreibersite* [(Fe,Ni)<sub>3</sub>P] and *Nickelphosphide* [(Ni,Fe)<sub>3</sub>P]: We lump these two IMA-  
586 approved phosphide species into *PC schreibersite* because they represent a continuous solid  
587 solution series, almost always with Fe > Ni, and they form by the same primary  
588 mechanisms.
- 589 • *Armalcolite* and *Ferropseudobrookite*: Fujimaki et al (1981a, 1981b) used  
590 “ferropseudobrookite” (Fe<sup>2+</sup>Ti<sub>2</sub>O<sub>5</sub>) as the name for the Mg-absent end-member related to  
591 armalcolite [(Mg,Fe<sup>2+</sup>)Ti<sub>2</sub>O<sub>5</sub>]. Though not an approved IMA mineral species, we refer to  
592 this occurrence as *PC ferropseudobrookite*.
- 593 • *Chromite*: Chromite (Fe<sup>2+</sup>Cr<sub>2</sub>O<sub>4</sub>) and other Cr-bearing oxide spinel group minerals are  
594 common primary phases in chondrules. Many occurrences conform to the IMA definition  
595 of chromite, but a few Cr-rich grains are closer to hercynite (Fe<sup>2+</sup>Al<sub>2</sub>O<sub>4</sub>) or  
596 magnesiochromite (MgCr<sub>2</sub>O<sub>4</sub>) end members, at times with significant spinel (MgAl<sub>2</sub>O<sub>4</sub>)  
597 and ulvospinel (Fe<sup>2+</sup>Ti<sub>2</sub>O<sub>4</sub>) content. We lump all of these Cr-bearing oxide spinel minerals  
598 together into *PC chromite*.

- 599 • *Roedderite and Merrihueite*: Roedderite and merrihueite,  $[(\text{Na},\text{K})_2\text{Mg}_5\text{Si}_{12}\text{O}_{30}]$  and  
600  $[(\text{K},\text{Na})_2(\text{Fe},\text{Mg})_5\text{Si}_{12}\text{O}_{30}]$ , respectively, form a continuous solid-solution of phases formed  
601 by the same primary process, and thus represent a single natural kind in our evolutionary  
602 system. Because most examples fall within the roedderite field, we lump occurrences  
603 together and assign the name *PC roedderite*.
- 604 • *Orthoenstatite*: Unlike in most terrestrial igneous rocks, the monoclinic (space group  $P2_1/c$ )  
605 form of  $\text{MgSiO}_3$ , clinoenstatite, is the most common polymorph. Therefore, for clarity we  
606 employ the common name “orthoenstatite” for orthorhombic  $\text{MgSiO}_3$  (space group  $Pbca$ )  
607 instead of the IMA-approved name, “enstatite.”
- 608 • *Silica Glass and Silicate Glass*: Glassy phases are important components of rapidly-  
609 quenched chondrules, with some chondrules approaching 100 vol % solid amorphous  
610 silicate. These condensed phases are not approved by the IMA, but we recognize *PC silica*  
611 *glass* (i.e., close to end-member  $\text{SiO}_2$ ) and *PC silicate glass*.

612

## 613 NATIVE ELEMENTS AND ALLOYS

614 Several alloys of iron and nickel, as well as the carbon allotrope graphite, occur as primary  
615 chondrule minerals. Iron-nickel alloys are among the most common of these phases, comprising  
616 several vol % of most chondrules and more than 90 vol % of some metal-rich examples (Brearley  
617 and Jones 1998; Scott and Krot 2014; Rubin and Ma 2020). Fe-Ni alloys, which typically  
618 incorporate Co, Cr, Cu, and other siderophile elements, condensed from the solar nebula at  
619 temperatures estimated between 1350 and 1450 K (Ebel and Grossman 2000; Campbell et al.

620 2005b). They occur as the IMA-approved minerals iron (though usually cited as “kamacite” in the  
621 meteoritics literature), taenite, tetrataenite, and awaruite, as well as the distinctive exsolved  
622 mixture of kamacite and taenite known as “plessite.” Fe-Ni alloys commonly hold significant  
623 amounts of other elements; high C, P, or Si contents, for example, may lead to exsolution of new  
624 minerals, such as graphite, carbides, schreibersite, perryite, or silica glass (see below). Note that  
625 alloys dominant in copper and in cobalt have been reported from chondrites, but they appear to be  
626 secondary phases and will be considered in Parts IV and V (Rubin 1990, 1994a; Brearley and Jones  
627 1998; Rubin and Ma 2020).

628

629 **Iron ( $\alpha$ -Fe):** Body-centered cubic (*Im3m*) iron, commonly referred to as kamacite in the  
630 meteoritics literature, is the most stable low-Ni iron alloy and is among the most common primary  
631 chondrule minerals. We designate this phase “PC iron” (see Table 2). PC iron is found with up to  
632 ~8 wt % Ni, though typical Ni contents are 3 to 7 wt %. Kamacite occurs in a range of textures  
633 (e.g., Brearley and Jones 1998; Rubin and Ma 2020), for example, as blebs to 50-micrometers  
634 diameter in mesostasis of type I chondrules, often in association with sulfides; in ordinary  
635 chondrites as polycrystalline intergrowths with taenite and troilite; as spheroidal grains, often  
636 concentrated near the chondrule edge; as globules up to 1-millimeter diameter in enstatite  
637 chondrites; in irregular masses, often in association with sulfides and/or carbides; and as irregular  
638 grains that are likely fragments from previous generations of chondrules. PC iron grains are  
639 sometimes zoned, with cores typically more Ni-rich than rims (Nagahara 1982).

640 While most PC iron crystallized as an igneous phase from the metal-rich fraction of immiscible  
641 metal-silicate chondrule melts, kamacite in CB group chondrules may have formed by  
642 condensation directly from a vapor plume generated by an impact on a differentiated body (Rubin

643 et al. 2003; Oulton et al. 2016; Rubin and Ma 2020). Kamacite in these CB metal-rich chondrules  
644 occurs in a distinctive morphology, as globules up to a centimeter in diameter.

645  
646 **Taenite [γ-(Fe,Ni)]**: The primitive cubic ( $Pm3m$ ) alloy of iron and nickel, referred to as  
647 “austenite” in the metallurgical literature, typically has ~25 to 35 wt % Ni. *PC taenite* commonly  
648 occurs with PC iron, sulfides, and other opaque phases in rounded grains; as crystals that are  
649 isolated or associated with kamacite; or as polycrystalline aggregates (Afiattalab and Wasson  
650 1980; Bevan and Axon 1980; Scott and Rajan 1981; Nagahara 1982; Brearley and Jones 1998).  
651 Taenite crystals, which are most abundant in Ni-rich LL ordinary chondrites, are commonly zoned  
652 from cores with 25 to 35 wt % Ni to rims that may exceed 50 wt % Ni (Wood 1967).

653 Taenite can incorporate significant amounts of P or C, which may exsolve as phosphides or  
654 carbides on cooling (e.g., Brearley and Jones 1998). In addition, under conditions of relatively  
655 slow cooling, taenite may exsolve thin (< 2-micrometers thick) lamellae of kamacite to produce  
656 the distinctive mixed phase known as “plessite” (Massalski et al. 1966; Buchwald 1975; Brearley  
657 and Jones 1998; Goldstein and Michael 2006).

658  
659 **Tetrataenite (FeNi)**: Tetrataenite, a low-temperature ordered Fe-Ni alloy (tetragonal,  
660  $P4/mmm$ ; Clarke and Scott 1980), is a widely distributed, though volumetrically minor, phase in  
661 type 3 (unequilibrated) ordinary chondrites (Bevan and Axon 1980; Scott and Rajan 1981;  
662 Nagahara 1982; Rubin 1994b; Rubin and Ma 2020). *PC tetrataenite* occurs as 10- to 60-  
663 micrometer-diameter grains or as rims up to 5-micrometers thick on taenite (Taylor and Heymann  
664 1971; Scott and Clarke 1979), forming through cooling and/or annealing of taenite below 350 °C  
665 (Clarke and Scott 1980). As such, tetrataenite is one of several chondrule minerals that spans a

666 continuous paragenetic range from primary to secondary. Though ideally a 50:50 mixture of Fe  
667 and Ni, the observed range of Ni in chondritic tetrataenite grains is 48 to 57 wt %, with minor Co  
668 and Cu. Metal grains in carbonaceous chondrites may significantly exceed 50 wt % Ni, resulting  
669 in fine-grained mixtures of tetrataenite and awaruite (Kimura and Ikeda 1992).

670

671 **Awaruite (Ni<sub>2</sub>Fe to Ni<sub>3</sub>Fe):** The Ni-dominant alloy awaruite, with face-centered cubic  
672 structure (*Fm3m*), is rare as a primary phase in chondrules (Taylor et al. 1981; Smith et al. 1993),  
673 and it is possible that all such occurrences are of secondary origin through aqueous alteration  
674 (Rubin, personal communication, 4 June 2020). *PC awaruite* typically occurs with 65 to 75 wt %  
675 Ni and forms as small anhedral grains in association with sulfides and carbides. Rubin (1991)  
676 described euhedral zoned crystals of presumably PC awaruite from a low-Fe olivine chondrule in  
677 the Allende CV chondrite. PC awaruite is thought to form in oxidizing nebular environments, in  
678 which oxidation of kamacite results in a Ni-enriched metal, crystallization of Ni-rich taenite, and  
679 subsequent transformation of taenite into tetrataenite and awaruite at temperatures below ~500 °C.  
680 Awaruite also forms via secondary processes in chondrules and chondrite matrices (Pederson  
681 1999; Rubin and Ma 2020).

682

683 **Graphite (C):** *PC graphite* is a common, if minor, primary chondrule mineral in enstatite  
684 chondrites, where it occurs as irregular to euhedral crystal inclusions up to 50-micrometers  
685 diameter in kamacite (Leitch and Smith 1980). Graphite probably formed by exsolution from a C-  
686 rich Fe-Ni alloy on cooling (Keil 1968). Keil (1968) noted that the amount of exsolved graphite  
687 increases with metamorphism; therefore, graphite is likely one of several chondrule minerals (e.g.,  
688 troilite, olivine, and plagioclase) that occurs in a continuum as both a primary and secondary phase.

689 Furthermore, other occurrences of less well-ordered graphite in chondrules have been ascribed to  
690 impact processes and are considered in Part IV of this series (Rubin 1997a; Rubin and Scott 1997).

691

## 692 **CARBIDES**

693 The iron carbides, cohenite and haxonite, are common primary chondrule phases (Brearley and  
694 Jones 1998; Rubin and Ma 2020). The rare iron carbide edscottite ( $\text{Fe}_5\text{C}_2$ ) has been reported as a  
695 matrix phase in the Semarkona LL3.0 ordinary chondrite, but it has not yet been observed as a  
696 primary chondrule phase (Ma and Rubin 2019).

697

698 **Cohenite [(Fe,Ni)<sub>3</sub>C]:** *PC cohenite* occurs in association with other opaque phases in some  
699 type 3 ordinary chondrites (Taylor et al. 1981; Scott et al. 1982; Scott and Jones 1990; Krot et al.  
700 1997b), as well as in enstatite chondrites (Mason 1966; Herndon and Rudee 1978; Rubin 1983;  
701 Shibata 1996). In unequilibrated ordinary chondrites it is found as polycrystalline masses with  
702 magnetite and sulfides in carbide-magnetite assemblages, which may have formed by reactions of  
703 kamacite and troilite with nebular gas (Taylor et al. 1981), though Krot et al. (1997b) and Rubin  
704 (personal communication; 27 March 2020) suggest a later origin by reaction with C-H-O fluids.  
705 In the CO3 chondrite Allan Hills 77307, cohenite occurs as grains < 30 micrometers in kamacite  
706 (Shibata 1996). PC cohenite contains up to ~4 wt % Ni (Scott and Jones 1990).

707

708 **Haxonite [(Fe,Ni)<sub>23</sub>C<sub>6</sub>]:** *PC haxonite* containing up to ~5 wt % Ni occurs with PC cohenite in  
709 the carbide-magnetite assemblages of unequilibrated (type 3) ordinary chondrites, as well as in  
710 CO3 and EH3 chondrites (Scott and Jones 1990; Rubin 1983; Shibata 1996; Rubin and Ma 2020).

711 An alternative view posits that carbide-magnetite assemblages are of secondary origin through  
712 parent-body aqueous alteration (Rubin, personal communication, 4 June 2020). If so, then all  
713 haxonite occurrences in chondrules may be secondary, as well.

714

#### 715 **NITRIDES AND OXYNITRIDES**

716 Osbornite (TiN) and nierite (Si<sub>3</sub>N<sub>4</sub>) have been reported from chondrites, but their presence  
717 has been ascribed to parent body metamorphism, shock alteration, or (in the case of some  
718 isotopically anomalous nierite grains) presolar origins (Buseck and Holdsworth 1972; Grossman  
719 et al. 1988; Scott 1988; Weisberg et al. 1988; Alexander et al. 1994; Russell et al. 1995; Rubin  
720 1997b; Hazen and Morrison 2020; Rubin and Ma 2020). Sinoite (Si<sub>2</sub>N<sub>2</sub>O) is known as both a  
721 primary chondrule mineral and as an impact product in enstatite chondrites (El Goresy et al. 2011;  
722 Lin et al. 2011; see also Part IV).

723

724 **Sinoite (Si<sub>2</sub>N<sub>2</sub>O):** Micrometer-scale *PC sinoite* needles, possibly condensed from nebular gas,  
725 occur in metal nodules from an EL3 clast from the Alhamata Sitta breccia (El Goresy et al. 2011;  
726 Lin et al. 2011). Associated minerals include graphite, oldhamite, enstatite, and Ca-rich  
727 clinopyroxene.

728

#### 729 **PHOSPHIDES**

730 With the exception of primary chondrule schreibersite, phosphide minerals are not known from  
731 the most unequilibrated chondrites. Occurrences of andreyivanovite (FeCrP) and florenskyite

732 (FeTiP) are also reported from chondrite meteorites, but their origins have been ascribed to impact  
733 processes (Ivanov et al. 2000; Zolensky et al. 2008).

734

735 **Schreibersite [(Fe,Ni)<sub>3</sub>P]:** *PC schreibersite* exsolves on cooling from P-rich Fe-Ni alloys in  
736 type 3 ordinary chondrites and enstatite chondrites, where it is closely associated with kamacite  
737 (Brearley and Jones 1998; Rubin and Ma 2020). It typically occurs as rims on, or inclusions in,  
738 kamacite, with individual grains as large as 300-micrometers in diameter. Schreibersite can contain  
739 up to ~50 wt % Ni, and often incorporates more than 1 wt % Co and Cr, as well (Wasson and Wai  
740 1970; Rambaldi and Wasson 1984; Zanda et al. 1994; see Brearley and Jones 1998, Table A3.32).  
741 Lehner et al. (2010) investigated trace and minor elements in schreibersite associated with  
742 kamacite and perryite and concluded that some schreibersite first formed by condensation from a  
743 reduced gas.

744 Ni-dominant grains of schreibersite have been recognized by the IMA as the mineral  
745 “Nickelphosphide” – ideally Ni<sub>3</sub>P, but originally described as (Ni,Fe)<sub>3</sub>P (Britvin et al. 1999).  
746 However, because this phase is evidently part of a continuous solid solution series, and a single  
747 paragenetic mode by exsolution from an Fe-Ni alloy on cooling is invoked, we lump  
748 nickelphosphide with the much more common schreibersite.

749

## 750 **SILICIDES**

751 Meteorites hold at least 8 different Fe-, Ni-, and Mn-bearing silicides (Rubin and Ma 2020), but  
752 perryite is the only example thought to be a primary chondrule mineral.

753

754 **Perryite [(Ni,Fe)<sub>8</sub>(Si,P)<sub>3</sub>]**: *PC perryite* is found as a widespread, if volumetrically minor, phase  
755 in type 3 unequilibrated enstatite chondrites (Keil 1968; Reed 1968; Lehner et al. 2010). It occurs  
756 in association with kamacite, schreibersite, sulfides, and other rare phases in the reduced enstatite  
757 chondrule mineral suite (Rubin and Ma 2020). The composition of PC perryite generally has > 60  
758 mol % Si in the Si-P site and > 90 mol % Ni in the Ni-Fe site (Wasson and Wei 1970; El Goresy  
759 et al. 1988; see Brearley and Jones 1998, Table A3.33). Lehner et al. (2010) suggest that perryite  
760 formed initially by condensation from a reduced gas and was then incorporated as inclusions in  
761 kamacite, while additional perryite precipitated from Si- and P-saturated Fe-Ni alloy on cooling.

762

### 763 **SULFIDES**

764 More than 50 sulfide minerals have been identified in meteorites (Rubin and Ma 2020), at least  
765 nine of which are thought to occur as primary chondrule minerals. However, the enumeration of  
766 primary versus secondary sulfide phases in chondrules (as well as in the matrix, refractory  
767 inclusions, and metal-rich portions of chondrites) is challenging (e.g., Weisberg and Kimura 2012;  
768 Singerling and Brearley 2018). Sulfide minerals arise from a continuum of processes, involving  
769 direct condensation from a hot gas phase, reactions between S-rich gas and condensed phases,  
770 crystallization from a melt, exsolution from metal, and a variety of alteration processes associated  
771 with impacts, metamorphism, and aqueous/hydrothermal interactions.

772 Troilite is by far the most common primary chondrule sulfide; it is the only sulfide to occur  
773 widely in CC, OC, and EC chondrules. The sulfides of chondrules in enstatite chondrites are of  
774 special interest, as these low-silica rocks contain unusual sulfides of elements such as Na, K, Mg,  
775 Ca, Mn, Cr, and Ti that more typically form oxides and silicates (Brearley and Jones 1998; Avril  
776 et al. 2013; Weyrauch et al. 2018; Rubin and Ma 2020). Thus, alabandite, caswellsilverite,

777 daubréelite, niningerite, oldhamite, and wassonite are confirmed primary phases. However, other  
778 sulfides from enstatite chondrites, including bornite, chalcopyrite, covellite, djerfisherite, idaite,  
779 pyrite, and pyrrhotite, are almost certainly secondary minerals that formed by impact and/or parent  
780 body processing (e.g., El Goresy et al. 1988; Weisberg and Kimura 2012; Ebel and Sack 2013).  
781 For representative analyses of chondrule sulfides see Brearley and Jones (1998), Tables A3.24 to  
782 A3.31.

783  
784 **Troilite (FeS):** *PC troilite* is one of the most abundant primary phases in chondrules (Brearley  
785 and Jones 1998, and references therein, Table A3.24). In unequilibrated ordinary chondrites it  
786 occurs as rounded grains with Fe-Ni alloys (Jones and Scott 1989; Jones 1990, 1996; Rubin et al.  
787 1999), as a constituent of carbide-magnetite assemblages (Krot et al. 1997b), as an accessory phase  
788 in silica-rich chondrules (Brigham et al. 1986), and in metal-troilite rims surrounding chondrules  
789 (Lauretta et al. 1996). In carbonaceous chondrites, PC troilite occurs, for example, in the  
790 chondrules of CO and CK chondrites as spherical or irregular metal-sulfide assemblages (Rubin  
791 et al. 1985; 1988; Shibata 1996; Singerling and Brearley 2018). And troilite comprises up to 10  
792 vol % of chondrules in some enstatite chondrites (El Goresy et al. 1988; Ikeda 1989a). Ikeda  
793 (1989a) recognized several different types of troilite-bearing EC nodules, including kamacite-  
794 troilite, niningerite-troilite, and djerfisherite-troilite nodules, as well as clasts in association with  
795 daubréelite (El Goresy et al. 1988).

796  
797 **Pentlandite [(Fe,Ni)<sub>9</sub>S<sub>8</sub>]:** *PC pentlandite* likely occurs as a primary chondrule mineral in  
798 unequilibrated ordinary chondrites (Jones and Scott 1989; Jones 1990, 1996), often intergrown  
799 with troilite in metal-sulfide or carbide-magnetite aggregates (Krot et al. 1997b). Barth et al. (2018)

800 report pentlandite in association with magnetite and troilite in a high-temperature association from  
801 the Acfer 094 unequilibrated carbonaceous chondrite – an occurrence that suggests formation by  
802 reaction of Fe-Ni metal with hot S-rich nebular gas prior to parent body accretion. Chondrules in  
803 carbonaceous chondrites also contain accessory pentlandite in association with Fe-Ni metal,  
804 troilite, and/or magnetite (Scott and Jones 1990). Note, however, that Rubin (personal  
805 communications, 27 March 2020) suggests that pentlandite occurrences in chondrules, as well as  
806 the carbide-magnetite assemblages in which they are found, are almost always secondary.

807  
808 **Alabandite (MnS):** *PC alabandite* is one of several unusual sulfides found in the highly  
809 reduced assemblages within chondrules of enstatite chondrites (Mason 1966; Buseck and  
810 Holdsworth 1972; Fogel 1997; Avril et al. 2013; Weyrauch et al. 2018). PC alabandite [(Mn,Fe)S]  
811 is found exclusively in EL chondrites, in which it typically incorporates 10 to 30 mol % FeS, and  
812 is sometimes given the name “ferroan alabandite” (e.g., Brearley and Jones 1998; Weisberg and  
813 Kimura 2012). Alabandite also forms a solid solution with niningerite (MgS), with compositions  
814 up to ~10 mol % MgS (Rubin 1984; Weyrauch et al. 2018; see Brearley and Jones 1998, Table  
815 A3.25 and A3.26).

816  
817 **Caswellsilverite (NaCrS<sub>2</sub>):** *PC caswellsilverite* is a rare accessory phase in chondrules of  
818 enstatite chondrites, found in association with alabandite, daubréelite, oldhamite, and other  
819 unusual sulfides (Mason 1966; El Goresy 1988; Ikeda 1989a; Rubin and Ma 2020).

820  
821 **Daubréelite (FeCr<sub>2</sub>S<sub>4</sub>):** *PC daubréelite* occurs as one of several unusual sulfides in reduced  
822 chondrule assemblages in enstatite chondrites (Mason 1966; Buseck and Holdsworth 1972; Ikeda

823 1989a; Izawa et al. 2010; Avril et al. 2013). It often occurs in association with troilite, from which  
824 it may have exsolved on cooling (El Goresy et al. 1988).

825  
826 **Niningerite (MgS)**: Keil and Snetsinger (1967) described the rare magnesium sulfide  
827 niningerite from reduced mineral assemblages in EH enstatite chondrites, in which it may  
828 constitute the most abundant chondrule sulfide mineral. *PC niningerite* has been described from  
829 several EH3 enstatite chondrites in association with other rare sulfides, notably oldhamite, and in  
830 nodules with Fe-Ni metal, troilite, and silicate (El Goresy et al. 1988; Ikeda 1989a; Izawa et al.  
831 2010; Avril et al. 2013; Weyrauch et al. 2018). Niningerite invariably incorporates iron (up to ~30  
832 mol % FeS in EH3, with greater FeS contents in equilibrated chondrules) and manganese (<20 mol  
833 % MnS); it typically displays Mg-Fe-Mn zoning (Ehlers and El Goresy 1988; see Brearley and  
834 Jones 1998, Table A3.25). The Fe-dominant phase, named keilite, is only known from enstatite  
835 chondrites that have been shock melted (Shimizu et al. 2002).

836  
837 **Oldhamite (CaS)**: *PC oldhamite* is a common accessory primary chondrule phase in enstatite  
838 chondrites, where it occurs as small grains in metal-sulfide nodules with other reduced phases,  
839 including alabandite, caswellsilverite, daubréelite, and niningerite (Mason 1966; Crozaz and  
840 Lundberg 1995; Fogel 1997; Nakamura-Messenger et al. 2012; Weyrauch et al. 2018). Calcium  
841 sulfide has also been reported as crystals up to 200-micrometers diameter within a metal matrix in  
842 the ungrouped, highly reduced meteorite Acfer 370 (Pratesi et al. 2019). Oldhamite in EH3  
843 chondrites is close to end-member composition, with minor Mg, Cr, and Fe (El Goresy et al. 1988;  
844 Ikeda 1989a).

845

846 **Sphalerite (ZnS):** *PC sphalerite* occurs as large unzoned primary crystals in EH3 enstatite  
847 chondrite Y-691, though it is more commonly encountered in chondrites as a secondary phase that  
848 occurs as “porous grains” associated with the breakdown of djerfisherite (El Goresy and Ehlers  
849 1989).

850  
851 **Wassonite (TiS):** Nakamura-Messenger et al. (2012) described *PC wassonite* as a primary  
852 chondrule phase from the Yamato 691 EH3 enstatite chondrite, where it was found as twelve sub-  
853 micron grains in a barred olivine chondrule crystallized from a melt.

854

## 855 **OXIDES**

856 Nine oxide phases, incorporating Mg, Ca, Fe<sup>2+</sup>, Al, Cr, Fe<sup>3+</sup>, Ti, and Zr as essential elements,  
857 have been described as primary chondrule minerals (Brearley and Jones 1998; Rubin and Ma 2017,  
858 2020). Of these phases, only three (spinel, chromite, and magnetite) are widespread as primary  
859 minerals in chondrules, while four (armalcolite, perovskite, rutile, and zirconolite) are known only  
860 as minor phases in plagioclase-olivine inclusions from carbonaceous chondrites (Sheng et al.  
861 1991a). A single occurrence of micrometer-scale corundum grains with high dislocation density  
862 from a chondrule in the Allende CV chondrite appears to be a shock phase (Müller et al. 1995) and  
863 is considered in Part IV.

864

## 865 **Spinel Group Oxides [(Mg, Fe<sup>2+</sup>)(Al,Cr,Fe<sup>3+</sup>)<sub>2</sub>O<sub>4</sub>]**

866 Three members of the spinel group of oxides – spinel (ideally MgAl<sub>2</sub>O<sub>4</sub>), chromite  
867 (Fe<sup>2+</sup>Cr<sub>2</sub>O<sub>4</sub>), and magnetite (Fe<sup>2+</sup>Fe<sup>3+</sup><sub>2</sub>O<sub>4</sub>) – are the most common primary oxide phases in

868 chondrules. Significant solid solution among other end-members, including hercynite  
869 ( $\text{Fe}^{2+}\text{Al}_2\text{O}_4$ ), magnesiochromite ( $\text{MgCr}_2\text{O}_4$ ), and ulvospinel ( $\text{Fe}^{2+}\text{Ti}_2\text{O}_4$ ), is observed (e.g.,  
870 Brearley and Jones 1998, see Table A3.6). However, almost all primary chondrule spinel group  
871 minerals appear to fall well within the compositional fields of three end-members – *PC spinel*, *PC*  
872 *chromite*, and *PC magnetite*. Note that spinel crystals in the chromite-hercynite-magnesiochromite  
873 compositional field have been described from chondrules in CV carbonaceous chondrites  
874 (Weinbruch et al. 1990; Müller et al. 1995), but we lump these examples together as PC chromite  
875 because they form a continuous solid solution with other Cr-rich oxide spinels and they arise by  
876 the same paragenetic processes. Note that we employ the names “*PC spinel*,” “*PC chromite*,” and  
877 “*PC magnetite*” to designate three distinct complex *phase regions* – not the end-member  
878 compositions.

879

880 **Spinel ( $\text{MgAl}_2\text{O}_4$ ):** Spinel, ranging in composition from near end-member  $\text{MgAl}_2\text{O}_4$  to  
881 examples with significant  $\text{Fe}^{2+}$ ,  $\text{Cr}^{3+}$ , and/or  $\text{Ti}^{4+}$ , is one of the most common primary oxide phases  
882 in chondrules. We use the name *PC spinel* to designate this complex phase space, which is found  
883 in unequilibrated ordinary chondrites (Ikeda 1980), notably in their Ca-Al-rich chondrules in  
884 association with fassaite and plagioclase (Bischoff and Keil 1983, 1984; McCoy et al. 1991a;  
885 Wang et al. 2016). PC spinel is an occasional minor phase in CO3 carbonaceous chondrites,  
886 typically in association with olivine in type I and II chondrules (McSween 1977b; Ikeda 1982). In  
887 CM chondrites, PC spinel occurs in association with fassaite (Simon et al. 1994), and as inclusions  
888 in forsterite (Fuchs et al. 1973) with variable  $\text{Fe}^{2+}$  and Cr contents to several wt %. Near end-  
889 member spinel grains are associated with fassaite, forsterite, and plagioclase in plagioclase-olivine

890 inclusions in CV chondrites (Sheng et al. 1991a). Finally, PC spinel has been identified from barred  
891 olivine-pyroxene chondrules in the Yamato-691 enstatite chondrite, where it occurs in association  
892 with fassaite and/or plagioclase (Ikeda 1988a, 1989b).

893

894 **Chromite (Fe<sup>2+</sup>Cr<sub>2</sub>O<sub>4</sub>):** Oxide spinel phases with significant Cr content are common primary  
895 and secondary accessory phases in a variety of chondrules and their associated opaque  
896 assemblages. Most of these occurrences conform to the IMA definition of chromite, as they are  
897 closer in composition to Fe<sup>2+</sup>Cr<sub>2</sub>O<sub>4</sub> than to other spinel end-members. Other examples, either on  
898 average or in zoned regions, may lie closer to the spinel (MgAl<sub>2</sub>O<sub>4</sub>), hercynite (Fe<sup>2+</sup>Al<sub>2</sub>O<sub>4</sub>), or  
899 magnesiochromite (MgCr<sub>2</sub>O<sub>4</sub>) end members, at times with significant ulvospinel (Fe<sup>2+</sup>Ti<sub>2</sub>O<sub>4</sub>)  
900 content, as well (for representative analyses see Brearley and Jones 1998, Table A3.6). For the  
901 purposes of primary chondrule mineralogy, we lump these compositionally varied Cr-bearing  
902 phases together as *PC chromite*.

903 *PC chromite* is known from relatively unequilibrated ordinary chondrites as euhedral crystals  
904 in mesostasis (Jones 1990; Johnson and Prinz 1991), as inclusions in olivine (Ruzicka 1990), and  
905 in Na-Al- and Na-Cr-rich chondrules associated with Na-rich glass and olivine (McCoy et al.  
906 1991a). Chromite crystals commonly incorporate inclusions of primary silicates, notably forsterite,  
907 Ca-poor pyroxene, and calcic pyroxene (Alwmark et al. 2011). Rare chromium-rich chondrules <  
908 300-micrometers in diameter feature chromite grains in mesostasis with plagioclase (Ramdohr  
909 1967; Krot et al. 1993). OC chromite is variable in composition, at times extending into the spinel  
910 compositional field, and grains are often zoned (Bunch et al. 1967; Ikeda 1980; Krot et al. 1993).

911 In type 3 carbonaceous chondrites, chromite occurs as a primary chondrule phase in type IIA  
912 chondrules (relatively oxidized and olivine-dominant) in the Allende CV3, Renazzo CR, in CO  
913 chondrites within olivine phenocrysts, and Adelaide (ungrouped) meteorites (Davy et al. 1978;  
914 Johnson and Prinz 1991; Weinbruch et al. 1994; Murakami and Ikeda 1994; Ikeda and Kimura  
915 1995; Wasson and Rubin 2003), though it is more commonly observed in assemblages that have  
916 been thermally altered (Tomeoka and Buseck 1990; Weinbruch et al. 1990; Müller et al. 1995).

917

918 **Magnetite (Fe<sup>2+</sup>Fe<sup>3+</sup><sub>2</sub>O<sub>4</sub>):** *PC magnetite* is found in a variety of contexts in chondrules, some  
919 of which may be primary in origin (though Rubin, personal communication, 4 June 2020, suggests  
920 that all chondrule magnetite occurrences are secondary). Barth et al. (2018) reported magnetite in  
921 association with pentlandite and troilite in a high-temperature association from the Acfer 094  
922 unequilibrated carbonaceous chondrite; they suggested that magnetite formed by reaction of Fe-  
923 Ni metal with hot O-rich nebular gas. In CO, CV, and other relatively unequilibrated carbonaceous  
924 chondrites, magnetite is often found in aggregates in association with kamacite and troilite  
925 (Haggerty and McMahon 1979; Nagahara and Kushiro 1982; Ikeda 1983; Scott and Jones 1990).  
926 Note that magnetite is also often found as a secondary phase in ordinary and carbonaceous  
927 chondrites (Brearley and Jones 1998), for example by the oxidation of troilite (Herndon et al.  
928 1975).

929

930 **Rutile (TiO<sub>2</sub>):** Rutile is known as a primary chondrule phase only as a minor accessory mineral  
931 from plagioclase-olivine inclusions (Sheng et al. 1991a). *PC rutile* occurs in grains up to 50-  
932 micrometers in diameter associated with armalcolite, ilmenite, perovskite, and fassaite.

933

934 **Ilmenite (FeTiO<sub>3</sub>)**: *PC ilmenite* is a minor primary accessory phase in Na-Al-rich chondrules  
935 in type 3 ordinary chondrites (Bischoff and Keil 1984). *PC ilmenite* also occurs as a minor  
936 accessory phase in plagioclase-olivine inclusions, where it is found as grains up to 50-micrometers  
937 in diameter with armalcolite, perovskite, and rutile (Sheng et al. 1991a).

938

939 **Armalcolite [(Mg,Fe<sup>2+</sup>)Ti<sub>2</sub>O<sub>5</sub>]**: Sheng et al. (1991a) report *PC armalcolite* as a rare accessory  
940 primary phase in plagioclase-olivine inclusions from carbonaceous chondrites, in which  
941 armalcolite is accompanied by several Ti-bearing oxides, including ilmenite, perovskite, rutile,  
942 and zirconolite. *PC armalcolite*'s Mg/Fe ratio ranges from 1.2 to 4.3.

943

944 **Ferropseudobrookite (Fe<sup>2+</sup>Ti<sub>2</sub>O<sub>5</sub>)**: Fujimaki et al (1981a, 1981b) described two euhedral  
945 crystals of "ferropseudobrookite" from an EL3 chondrite, Allan Hills 77015, in a unique Mg-poor  
946 chondrule with albite, a silica mineral, and glass. Note that ferropseudobrookite (ideally  
947 Fe<sup>2+</sup>Ti<sub>2</sub>O<sub>5</sub>, though here it contains significant Ca, Ti, and Cr in the Fe<sup>2+</sup> site) is not an approved  
948 IMA species. Nevertheless, we recognize *PC ferropseudobrookite*, as this Fe<sup>2+</sup>-dominant, Mg-  
949 absent mineral differs from both armalcolite and pseudobrookite (Fe<sup>3+</sup><sub>2</sub>TiO<sub>5</sub>).

950

951 **Perovskite (CaTiO<sub>3</sub>)**: *PC perovskite* is one of several minor accessory phases found as primary  
952 chondrule minerals only in plagioclase-olivine inclusions (Sheng et al. 1991a). It occurs as 10- to  
953 50-micrometer-diameter grains in association with armalcolite, ilmenite, and rutile.

954

955        **Zirconolite (CaZrTi<sub>2</sub>O<sub>7</sub>):** *PC zirconolite* occurs as micron-scale irregular blebs surrounding  
956 perovskite in plagioclase-olivine inclusions (POIs) from unequilibrated carbonaceous chondrites  
957 (Sheng et al. 1991a). Zirconolite grains from POIs feature significant Fe<sup>2+</sup> substitution for Ca,  
958 while they hold as much as 10 wt % Y<sub>2</sub>O<sub>3</sub> plus REE oxides.

959

## 960 **PHOSPHATES**

961        Most chondritic phosphate minerals appear to be secondary phases, formed through aqueous  
962 and thermal alteration of prior P-bearing phases, notably as fine-grained constituents of matrices  
963 (e.g., Rubin and Grossman 1985; Jones et al. 2014; Lewis and Jones 2016; Rubin and Ma 2017).  
964 However, merrillite has been found in unusual glass-rich, Si-rich, or Cr-rich chondrules from  
965 unequilibrated ordinary chondrites – occurrences that probably represent primary chondrule  
966 mineralization.

967

968        **Merrillite [Ca<sub>9</sub>NaMg(PO<sub>4</sub>)<sub>7</sub>]:** Krot and Rubin (1994) report two occurrences of merrillite  
969 from glass-rich chondrules in ordinary chondrites, which we provisionally classify as *PC*  
970 *merrillite*. Two anhedral merrillite crystals (~150-micrometers maximum dimension) are  
971 associated with olivine in a glass chondrule in the Hedjaz (L3.7) ordinary chondrite, while a spinel  
972 grain in a glass chondrule from Allan Hills 77043 (L3.5) holds a 10-micrometer-diameter euhedral  
973 merrillite inclusion. Brigham et al. (1986) describe merrillite from a silica-pyroxene chondrule in  
974 the Bremervorde (H3) ordinary chondrite, while Krot et al. (1993) record merrillite as a relatively  
975 common accessory mineral in unusual Cr-rich chondrules, for example in Raguli (H3.8). As with  
976 merrillite occurrences in glass-rich chondrules, it is not certain whether these grains formed during

977 initial cooling of a P-rich precursor, most likely a P-rich Fe-Ni alloy (i.e., primary origin), or during  
978 a subsequent alteration process (Jones et al. 2014; Lewis and Jones 2016).

979

## 980 **SILICATES**

981 Silicate minerals, most notably Mg-Fe olivine, Ca-rich and Ca-poor pyroxenes, and plagioclase,  
982 are the dominant phases in most chondrules. Relatively few other silicates have been reported as  
983 primary phases in chondrules – a reflection of their igneous origins from nebular precursors.

984

### 985 **Silica Group Minerals (SiO<sub>2</sub>)**

986 Silica-rich chondrules constitute an important, if volumetrically minor, compositional extreme  
987 in unequilibrated chondrite meteorites (Brearley and Jones 1998; Krot et al. 2004b; Scott and Krot  
988 2014; Rubin and Ma 2020). In addition, silica forms rims around Mg-rich chondrules from CR  
989 chondrites (Krot et al. 2004b). Three phases – cristobalite, tridymite, and silica glass – have been  
990 reported as primary chondrule minerals (Brearley and Jones 1998; Kimura et al. 2005; Hezel et al.  
991 2006). Additionally, quartz occurs as a secondary phase in metamorphosed enstatite chondrites  
992 that were re-equilibrated at  $T < 867\text{ }^{\circ}\text{C}$  (Kimura et al. 2005), while coesite, seifertite, and stishovite  
993 have been identified as silica polymorphs formed during shock events to  $P > 0.6\text{ GPa}$  (Rubin and  
994 Ma 2020).

995

996 **Cristobalite (SiO<sub>2</sub>)**: *PC cristobalite* has been reported from silica-rich chondrules in many  
997 type 3 and type 4 ordinary and enstatite chondrites, where it occurs in association with low-Ca  
998 pyroxene and may approach 30 vol % of some chondrules (Rubin 1983; Bridges et al. 1995;  
999 Brigham et al. 1986; Brearley and Jones 1998; Kimura et al. 2005; Hezel et al. 2005; Rubin and

1000 Ma 2020). Textures and associations suggest that cristobalite is the liquidus phase in some SiO<sub>2</sub>-  
1001 dominant chondrules, so it crystallized from the original chondrule melt (Kimura et al. 2005).

1002

1003 **Tridymite (SiO<sub>2</sub>)**: *PC tridymite* occurs in many silica-rich chondrules in type 3 and type 4  
1004 ordinary and enstatite chondrites (Ikeda 1989b; Schulze et al. 1994; Bridges et al. 1995; Newton  
1005 et al. 1995; Brearley and Jones 1998; Kimura et al. 2005; Hezel et al. 2004; Rubin and Ma 2020).  
1006 At low-Mg, high-Si compositions, tridymite is the liquidus phase rather than cristobalite; therefore,  
1007 tridymite is assumed to be a primary chondrule mineral that crystallized from melt (Kimura et al.  
1008 2005).

1009

1010 **Silica Glass (SiO<sub>2</sub>)**: *PC silica glass* (SiO<sub>2</sub> > 90 mol %), in association with primary low-Ca  
1011 pyroxene and secondary fayalitic olivine, is an important constituent of silica-rich chondrules,  
1012 which represent less than 2 vol % of ordinary chondrites (Brigham et al. 1986; Wasson and Krot  
1013 1994; Brearley and Jones 1998). Silica-glass-rich chondrules have also been described from  
1014 carbonaceous chondrites (Olsen 1983; Kimura et al. 2005), and from an enstatite chondrite as  
1015 isolated < 5-micrometer diameter inclusions in Fe-Ni alloys, presumably exsolved from the Si-  
1016 rich metal on cooling (Ivanov et al. 1996). Kimura et al. (2005) suggest that some occurrences of  
1017 silica glass represent the final product from rapid cooling of a Si-rich chondrule melt.

1018

1019 **Olivine [(Mg,Fe)<sub>2</sub>SiO<sub>4</sub>]**: Ferromagnesian olivine group minerals are found in all chondrite  
1020 groups and are among the most abundant chondrule primary phases. Hundreds of references in  
1021 work spanning the past half century document occurrences of olivine, which occurs in numerous

1022 different textures and contexts within chondrules (as well as in CAIs, AOAs, and other primary  
1023 meteoritic constituents). This diversity reflects a variety of primary mineralization processes,  
1024 including crystallization from a chondrule melt, condensation from nebular gas, and condensation  
1025 within an impact plume, as well as subsequent modification via reaction with hot nebular gases  
1026 (Brearley and Jones 1998; Scott and Krot 2014; Rubin and Ma 2020).

1027 An important question in the context of the evolutionary system of mineralogy is whether there  
1028 are multiple natural kinds of primary chondrule olivine (as well as other major silicate phases,  
1029 including primary chondrule pyroxene and plagioclase, for example). Numerous attributes of an  
1030 olivine occurrence provide insight on its paragenesis and subsequent history, including major,  
1031 minor, and trace element composition; stable isotope composition; grain morphology and zoning;  
1032 chondrule texture; dislocation density; solid inclusions; and petrographic context. If sufficiently  
1033 comprehensive data resources become available, then cluster analysis might reveal several  
1034 different kinds of primary chondrule olivine with idiosyncratic combinations of attributes.  
1035 However, until such time as those data resources are developed, we recognize *PC olivine* as the  
1036 only primary chondrule olivine. Note that in a few instances the most FeO-rich zoned regions of  
1037 some primary olivine grains may extend into the fayalite field, with  $Fe > Mg$ . Therefore, we lump  
1038 all of these examples into *PC olivine*, which represents a wide range of  $[(Mg,Fe)_2SiO_4]$   
1039 compositions.

1040 A few instances of the Fe-dominant olivine, fayalite, occur (1) in rare silica-bearing chondrules  
1041 with cristobalite and Ca-free pyroxene (Brigham et al. 1986; Wasson and Krot 1994); (2) as rims  
1042 around forsterite in type I chondrules (Hua et al. 1988; Murakami and Ikeda 1994; Krot et al.  
1043 1995); and (3) as Fag8-99 grains to 100-micrometers diameter in association with magnetite, troilite,  
1044 and pentlandite (Hua and Buseck 1995). These occurrences have all been ascribed to secondary

1045 processes in chondrites (Krot et al. 1997b; Brearley and Jones 1998; Brearley 2014), though a few  
1046 earlier researchers suggested that fayalite rims could be primary as a consequence of condensation  
1047 from an oxidized nebular gas (e.g., Hua et al. 1988; Weinbruch et al. 1990, 1994; Krot and Rubin  
1048 1996; Krot et al. 1997b).

1049 In the most unequilibrated ordinary chondrites, olivine phenocrysts, often nucleated on prior  
1050 generations of relict olivine (Rubin 2006; Rubin and Ma 2020), are invariably Mg-rich (Fo<sub>65-99</sub>)  
1051 with minor Mg-Fe zoning— attributes that reflect crystallization from the melt (Rubin and Wasson  
1052 1987; Jones 1990; Weinbruch et al. 1990, 1994; Brearley and Jones 1998, see Table A3.1). Olivine  
1053 of similar composition occurs as inclusions in clinoenstatite (Jones 1994), while more Fe-rich  
1054 (Fo<sub>60-70</sub>) micrometer-scale crystallites may occur in the mesostasis (Töpel-Schadt and Müller  
1055 1985). Within a given unequilibrated meteorite, olivine compositions in adjacent chondrules may  
1056 differ significantly; however, olivine chemistry re-equilibrates by inter-chondrule diffusion as a  
1057 consequence of parent-body alteration. Therefore, for meteorites of grade 3.6 and higher, the  
1058 olivine phenocrysts in adjacent chondrules typically attain uniform compositions in major and  
1059 minor elements (McCoy et al. 1991b; Sears et al. 1992).

1060 Carbonaceous chondrites display a wider range of both averaged and zoned olivine  
1061 compositions, with phenocrysts in CO3, CM2, and CV3 chondrites covering the range from near  
1062 end-member forsterite in type I chondrules to Fo<sub>37-50</sub> in the rims of zoned olivine in type II  
1063 chondrules (McSween 1977a; Desnoyers 1980; Cohen et al. 1983; Scott and Taylor 1983; Sheng  
1064 et al. 1991b; Murikami and Ikeda 1994; Simon et al. 1995; Brearley and Jones 1998, and references  
1065 therein).

1066 Primary olivine in the ferromagnesian chondrules of type 3 enstatite chondrites is uniformly  
1067 forsteritic, with most samples Fo<sub>92-99</sub> (Grossman et al. 1985; Ikeda 1988b), though rare zoned  
1068 examples display more fayalitic rims to Fo<sub>75</sub> (Lusby et al. 1987).

1069

### 1070 **Low-Calcium Pyroxenes [(Mg,Fe,Ca)SiO<sub>3</sub>]**

1071 Low-Ca pyroxene group minerals, ideally (Mg, Fe<sup>2+</sup>, Ca)<sub>2</sub>Si<sub>2</sub>O<sub>6</sub>, but often with significant Al  
1072 and/or Ti and most commonly with less than 40 mol % of the Fe end-member, are extremely  
1073 common primary constituents of chondrules (Ikeda 1982; Noguchi 1989; Brearley and Jones 1998,  
1074 Table A3-2; Rubin and Ma 2020). Almost all primary chondrule pyroxenes are either low-Ca  
1075 varieties (orthoensatite, clinoenstatite, and pigeonite) or high-Ca varieties (diopside, augite, and  
1076 “fassaite”). Note that iron-rich pyroxenes, including those with greater than 50 mol % hedenbergite  
1077 [(Ca,Fe)SiO<sub>3</sub>; Sheng et al. 1991] and ferrosilite (FeSiO<sub>3</sub>; Rubin and Ma 2020) components, are  
1078 invariably of secondary origin. Indeed, many primary chondrule pyroxenes lie relatively close to  
1079 the MgSiO<sub>3</sub>—CaMgSi<sub>2</sub>O<sub>6</sub> join.

1080 Orthopyroxene is the most common low-Ca pyroxene in terrestrial igneous rocks; however,  
1081 orthoenstatite (officially named “enstatite” by the IMA) is relatively uncommon as a primary  
1082 chondrule phase compared to clinoenstatite and pigeonite, which are both monoclinic (*P*<sub>21/c</sub>)  
1083 pyroxenes with similar unit-cell dimensions. Clinoenstatite is defined by IMA protocols as end-  
1084 member MgSiO<sub>3</sub>, whereas pigeonite is ostensibly a more Ca- and Fe-rich variant, with up to 15  
1085 mol % CaSiO<sub>3</sub>. A continuous solid solution exists among clinoenstatite, clinoferrosilite (FeSiO<sub>3</sub>),

1086 and pigeonite. However, Ca-poor chondrule clinoenstatite is often found as phenocrysts  
1087 surrounded by a significantly more Ca-rich pigeonite layer. We therefore recognize *PC*  
1088 *clinoenstatite* and *PC pigeonite*, along with *PC orthoenstatite*, as distinct natural kinds in the Mg-  
1089 Fe-(Ca) pyroxene solid solution, each spanning a significant range of Mg-Fe-Ca phase space. Note,  
1090 however, that in the absence of coexisting phases with contrasting Ca contents, the distinction  
1091 between “clinoenstatite” and “pigeonite” may be arbitrary.

1092

1093 **Orthoenstatite [(Mg,Fe)SiO<sub>3</sub>]:** Orthorhombic enstatite (space group *Pbca*) is the stable low-  
1094 temperature form of (Mg,Fe)SiO<sub>3</sub>, and is thus the low-Ca pyroxene phase most commonly found  
1095 in gradually cooled terrestrial igneous rocks (e.g., Deer et al. 1966). Nevertheless, it is significantly  
1096 less common than clinoenstatite as a primary phase in rapidly cooled chondrules and may, in some  
1097 instances, point to a secondary process from thermal metamorphism and consequent inversion of  
1098 clinoenstatite.

1099 In ordinary and carbonaceous chondrites orthoenstatite occurs as rare phenocrysts in association  
1100 with clinoenstatite and forsterite (Ikeda 1982; Watanabe et al. 1986; Noguchi 1989; Jones 1996).  
1101 Orthoenstatite is also found as layers surrounding clinoenstatite in some chondrules in the Allende  
1102 CV3 carbonaceous chondrite (Noguchi 1989), while in EH3 enstatite chondrites orthoenstatite has  
1103 been reported as the dominant pyroxene in barred olivine-pyroxene chondrules (Zhang et al. 1996).

1104

1105 **Clinoenstatite [(Mg,Fe)SiO<sub>3</sub>]:** *PC clinoenstatite* is the most common pyroxene in  
1106 ferromagnesian chondrules, occurring prominently as phenocrysts in unequilibrated ordinary  
1107 chondrites. The widespread occurrence of this high-temperature polymorph of MgSiO<sub>3</sub>, rather

1108 than orthoenstatite, points to its formation from a melt at > 985 °C (Boyd and Schairer 1964), with  
1109 subsequent rapid cooling of chondrules. Examples from numerous meteorites show FeSiO<sub>3</sub>  
1110 contents ranging from <1 to ~35 mol % (Brearley and Jones 1998, see Figures 10, 14, 23, 24, 29,  
1111 33, 38, 41, 47, 49, 53, 55, 56, 58, 59, 62, 65, and 66; Table A3.2). Clinoenstatite is often  
1112 polysynthetically twinned (e.g., Müller et al. 1995) and is commonly encased in more calcic  
1113 pyroxenes, either augite or by a layer of pigeonite surrounded by augite (Noguchi 1989).

1114

1115 **Pigeonite [(Mg,Fe,Ca)SiO<sub>3</sub>]**: Pigeonite with 5- to 15-mol % CaSiO<sub>3</sub> component occurs in the  
1116 chondrules of type 3 ordinary chondrites, both as individual crystals and as a thin layer between  
1117 clinoenstatite cores and augitic mantles (Noguchi 1989). Pigeonite often displays exsolution  
1118 lamellae of calcic clinopyroxene (space group *C2/c*) or anti-phase domains (a consequence of high-  
1119 temperature inversion) – both of which may point to multiple heating and cooling events  
1120 (Ashworth and Barber 1977). In carbonaceous chondrites, low-Fe pigeonite (Fs<sub><02</sub>) also occurs in  
1121 close association with augite, for example as intergrowths in the Cochabamba CM2 chondrite  
1122 (Müller et al. 1979), or as an intermediate layer between a clinoenstatite core and augite  
1123 overgrowth in the Allende CV3 chondrite (Noguchi 1989). In addition, the plagioclase-olivine  
1124 inclusions of CV chondrites sometimes hold Fe-poor (Fs<sub><01</sub>), Al-rich (to several mol %) pigeonite  
1125 (Sheng et al. 1991a). Finally, EH3 enstatite chondrites hold a variety of pyroxenes, including  
1126 pigeonite (Kitamura et al. 1987; Ikeda 1989b), some of which hold greater than 10 mol % CaSiO<sub>3</sub>  
1127 component (Ikeda 1988b; Kitamura et al. 1988).

1128

1129 **High-Calcium Clinopyroxenes [(Ca,Mg,Fe)(Mg,Fe,Al,Ti<sup>3+</sup>)(Al,Ti<sup>4+</sup>,Si)SiO<sub>6</sub>]**

1130 Clinopyroxenes with  $\text{Ca} \sim (\text{Mg} + \text{Fe})$  are common primary phases in chondrules. The  
1131 nomenclature of these monoclinic pyroxenes (space group  $\text{C2}_1/\text{c}$ ) is complicated by the frequent  
1132 use of two approved IMA names, diopside ( $\text{CaMgSi}_2\text{O}_6$ ) and augite [ $(\text{Ca},\text{Mg},\text{Fe})_2\text{Si}_2\text{O}_6$ ], in  
1133 concert with unapproved or discredited terminology, including “fassaite,” “Al-Ti-diopside,” and  
1134 “aluminous diopside” (Morimoto et al. 1988; Sack and Ghiorso 2017; Rubin and Ma 2017, 2020;  
1135 see [ruff.info/ima](http://ruff.info/ima), accessed 7 April 2020). In extreme instances, clinopyroxene compositions may  
1136 approach such end-members as kushiroite ( $\text{CaAl}_2\text{SiO}_6$ ; Kimura et al. 2009), grossmanite  
1137 ( $\text{CaTi}^{3+}\text{AlSiO}_6$ ; Ma and Rossman 2009), or the as yet unnamed end-member ( $\text{CaMgTi}^{4+}\text{SiO}_6$ ), all  
1138 of which extend the continuous clinopyroxene compositional range to  
1139 [ $(\text{Ca},\text{Mg},\text{Fe})(\text{Mg},\text{Fe},\text{Al},\text{Ti}^{3+})(\text{Al},\text{Ti}^{4+},\text{Si})\text{SiO}_6$ ]. Specific instances of compositional extremes, for  
1140 example Al- and Ti-rich clinopyroxenes, reflect the idiosyncratic average compositions of their  
1141 host chondrules. However, inasmuch as these calcic clinopyroxenes all form in similar ways within  
1142 a molten droplet, we recognize only one kind of primary chondrule calcic clinopyroxene, *PC*  
1143 *augite*.

1144  
1145 **Augite [ $(\text{Ca},\text{Mg},\text{Fe})(\text{Mg},\text{Fe},\pm\text{Al},\pm\text{Ti}^{3+})(\pm\text{Al},\pm\text{Ti}^{4+},\text{Si})\text{SiO}_6$ ]:** *PC augite* occurs commonly in  
1146 chondrules in type 3 ordinary chondrites, carbonaceous chondrites, and enstatite chondrites, both  
1147 as phenocrysts and as overgrowths (< 20-micrometers thick) on clinoenstatite, at times with a thin  
1148 intermediate pigeonite layer. Augite also is found as exsolution lamellae in low-Ca pyroxene.  
1149 While compositions vary significantly, most *PC augite* have  $\text{CaSiO}_3$  from 30 to 45 mol % and  
1150  $\text{FeSiO}_3$  from ~0 to 15 mol % (Brearley and Jones 1998; see figures 10, 17, 23, 25, 29, 34, 38, 42,

1151 47, 49, 60, 65, and 67; Table A3.3). Examples of PC augite that are close to diopside in  
1152 composition (i.e., with  $\text{MgSiO}_3 > 35$  mol %,  $\text{CaSiO}_3 > 45$  mol %, and correspondingly low Fe,  
1153 Al, and Ti) have been reported by Noguchi (1989) as crystals ( $\text{Wo}_{48-50}$ ) in glass in a single  
1154 chondrule from the ALH-77003 CO chondrite. Additional reports of chondrule “fassaite” crystals  
1155 in glassy mesostasis with a wide range of compositions rich in Al and Ti have been reported from  
1156 Al-rich and Ca-Al-rich chondrules in type 3 ordinary chondrites (Bischoff and Keil 1984; Wang  
1157 et al. 2016). Al-Ti-rich clinopyroxenes are also recorded from low-Fe chondrules and plagioclase-  
1158 olivine inclusions in Allende and other CV3 meteorites (Noguchi 1989; Sheng et al. 1991a), as  
1159 well as in CR chondrites (Noguchi 1995).

1160

#### 1161 **Plagioclase Feldspar Group ( $\text{CaAl}_2\text{Si}_2\text{O}_8$ to $\text{NaAlSi}_3\text{O}_8$ )**

1162 Plagioclase feldspar is a common phase in typical ferro-magnesian chondrules of ordinary  
1163 chondrites, especially in devitrified mesostasis, where it may represent both a primary phase  
1164 formed on initial chondrule cooling and a secondary phase crystallized during subsequent  
1165 metamorphism in the parent body (Brearley and Jones 1998; Lewis and Jones 2016, 2019). This  
1166 continuum from primary to secondary feldspar is reflected as increases in the average size of  
1167 plagioclase crystallites, the volume ratio of mesostasis crystals to glass, and the degree of  
1168 plagioclase Al-Si disorder. The range of chondrule plagioclase compositions in ordinary  
1169 chondrites, though usually well within the anorthite field ( $\text{An}_{60-90}$ ; Ikeda 1982; Miúra and  
1170 Tomisaka 1984), occasionally extends to  $\text{An}_{02}$  within the albite field in unequilibrated ordinary  
1171 chondrites (Brearley and Jones 1998, see Table A3.5; Lewis and Jones 2019, and references

1172 therein). In addition, a near end-member albite occurrence is associated with silica in a single  
1173 chondrule (Fujimaki et al. 1981a, 1981b).

1174 Plagioclase-rich chondrules are found in some type 3 CO chondrites, in which primary calcic  
1175 plagioclase laths (An<sub>70-90</sub>) occur in association with augite and orthopyroxene (Greshake 1997;  
1176 Jones 1997; Brearley and Jones 1998). Plagioclase also plays a significant role in varied, less  
1177 common Al-(Ca)-rich chondrules in ordinary chondrites, in which calcic plagioclase occurs as a  
1178 fine-grained mineral in both the groundmass and mesostasis (Wang et al. 2016). Note, however,  
1179 that albitic plagioclase is not a primary phase in Na-Al-rich chondrules, in which Na-rich glass is  
1180 the dominant sodium phase.

1181 Plagioclase occurs occasionally as a primary phase in the chondrules of carbonaceous  
1182 chondrites. An<sub>>80</sub> is found as a primary phase in a small fraction of Allende (CV3) ferromagnesian  
1183 chondrules, at times in association with low-calcium pyroxenes (Simon and Haggerty 1980;  
1184 Noguchi 1989; Brearley and Jones 1998, see Table A3.5). CV chondrites also hold plagioclase-  
1185 olivine inclusions, in which calcic plagioclase (commonly An<sub>~95</sub>) and forsteritic olivine  
1186 phenocrysts are the dominant phases (Sheng et al. 1991a). Plagioclase (~An<sub>90</sub>) was also reported  
1187 in association with augite in a single silica-bearing chondrule from the Murchison CM chondrite  
1188 (Olsen 1983). In addition, plagioclase is not uncommon as a phase in the mesostasis of  
1189 carbonaceous chondrites (Murakami and Ikeda 1994; Ikeda and Kimura 1995). Plagioclase (An<sub>48-  
1190 88</sub>) has also been reported as a primary phase in enstatite chondrites, occurring as laths in  
1191 mesostasis (Ikeda 1988b, 1989b), as well as in Al-rich chondrules (Bischoff et al. 1985; Wang et  
1192 al. 2016).

1193 Most reports of primary plagioclase feldspar, especially in type I chondrules, lie in the calcium-  
1194 dominant field, if not close to anorthite ( $An_{>80}$ ). By contrast, most albitic plagioclase (and all K-  
1195 bearing feldspars) are described as secondary in origin (e.g., Ikeda 1989b; Rubin and Kallemeyn  
1196 1989, 1994; Schulze et al. 1994; Lewis and Jones 2016, 2019). We recognize two primary  
1197 chondrite feldspar group minerals. Most occurrences of primary chondrule plagioclase lie well  
1198 within the anorthite range, though a few outliers may display sodium content greater than calcium  
1199 as part of a continuous solid solution. We name all such phases as *PC anorthite*. In addition, the  
1200 common occurrences of Na-rich plagioclase ( $An_{02}$  to  $An_{32}$ ) in FeO-rich chondrules in the  
1201 unequilibrated Semarkona (LL3.00) chondrite (Lewis and Jones 2019), as well as the rare  
1202 occurrence of albite with silica reported by Fujimaki et al. (1981a), are designated *PC albite*.

1203  
1204 **Anorthite [(Ca,Na)(Al,Si)<sub>2</sub>Si<sub>2</sub>O<sub>8</sub>]:** *PC anorthite* is a common phase as phenocrysts or as  
1205 crystallites in mesostasis in both ordinary and carbonaceous chondrites.

1206  
1207 **Albite (NaAlSi<sub>3</sub>O<sub>8</sub>):** Fujimaki et al. (1981a, 1981b) report a rare occurrence of *PC albite*  
1208 ( $Ab_{>98}$ ) associated with silica and ferropseudobrookite in a single chondrule from the L3 ordinary  
1209 chondrite ALH77015.

1210  
1211 **Nepheline [Na<sub>3</sub>K(Al<sub>4</sub>Si<sub>4</sub>O<sub>16</sub>):** Most chondrules are too silica-rich to form feldspathoids as  
1212 stable primary phases. However, nepheline has been reported as both a primary and (more  
1213 commonly) secondary phase (Ikeda 1988b; Sheng et al. 1991a). *PC nepheline* is found as

1214 epitaxially-oriented intergrowths with anorthite in unequilibrated ordinary chondrites (Ikeda  
1215 1982), including in some plagioclase-rich chondrules (Jones 1997). It also occurs in association  
1216 with Na-bearing plagioclase in Al-Ca-Na-rich chondrules in ordinary chondrites (Brearley and  
1217 Jones 1998; Rubin and Ma 2020). Note, however, that some experts suggest that all nepheline  
1218 occurrences in chondrules are of secondary origin (R. Jones, personal communication, June 4,  
1219 2020).

1220

1221 **Sapphirine [Mg<sub>4</sub>(Mg<sub>3</sub>Al<sub>9</sub>)O<sub>4</sub>(Si<sub>3</sub>Al<sub>9</sub>O<sub>36</sub>):** *PC sapphirine* is one of several minor accessory  
1222 phases found as primary chondrule minerals only in plagioclase-olivine inclusions (POIs) from the  
1223 Allende CV carbonaceous chondrite (Sheng et al. 1991a). Sapphirine occurs as widely distributed  
1224 5- x 25-micrometer crystal prisms in a Na- and Cl-rich mesostasis. Sapphirine from POIs  
1225 incorporates excess Mg + Si at the expense of Al, as well as significant Cr and Ti, in accord with  
1226 experimental studies of sapphirine crystallization from a melt (Sheng et al. 1991b).

1227

1228 **Merrihueite [(K,Na)<sub>2</sub>(Fe,Mg)<sub>5</sub>Si<sub>12</sub>O<sub>30</sub>] and Roedderite [(Na,K)<sub>2</sub>Mg<sub>5</sub>Si<sub>12</sub>O<sub>30</sub>]:** Silica-rich  
1229 chondrules in several unequilibrated ordinary and enstatite chondrites have been reported to hold  
1230 minerals of the merrihueite-roedderite solid solution series (Dodd et al. 1965; Rambaldi et al. 1986;  
1231 Krot and Wasson 1994). Wood and Holmberg (1994) proposed that these unusual silicates formed  
1232 by the reaction of silica-rich phases with alkali-rich nebular gas. The compositions of these  
1233 occurrences span the range from  $0.1 < \text{Na}/(\text{Na}+\text{K}) < 0.8$ , and with  $0 < \text{Fe}/(\text{Fe}+\text{Mg}) < 0.8$  (Wood  
1234 and Holmberg 1994). IMA protocols could thus assign as many as four different mineral names to  
1235 the Na-Mg (roedderite), K-Fe (merrihueite), Na-Fe, and K-Mg compositional variants, all of which  
1236 are observed in these meteorites. However, these minerals form a continuous solid-solution of

1237 phases formed by the same primary process, and thus represent a single natural kind in our  
1238 evolutionary system. Because most examples fall within the roedderite field, we assign the name  
1239 *PC roedderite* to these examples. Note, however, that some experts ascribe all such occurrences  
1240 to secondary process (R. Jones, personal communications, June 4, 2020).

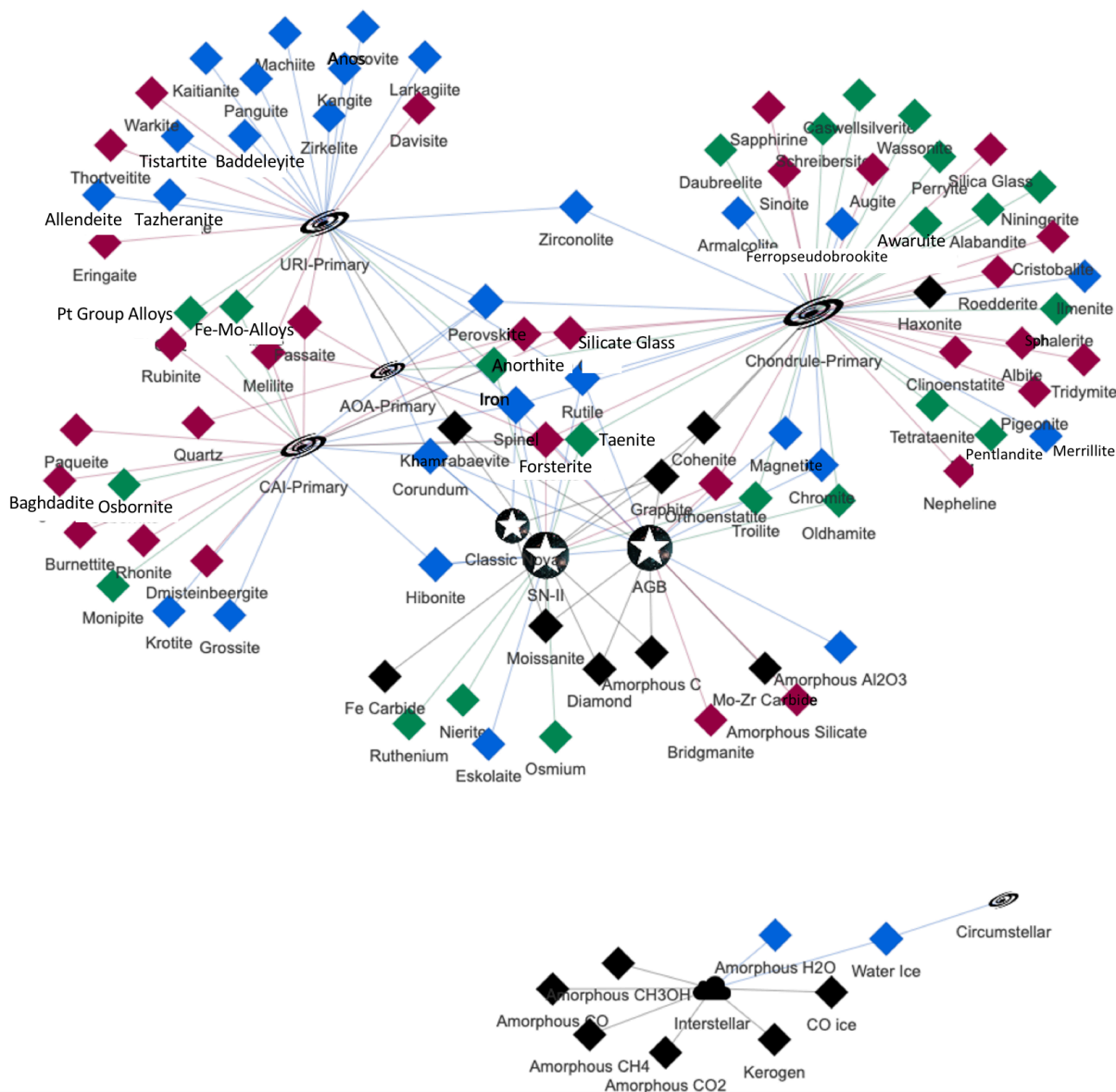
1241  
1242 **Silicate Glass (Ca,Mg,Al,Si,O):** *PC silicate glass* is an important constituent of many chondrules.  
1243 In extreme cases, chondrules can be >99 vol % silicate glass, with a significant population having  
1244 55 to 85 vol % glass (Krot and Rubin 1994). Silicate glass as a primary phase in chondrules spans  
1245 a wide range of compositions (Brealey and Jones 1998, and references therein). As with other  
1246 common silicate phases in chondrules, cluster analysis of large databases of silicate glass might  
1247 reveal distinctive natural kinds that could warrant a splitting of PC silicate glass.

1248 **NETWORK GRAPH OF STELLAR AND PRIMARY NEBULAR MINERALS**

1249 The evolutionary system of mineralogy can be illustrated using bipartite mineral network  
1250 graphs, which display relationships among mineral phases and their attributes, in this instance their  
1251 paragenetic modes and chemical groups (Morrison et al. 2017, 2020; Hazen et al. 2019b; Hazen  
1252 and Morrison 2020; Morrison and Hazen 2020). **Figure 2** displays a bipartite force-directed  
1253 network graph of primary stellar, interstellar, and nebular minerals formed prior to ~4561 Ma, in  
1254 which 96 different phases, including 10 amorphous condensed phases, are represented by  
1255 diamond-shaped nodes. Each of these mineral nodes is linked to one or more nodes representing a  
1256 paragenetic mode of formation. Three different star-shaped nodes (AGB, SN-II, and CNova)  
1257 represent stellar environments that impart distinctive isotopic signatures to minerals. A cloud-  
1258 shaped node indicates interstellar dense molecular clouds (DMC), whereas five flattened disk icons  
1259 represent different primary mineral-forming nebular environments (Circumstellar, CAI, AOA,  
1260 URI, and PC).

1261 Information about mineral compositions is indicated by the color of diamond-shaped mineral  
1262 nodes: black (C-bearing), green (lacking C or O), blue (contains O, but not C or Si), and red  
1263 (contains Si and O). The sizes of the star-, cloud-, and disk-shaped symbols indicate the numbers  
1264 of different minerals to which they are associated.

1265 Note that while most mineral nodes are members of a well-connected network, 8 low-  
1266 temperature interstellar and nebular condensed molecular phases, all formed at  $T < 100$  K, form a  
1267 separate network from 88 high-temperature stellar and nebular condensates ( $T \gg 300$  K). In future  
1268 contributions to this series, which will consider phases formed at intermediate temperatures in  
1269 planetary surface environments, new links will occur between these two mineral-forming  
1270 environments.



1271  
 1272 Figure 2. Bipartite force-directed network graph (Morrison et al. 2017) of primary stellar, interstellar, and  
 1273 nebular minerals linked to their modes of paragenesis. Diamond-shaped nodes represent condensed  
 1274 crystalline and amorphous phases [black (C-bearing), green (not C or O), blue (contains O, but not C or Si),  
 1275 and red (contains Si + O)]. Star-shaped nodes represent three types of host stars— asymptotic giant branch  
 1276 stars (AGB), Type II supernovae (SN-II), and classical novae (CNova); the cloud-shaped node represents  
 1277 dense molecular clouds (DMC); and five disk-shaped nodes indicate circumstellar environments, CAI,  
 1278 AOA, URI, and PC minerals. The sizes of paragenetic mode nodes correspond to the numbers of links to  
 1279 mineral nodes. Note that 8 low-temperature phases of the interstellar medium are not linked to 88 high-  
 1280 temperature primary phases of stellar and nebular environments.  
 1281

1282 This bipartite network of mineral evolution is a visual representation of all confirmed stellar,  
1283 interstellar, and primary nebular minerals described in Parts I, II, and III of the evolutionary system  
1284 of mineralogy. Of the 96 species in Figure 2, spinel is the most ubiquitous, occurring in 7 of the 9  
1285 different paragenetic modes considered thus far; consequently, spinel assumes a highly centralized  
1286 position in this network graph. Iron, corundum, and forsterite, each linked to 5 modes of formation,  
1287 were the next most widespread minerals prior to the formation of planetesimals. On the other hand,  
1288 more than two-thirds of these minerals – 68 of 96 species – are thus far only recorded from a single  
1289 paragenetic mode.

1290 Of the 43 primary chondrule mineral species considered in Part III, 27 occur here for the first  
1291 time. This significant increase in mineral diversity associated with chondrule formation in part  
1292 reflects chemical fractionation within the solar nebula and the consequent increasing importance  
1293 of such key elements as Na, K, Cr, Mn, and S, all of which are moderately volatile and thus were  
1294 incorporated into solid phases as the nebular disk cooled.

1295 The topology of this network graph reflects important aspects of mineral evolution. Nodes for  
1296 a few of the commonest minerals (fewer than 20 species) are centrally located; those diamond-  
1297 shaped icons are surrounded by several nodes for paragenetic modes. But the majority of minerals  
1298 are represented by starbursts of nodes that decorate the periphery of the graph, each diamond  
1299 representing a species that at this stage of mineral evolution is only linked to a single paragenetic  
1300 mode. In future contributions, as we add new paragenetic modes, many new mineral species  
1301 formed by different processes at new combinations of temperature, pressure, and composition will  
1302 enhance this pattern. New starbursts will appear, while a greater number of minerals will have  
1303 multiple links to paragenetic modes and thus shift to the network's crowded interior. In this way,

1304 as new modes of mineral paragenesis are considered, this information-rich graphical approach will  
1305 provide a dynamic, interactive view of the entire sweep of mineral evolution.

1306

## 1307 **IMPLICATIONS**

1308 Part III of the evolutionary system of mineralogy represents a vital transition between the  
1309 genesis of dust and gas in stars and the solid condensed phases that would become planets and  
1310 moons. Dynamic electromagnetic, shock front, and impact processes provided the principal high-  
1311 temperature sources required to form igneous droplets – the chondrules that accreted to become  
1312 the first macroscopic rocks of our solar system. However, soon thereafter gravity took control as  
1313 planetesimals began to form and collide and new suites of minerals emerged.

1314 The catalog of 43 phases is misleading in at least two ways regarding the diversity and  
1315 distribution of primary chondrule minerals. First, the primary origins of 8 of these phases  
1316 (awaruite, graphite, haxonite, pentlandite, magnetite, merrillite, nepheline, and roedderite) have  
1317 been questioned. For each of these minerals, some experts assert that all chondrule occurrences  
1318 formed by secondary processes. Of the remaining 35 minerals, an additional 15 (sinoite, perryite,  
1319 alabandite, caswellsilverite, daubréelite, niningerite, oldhamite, sphalerite, wassonite, rutile,  
1320 armacolite, ferropseudobrookite, perovskite, zirconolite, and sapphirine) are extremely rare and of  
1321 restricted occurrence, while 7 more (tetrataenite, cohenite, schreibersite, magnetite, ilmenite,  
1322 cristobalite, and silica glass) are more widespread but volumetrically minor. Thus, only a dozen  
1323 phases probably account for more than 99 vol. % of primary chondrule mineralogy. This  
1324 distribution reflects the mineralogical parsimony of high-temperature assemblages of the nebula's  
1325 major rock-forming elements – in essence, a nebular manifestation of J. Willard Gibbs' "phase  
1326 rule" (Gibbs 1876-1878). We will discover a similar restricted mineral diversity among the  
1327 primary phases that arise from planetesimal differentiation into mantle and core (the subject of  
1328 Part IVA). However, a dramatic rise in mineral diversity occurred as a consequence of pervasive  
1329 alteration of these equilibrium phases – reworking by impact processes (Part IVB), as well as

1330 aqueous, hydrothermal, and metamorphic alteration that resulted in hundreds of new minerals  
1331 before the assembly of today's planets and moons (Part V).

1332 This study of primary meteorite phases reveals an intriguing sociological aspect to the science  
1333 of meteorite mineralogy. The bold outlines of primary chondrule mineralogy, on which our  
1334 contribution is grounded, were made in the 1960s and 1970s. Thousands of publications expanded  
1335 and refined that knowledge base in the 1980s and 1990s. By 1998, Adrian Brearley and Rhian  
1336 Jones could summarize chondrite mineralogy and petrology in a 398-page treatise with more than  
1337 1000 references by almost as many coauthors. Our review of chondrule mineralogy would not  
1338 have been possible without that immense body of research and the summary of Brearley and Jones  
1339 (1998).

1340 Mineralogical fashion, and funding, has changed. While many dedicated workers continue to  
1341 probe these most ancient rocks and make important discoveries, the study of meteorite mineralogy  
1342 and petrology appears to be less of a priority than in decades past. New discoveries, particularly  
1343 related to scarce isotopes and to submicron-scale phases discovered by microbeam techniques, are  
1344 breathtaking. Nevertheless, one comes away from this vast literature feeling that much more  
1345 remains to be discovered about chondrites and their ancient mineralogy. Thousands of meteorites  
1346 have been collected, but remain to be investigated. Numerous trace elements and stable isotope  
1347 systems are yet to be explored. Undiscovered nanoscale minerals and poorly-characterized non-  
1348 crystalline solid phases beckon. We suspect that another golden age of meteorite mineralogy,  
1349 perhaps including the promise of data-driven discovery using large and growing planetary  
1350 materials data resources, lies before us.

1351

1352 **ACKNOWLEDGMENTS**

1353 We are deeply grateful to reviewers Rhian Jones and Alan Rubin, as well as Associate Editor  
1354 Steven Simon, for their meticulous, thoughtful, and constructive reviews of this manuscript, which  
1355 was substantially improved as a consequence. We are also grateful to Denton Ebel and Alan Rubin,  
1356 who contributed invaluable detailed reviews of an earlier version of this contribution. Rubin and  
1357 Chi Ma provided access to important work in press, including a draft of their forthcoming book,  
1358 *Meteorite Mineralogy*. We are grateful to Conel O.M'D. Alexander, Asmaa Boujibar, Carol  
1359 Cleland, Robert T. Downs, Olivier Gagné, Sergey Krivovichev, Glenn MacPherson, Larry Nittler,  
1360 Michael Walter, and Shuang Zhang for thoughtful discussions and comments.

1361 This publication is a contribution to the Deep Carbon Observatory, the 4D Initiative, and the  
1362 Deep-time Digital Earth (DDE) program. Studies of mineral evolution and mineral ecology have  
1363 been supported by the Deep Carbon Observatory, the Alfred P. Sloan Foundation, the W. M. Keck  
1364 Foundation, the John Templeton Foundation, the NASA Astrobiology Institute ENIGMA team, a  
1365 private foundation, and the Carnegie Institution for Science. Any opinions, findings, or  
1366 recommendations expressed herein are those of the authors and do not necessarily reflect the views  
1367 of the National Aeronautics and Space Administration.

1368

## REFERENCES

- 1369
- 1370 Abel, T., Bryan, G.L., and Norman, M.L. (2002) The formation of the first stars in the universe.  
1371 Science, 295, 93-98.
- 1372 Abreu, N.M., and Brearley, A.J. (2011) Deciphering the nebular and asteroidal record of silicates  
1373 and organic material in matrix of the reduced CV3 chondrite Vigarano. Meteoritics & Planetary  
1374 Science, 46, 252-274.
- 1375 Afiattalab, F., and Wasson, J.T. (1980) Composition of the metal phases in ordinary chondrites:  
1376 Implications regarding classification and metamorphism. Geochimica et Cosmochimica Acta,  
1377 44, 431-446.
- 1378 Akridge, D.G., and Sears, D.W.G. (1999) The gravitational and aerodynamic sorting of meteoritic  
1379 chondrules and metal: Experimental results with implications for chondritic meteorites. Journal  
1380 of Geophysical Research, 104, 11853–11864.
- 1381 Alexander, C.O.M'D., and Ebel, D.S. (2012) Questions, questions: Can the contradictions between  
1382 the petrologic, isotopic, thermodynamic, and astrophysical constraints on chondrule formation  
1383 be resolved? Meteoritics & planetary Science, 47, 1157-1175.
- 1384 Alexander, C.O.M'D., Swan, P., and Prombo, C.A. (1994) Occurrence and implications of silicon  
1385 nitride in enstatite chondrites. Meteoritics, 29, 79-85.
- 1386 Alexander, C.M.O'D., Grossman, J.N., Ebel, D.S., and Ciesla, F.J. (2008) The formation  
1387 conditions of chondrules and chondrites. Science, 320, 1617–1619.
- 1388 Alwmark, C., Schmitz, B., Holm, S., Marone, F., and Stampanoni, M. (2011) A 3-D study of  
1389 mineral inclusions in chromite from ordinary chondrites using synchrotron radiation X-ray  
1390 tomographic microscopy—Method and application. Meteoritics & Planetary Science, 46, 1071-  
1391 1081.

- 1392 Amelin, Y., and Krot, A.N. (2007) Pb isotopic ages of the Allende chondrules. *Meteoritics &*  
1393 *Planetary Science*, 42, 1321-1335.
- 1394 Amelin, Y., Krot, A.N., Hutcheon, I.D., and Ulyanov, A.A. (2002) Lead isotopic ages of  
1395 chondrules and calcium–aluminum-rich inclusions. *Science*, 297, 1678–1683.
- 1396 Amelin, Y., Kaltenbach, A., Iizuka, T., Stirling, C.H., Ireland, T.R., Petaev, M., and Jacobsen, S.B.  
1397 (2010) U–Pb chronology of the Solar System’s oldest solids with variable  $^{238}\text{U}/^{235}\text{U}$ . *Earth and*  
1398 *Planetary Science Letters*, 300, 343–350.
- 1399 Ashworth, J.R., and Barber, D.J. (1977) Electron microscopy of some stony meteorites.  
1400 *Philosophical Transactions of the Royal Society of London*, A286, 493-506.
- 1401 Asphaug, E., Jutzi, M., and Movshovitz, N. (2011) Chondrule formation during planetesimal  
1402 accretion. *Earth and Planetary Science Letters*, 308, 369-379.
- 1403 Avril, C., Malavergne, V., Caracas, R., Zanda, B., Reynard, B., Charon, E., Bobocioiu, E., Brunet,  
1404 F., Borensztajn, S., Pont, S., Tarrida, M., and Guyot, F. (2013) Raman spectroscopic properties  
1405 and Raman identification of CaS-MgS-MnS-FeS-Cr<sub>2</sub>FeS<sub>4</sub> sulfides in meteorites and reduced  
1406 sulfur-rich systems. *Meteoritics & Planetary Science*, 48, 1415-1426.
- 1407 Baecker, B., Rubin, A.E., and Wasson, J.T. (2017) Secondary melting events in Semarkona  
1408 chondrules revealed by compositional zoning in low-Ca pyroxene. *Geochimica et*  
1409 *Cosmochimica Acta*, 211, 256-279.
- 1410 Barth, M.I.F., Harries, D., Langenhorst, F., and Hoppe, P. (2018) Sulfide-oxide assemblages in  
1411 Acfer 094 – Clues to nebular metal-gas interactions. *Meteoritics & Planetary Science*, 53, 187-  
1412 203.

- 1413 Bell, K.R., Cassen, P.M., Wasson, J.T., and Woolum, D.S. (2000) The FU Orionis phenomenon  
1414 and solar nebula material. In V. Mannings, A.P. Boss, and S.S. Russell, Eds., *Protostars and*  
1415 *Planets IV*, pp. 897-926. University of Arizona Press.
- 1416 Berg, T., Maul, J., Schönense, G., Marosits, E., Hoppe, P., Ott, U., and Palme, H. (2009) Direct  
1417 evidence for condensation in the early solar system and implications for nebular cooling rates.  
1418 *The Astrophysical Journal*, 702, L172-L176.
- 1419 Bertout, C. (1989) T Tauri stars—wild as dust. *Annual Reviews of Astronomy and*  
1420 *Astrophysics*, 27, 351-395.
- 1421 Bertulani, C.A. (2013) *Nuclei in the Cosmos*. World Scientific.
- 1422 Bevan, A.W.R., and Axon, H.J. (1980) Metallography and thermal history of the Tieschitz  
1423 unequilibrated meteorite – metallic chondrules and the origin of polycrystalline taenite. *Earth*  
1424 *and Planetary Science Letters*, 47, 353-360.
- 1425 Bigolski, J.N., Weisberg, M.K., Connolly, H.C. Jr., and Ebel, D.S. (2016) Microchondrules in  
1426 three unequilibrated ordinary chondrites. *Meteoritics & Planetary Science*, 51, 235-260.
- 1427 Bischoff, A., and Keil, K. (1983) Ca-Al-rich chondrules in ordinary chondrites. *Nature*, 303, 588-  
1428 592.
- 1429 Bischoff, A., and Keil, K. (1984) Al-rich objects in ordinary chondrites: Related origin of  
1430 carbonaceous and ordinary chondrites and their constituents. *Geochimica et Cosmochimica*  
1431 *Acta*, 48, 693-709.
- 1432 Bischoff, A., Keil, K., and Stöffler, D. (1985) Perovskite-hibonite-spinel-bearing inclusions and  
1433 Al-rich chondrules and fragments in enstatite chondrites. *Chemie der Erde*, 44, 97-106.
- 1434 Bischoff, A., Wurm, G., Chaussidon, M., Horstmann, M., Metzler, K., Weyrauch, M., and  
1435 Weinauer, J. (2017) The Allende multicomponent chondrule (ACC) – Chondrule formation in

- 1436 a local super-dense region of the early solar system. *Meteoritics & Planetary Science*, 52, 906-  
1437 924.
- 1438 Bizzarro, M., Connelly, J.N., and Krot, A.N. (2017) Chondrules—Ubiquitous chondritic solids  
1439 tracking the evolution of the solar protoplanetary disk. In *Formation, evolution, and dynamics*  
1440 *of young solar systems. Astrophysics and Space Science Library. Cham, Switzerland: Springer*  
1441 *International Publishing AG. pp. 161–195.*
- 1442 Bollard, J., Connelly, J.N., and Bizzarro, M. (2015) Pb-Pb dating of individual chondrules from  
1443 the CBa chondrite Gujba: Assessment of the impact plume formation model. *Meteoritics &*  
1444 *Planetary Science*, 50, 1197-1216.
- 1445 Bollard, J., Connelly, J.N., Whitehouse, M.J., Pringle, E.A., Bonal, L., Jørgensen, J.K., Nordlund,  
1446 A., Moynier, F., and Bizzarro, M. (2017) Early formation of planetary building blocks inferred  
1447 from Pb isotopic ages of chondrules. *Science Advances*, 3:e1700407.
- 1448 Bond, H.E., Nelan, E.P., VandenBerg, D.A., Schaefer, G.H., and Harmer, D. (2013) HD 140283:  
1449 A star in the solar neighborhood that formed shortly after the Big Bang. *The Astrophysical*  
1450 *Journal*, 765, L12 (5 pp).
- 1451 Boss, A.P. (1996) A concise guide to chondrule formation models. In R.H. Hewins, R.H. Jones  
1452 and E.R.D. Scott, Eds., *Chondrules and the Protoplanetary Disk*, pp. 257-264. Cambridge  
1453 University Press.
- 1454 Boss, A.P., and Durisen, R.H. (2005) Sources of shock waves in the protoplanetary disk.  
1455 *Astronomical Society of the Pacific Conference Series*, 341, 821-838.
- 1456 Bouvier, A., and Wadhwa, M. (2010) The age of the Solar System redefined by the oldest Pb-Pb  
1457 age of a meteoritic inclusion. *Nature Geoscience*, 3, 637-641.

- 1458 Bowman, J.D., Rogers, A.E.E., Monsalve, R.A., Mozdzen, T.J., and Mahesh, N. (2018) An  
1459 absorption profile centred at 78 megahertz in the sky-averaged spectrum. *Nature*, 555, 67-70.
- 1460 Boyd, F.R., and Schairer, J.F. (1964) The system  $\text{MgSiO}_3\text{-CaMgSi}_2\text{O}_6$ . *Journal of Petrology*, 5,  
1461 275-309.
- 1462 Bradley, J.P. (1994a) Nanometer-scale mineralogy and petrography of fine-grained aggregates in  
1463 anhydrous interplanetary dust particles. *Geochimica et Cosmochimica Acta*, 58, 2123-2134.
- 1464 Bradley, J.P. (1994b) Chemically anomalous, pre-accretionally irradiated grains in interplanetary  
1465 dust from comets. *Science*, 265, 925-929.
- 1466 Brearley, A.J. (2014) Nebular versus parent body processing. *Treatise on Geochemistry*, Second  
1467 Edition, 1, 247-268.
- 1468 Brearley, A.J., and Jones, R.H. (1998) Chondritic meteorites. *Reviews in Mineralogy*, 36, 3.01-  
1469 3.398.
- 1470 Bridges, J.C., Franchi, L.A., Hutchison, R., Morse, A.D., Long, J.V.P., and Pillinger, C.T. (1995)  
1471 Cristobalite- and tridymite-bearing clasts in Parnallee (LL3) and Farmington (L5). *Meteoritics*,  
1472 30, 715-727.
- 1473 Brigham, C.A., Yabuki, H., Ouyang, Z., Murrell, M.T., El Goresy, A., and Burnett, D.S. (1986)  
1474 Silica-bearing chondrules and clasts in ordinary chondrites. *Geochimica et Cosmochimica*  
1475 *Acta*, 50, 1655-1666.
- 1476 Britvin, S.N., Kolomensky, V.D., Boldyreva, M.M., Bogdanova, A.N., Kretser, Y.L., Boldyreva,  
1477 O.N., and Rudashesky, N.S. (1999) Nickelphosphide  $(\text{Ni,Fe})_3\text{P}$ , the nickel analog of  
1478 schreibersite. *Zapiski Vserossijskogo Mineralogicheskogo Obshchestva*, 128, 64-72.
- 1479 Buchwald, V.F. (1975) *Handbook of Iron Meteorites*. University of California Press.

- 1480 Budde, G., Kleine, T., Kruijer, T.S., Burkhardt, C., and Metzler, K. (2015) Tungsten isotopic  
1481 constraints on the age and origin of chondrules. Proceedings of the National Academy of  
1482 Sciences USA, 113, 2886-2891.
- 1483 Budde, G., Burkhardt, C., Brennecka, G.A., Fischer-Gödde, M., Kruijer, T.S., and Kleine, T.  
1484 (2016) Molybdenum isotopic complementarity of chondrules and matrix and the dichotomy of  
1485 carbonaceous and noncarbonaceous meteorites. Earth and Planetary Science Letters, 454, 293-  
1486 303.
- 1487 Bullock, E.M., MacPherson, G.J., Nagashima, K., Krot, A.N., Petaev, M.I., Jacobsen, S.B., and  
1488 Ulyanov, A.A. (2012) Forsterite-bearing Type B refractory inclusions from CV3 chondrites:  
1489 From aggregates to volatilized melt droplets. Meteoritics & Planetary Science, 47, 2128–2147.
- 1490 Bunch, T.E., Keil, K., and Snetsinger, K.G. (1967) Chromite compositions in relation to chemistry  
1491 and texture of ordinary chondrites. Geochimica et Cosmochimica Acta, 31, 1568-1582.
- 1492 Burbidge, E.M., Burbidge, G.R., Fowler, W.A., and Hoyle, F. (1957) Synthesis of the elements in  
1493 stars. Review of Modern Physics, 29, 547-650.
- 1494 Burke, E.A.J. (2006) The end of CNMMN and CCM—Long live the CNMNC! Elements, 2, 388.
- 1495 Burkhardt, C., Kleine, T., Oberli, F., Pack, A., Bourdon, B., and Wieler, R. (2011) Molybdenum  
1496 isotopic anomalies in meteorites: Constraints on solar nebula evolution and the origin of the  
1497 Earth. Earth and Planetary Science Letters, 312, 390-400.
- 1498 Burkhardt, C., Dauphas, N., Hans, U., Bourdon, B., and Kleine, T. (2019) Elemental and isotopic  
1499 variability in solar system materials by mixing and processing of primordial disk reservoirs.  
1500 Geochimica et Cosmochimica Acta, 261, 145-170.
- 1501 Buseck, P.R., and Holdsworth, E.F. (1972) Mineralogy and petrology of the Yilmia enstatite  
1502 chondrite. Meteoritics, 7, 429-447.

- 1503 Cameron, A.G.W. (1957) Nuclear reactions in stars and nucleogenesis. Publications of the  
1504 Astronomical Society of the Pacific, 69, 201-222.
- 1505 Campbell, A.J., and Humayun, M. (2004) Formation of metal in the CH chondrites ALH 85085  
1506 and PCA 91467. *Geochimica et Cosmochimica Acta*, 68, 3409-3422.
- 1507 Campbell, A.J., Humayun, M., and Weisberg, M.K. (2002) Siderophile element constraints on the  
1508 formation of metal in the metal-rich chondrites Bencubbin, Weatherford, and Gujba.  
1509 *Geochimica et Cosmochimica Acta*, 66, 647-660.
- 1510 Campbell, A.J., Humayun, M., and Weisberg, M.K. (2005a) Compositions of unzoned and zoned  
1511 metal in the CBb chondrites HH 237 and QUE 94627. *Meteoritics & Planetary Science*, 40,  
1512 1131-1148.
- 1513 Campbell, A.J., Zanda, B., Perron, C., Meibom, A., and Petaev, M.I. (2005b) Origin and thermal  
1514 history of Fe-Ni metal in primitive chondrites. *Astronomical Society of the Pacific Conference  
1515 Series*, 341, 407-431.
- 1516 Chambers, J.E. (2004) Planetary accretion in the early solar system. *Earth and Planetary Science  
1517 Letters*, 223, 241-252.
- 1518 Charles, C.R.J., Robin, P.-Y.F., Davis, D.W., and McCausland, P.J.A. (2018) Shapes of  
1519 chondrules determined from the petrofabric of the CR2 chondrite NWA 801. *Meteoritics &  
1520 Planetary Science*, 53, 935-951.
- 1521 Chaumard, N., Humayun, M., Zanda, B., and Hewins, R.H. (2018) Cooling rates of type I  
1522 chondrules from Renazzo: Implications for chondrule formation. *Meteoritics & Planetary  
1523 Science*, 53, 984-1005.
- 1524 Chiang, E., and Youdin, A.N. (2010) Forming planetesimals in solar and extrasolar nebulae.  
1525 *Annual Review of Earth and Planetary Sciences*, 38, 493-522.

- 1526 Clarke, R.S. Jr., and Scott, E.R.D. (1980) Tetrataenite - ordered FeNi, a new mineral in meteorites.  
1527 American Mineralogist, 65, 624-630.
- 1528 Cody, G.D., Heying, E., Alexander, C.M.O'D., Nittler, R.R., Kilcoyne, A.L.D., Sandford, S.A.,  
1529 and Stroud, R.M. (2011) Establishing a molecular relationship between chondritic and  
1530 cometary organic solids. Proceedings of the National Academy of Science USA, 108, 19171-  
1531 19176.
- 1532 Cohen, R.E., Kornacki, A.S., and Wood, J.A. (1983) Mineralogy and petrology of chondrules and  
1533 inclusions in the Mokoia CV3 chondrites. Geochimica et Cosmochimica Acta, 47, 1739-1757.
- 1534 Connelly, J.N., and Bizzarro, M. (2009) Pb-Pb dating of chondrules from CV chondrules by  
1535 progressive dissolution. Chemical Geology, 259, 143-151.
- 1536 Connelly, J.N., and Bizzarro, M. (2018) The absolute Pb-Pb isotope ages of chondrules: Insights  
1537 into the dynamics of the solar protoplanetary disk. In S.A. Russell, H.C. Connolly Jr., and A.N.  
1538 Krot, Eds., Chondrules: Records of Protoplanetary Disk Processes, pp.300-323. Cambridge  
1539 University Press.
- 1540 Connelly, J.N., Amelin, Y., Krot, A.N., and Bizzarro, M. (2008) Chronology of the solar system's  
1541 oldest solids. The Astrophysical Journal, 67, L121-L124.
- 1542 Connelly, J.N., Bizzarro, M., Krot, A.N., Nordlund, Å., Wielandt, D., and Ivanova, M.A. (2012)  
1543 The absolute chronology and thermal processing of solids in the solar protoplanetary disk.  
1544 Science, 338, 651-655.
- 1545 Connolly, H.C. Jr., and Desch, S.J. (2004) On the origin of the "kleine Kugelchen" called  
1546 chondrules. Chemie der Erde – Geochemistry, 64, 95-125.
- 1547 Connolly, H.C. Jr., and Jones, R.H. (2016) Chondrules: The canonical and noncanonical views.  
1548 Journal of Geophysical Research: Planets, 121, 1885-1899.

- 1549 Connolly, H.C. Jr., Jones, B.D., and Hewins, R.H. (1998) The flash melting of chondrules: An  
1550 experimental investigation into melting history and physical nature of chondrule precursors.  
1551 *Geochimica et Cosmochimica Acta*, 62, 2725-2735.
- 1552 Crozaz, G., and Lundberg, L. (1995) The origin of oldhamite in unequilibrated enstatite chondrites.  
1553 *Geochimica et Cosmochimica Acta*, 59, 3817-3831.
- 1554 Cullivier, P., Chaumard, N., Leroux, H., Zanda, B., Hewins, R.H., Jacob, D., and Devouard, B.  
1555 (2018) A TEM study of exsolution in Ca-rich pyroxenes from the Paris and Renazzo chondrites:  
1556 Determination of type I chondrule cooling rates. *Meteoritics & Planetary Science*, 53, 482-492.
- 1557 Cuzzi, J.N., and Alexander, C.M.O'D. (2006) Chondrule formation in particle-rich nebular regions  
1558 at least hundreds of kilometers across. *Nature*, 441, 483-485.
- 1559 Cuzzi, J.N., Hogan, R.C., Paque, J.M., and Dobrovolskis, A.R. (2001) Size-selective concentration  
1560 of chondrules and other small particles in protoplanetary nebula turbulence. *The Astrophysical*  
1561 *Journal*, 546, 496-508.
- 1562 D'Alessio, P., Calvet, N., and Woolum, D.S. (2005) Thermal structure of protoplanetary disks.  
1563 *Astronomical Society of the Pacific Conference Series*, 341, 353-372.
- 1564 Davis, A.M. (2011) Stardust in meteorites. *Proceedings of the National Academy of Sciences*  
1565 *USA*, 108, 19142-19146.
- 1566 Davis, A.M., and Richter, F.M. (2014) Condensation and evaporation of solar system materials.  
1567 In A.M. Davis, H.D. Holland, and K.K. Turekian, Eds., *Treatise on Geochemistry*, Vol. 1:  
1568 *Meteorites, Comets, and Planets*, Second Edition, pp.335-360. Elsevier-Pergamon.
- 1569 Davis, A.M., Hashimoto, A., Clayton, R.N., and Mayeda, T.K. (1990) Isotope mass fractionation  
1570 during evaporation of forsterite (Mg<sub>2</sub>SiO<sub>4</sub>). *Nature*, 347, 655-658.
- 1571 Davy, R., Whitehead, S.G., and Pitt, G. (1978) The Adelaide meteorite. *Meteoritics*, 13, 121-140.

- 1572 Deer, W.A., Howie, R.A., and Zussman, J. (1966) An Introduction to the Rock-Forming Minerals.  
1573 John Wiley and Sons.
- 1574 Desch S.J., and Connolly H.C. Jr. (2002) A model for the thermal processing of particles in solar  
1575 nebula shocks: Application to the cooling rates of chondrules. *Meteoritics & Planetary Science*,  
1576 37, 183–207.
- 1577 Desch, S.J., and Cuzzi, J.N. (2000) The generation of lightning in the solar nebula. *Icarus*, 143,  
1578 87-105.
- 1579 Desch, S.J., Morris, M.A., and Connolly, H.C. Jr. (2010) A critical examination of the x-wind  
1580 model chondrule and calcium-rich, aluminum-rich inclusion formation and radionuclide  
1581 production. *The Astrophysical Journal*, 725, 692-711.
- 1582 Desch, S.J., Morris, M.A., Connolly, H.C. Jr., and Boss, A.P. (2012) The importance of  
1583 experiments: Constraints on chondrule formation models. *Meteoritics & Planetary Science*, 47,  
1584 1139-1156.
- 1585 Desch, S.J., Kalyaan, A., and Alexander, C.M.O'D. (2018) The effect of Jupiter's formation on the  
1586 distribution of refractory elements and inclusions in meteorites. *The Astrophysical Journal*  
1587 Supplement Series, 238, 11 (31 pp).
- 1588 Desnoyers, C. (1980) The Niger (I) carbonaceous chondrite and implications for the origin of  
1589 aggregates and isolated olivine grains in C2 chondrite. *Earth and Planetary Science Letters*, 47,  
1590 223-234.
- 1591 Dobriça, E., and Brearley, A.J. (2016) Microchondrules in two unequilibrated ordinary chondrites:  
1592 Evidence for formation by splattering from chondrules during stochastic collisions in the solar  
1593 system. *Meteoritics & Planetary Science*, 51, 884-905.
- 1594 Dodd, R.T., Schmus, W.R., and Marvin, U.B. (1965) Merrihueite, a new alkali-ferromagnesian

- 1595 silicate from the Mezö-Madaras chondrite. *Science*, 149, 972-974.
- 1596 Downs, R.T. (2006) The RRUFF Project: an integrated study of the chemistry, crystallography,  
1597 Raman and infrared spectroscopy of minerals. Program and Abstracts of the 19th General  
1598 Meeting of the International Mineralogical Association in Kobe, Japan. 003-13.
- 1599 Downs, R.T., and Hall-Wallace, M. (2003) The American Mineralogist Crystal Structure  
1600 Database. *American Mineralogist*, 88, 247-250.
- 1601 Ebel, D.S. (2006) Condensation of rocky materials in astrophysical environments. In D.S. Lauretta  
1602 and H.Y. McSween Jr., Eds., *Meteorites and the Early Solar System II*, pp. 253-277. University  
1603 of Arizona Press.
- 1604 Ebel, D.S., and Alexander, C.M.O'D. (2011) Equilibrium condensation from chondritic porous  
1605 IDP enriched vapor: Implications for Mercury and enstatite chondrite origins. *Planetary and  
1606 Space Science*, 59, 1888-1894.
- 1607 Ebel, D.S., and Grossman, L. (2000) Condensation in dust-rich systems. *Geochimica et  
1608 Cosmochimica Acta*, 65, 469-477.
- 1609 Ebel, D.S., and Sack, R.O. (2013) Djerfisherite: Nebular source of refractory potassium.  
1610 *Contributions to Mineralogy and Petrology*, 166, 923-934.
- 1611 Ebel, D.S., Weisberg, M.K., and Beckett, J.R. (2012) Thermochemical stability of low-iron,  
1612 manganese-enriched olivine in astrophysical environments. *Meteoritics & Planetary Science*,  
1613 47, 585-593.
- 1614 Ebel, D.S., Alexander, C.M.O'D., and Libourel, G. (2018) Vapor-melt exchange: Constraints on  
1615 chondrite formation conditions and processes. In S.A. Russell, H.C. Connelly, and A.N. Krot,  
1616 Eds., *Chondrules: Records of Protoplanetary Disk Processes*, pp.151-174. Cambridge  
1617 University Press.

- 1618 Ebert, S., and Bischoff, A. (2016) genetic relationship between Na-rich chondrules and Ca, Al-  
1619 rich inclusions? – Formation of Na-rich chondrules by melting of refractory and volatile  
1620 precursors in the solar nebula. *Geochimica et Cosmochimica Acta*, 177, 182-204.
- 1621 Ehlers, K., and El Goresy, A. (1988) Normal and reverse zoning in niningerite: a novel key  
1622 parameter to the thermal histories of EH-chondrites. *Geochimica et Cosmochimica Acta*, 52,  
1623 877-887.
- 1624 El Goresy, A., and Ehlers, K. (1989) Sphalerite in EH chondrites: 1. Textural relations,  
1625 compositions, diffusion profiles, and pressure temperature histories. *Geochimica et*  
1626 *Cosmochimica Acta*, 53, 1657-1668.
- 1627 El Goresy, A., Yabuki, H., Ehlers, K., Woolum, D., and Pernicka, E. (1988) Qingzhen and Yamato-  
1628 691: A tentative alphabet for EH chondrites. *Proceedings of the NIPR Symposium on Antarctic*  
1629 *Meteorites*, 1, 65-101.
- 1630 El Goresy, A., Zinner, E., Matsunami, S., Palme, H., Spettel, B., Lin, Y., and Nazarov, M. (2002)  
1631 Efremovka 101.1: A CAI with ultrarefractory REE patterns and enormous enrichments of Sc,  
1632 Zr, and Y in fassaite and perovskite. *Geochimica et Cosmochimica Acta*, 66, 1459–1491.
- 1633 El Goresy, A., Boyer, M., and Miyahara, M. (2011) Almahata Sita MS-17 EL-3 chondrite  
1634 fragment: contrasting oldhamite assemblages in chondrules and matrix and significant  
1635 oldhamite REE-patterns. *Meteoritics & Planetary Sciences*, 46, Abstract #5079.
- 1636 Fedkin, A.V., and Grossman, L. (2013) Vapor saturation of sodium: Key to unlocking the origin  
1637 of chondrules. *Geochimica et Cosmochimica Acta*, 112, 225-250.
- 1638 Fedkin, A.V., Grossman, L., Humayun, M., Simon, S.B., and Campbell, A.J. (2015) Condensates  
1639 from vapor made by impacts between metal-, silicate-rich bodies: Comparison with metal and  
1640 chondrules in CB chondrites. *Geochimica et Cosmochimica Acta*, 164, 236-261.

- 1641 Fogel, R.A. (1997) On the significance of diopside and oldhamite in enstatite chondrites and  
1642 aubrites. *Meteoritics*, 32, 577-591.
- 1643 Friedrich, J.M., Weisberg, M.K., Ebel, D.S., Biltz, A.E., Corbett, B.M., Iotzov, I.V., Khan, W.S.,  
1644 and Wolman, M.D. (2015) Chondrule size and related physical properties: A compilation and  
1645 evaluation of current data across all meteorite groups. *Chemie der Erde*, 75, 419-443. DOI:  
1646 10.1016/j.chemer.2014.08.003
- 1647 Friend, P., Hezel, D.C., and Mucerschi, D. (2016) The conditions of chondrule formation, Part II:  
1648 Open system. *Geochimica et Cosmochimica Acta*, 173, 198-209.
- 1649 Fu, R.R., Weiss, B.P., Schrader, D.L., and Johnson, B.C. (2018) Records of magnetic fields in the  
1650 chondrule formation environment. In S.A. Russell, H.C. Connolly Jr., and A.N. Krot, Eds.,  
1651 Chondrules: Records of Protoplanetary Disk Processes, pp. 324-339. Cambridge University  
1652 Press.
- 1653 Fuchs, L.H. (1966) Djerfisherite, alkali copper-iron sulfide: a new mineral. *Science*, 153, 166-167.
- 1654 Fuchs, L.H., Olsen, E., and Jensen, K.J. (1973) Mineralogy, mineral chemistry, and composition  
1655 of the Murchison (C2) meteorite. *Smithsonian Contributions to Earth Science*, 10, 1-39.
- 1656 Fujimaki, H., Matsu-Ura, M., Sunagawa, I, and Aoki, K. (1981a) Chemical compositions of  
1657 chondrules and matrices in the ALHA-77015 chondrite (L3). *Memoirs of the NIPR Special*  
1658 *Issue*, 20, 161-174.
- 1659 Fujikami, H., Matsu-Ura, M., Aoki, K, and Sunagawa, I. (1981b) Ferropseudobrookite-silica  
1660 mineral-albite-chondrule in the ALH-7701 5 chondrite (L3). *Memoirs of the NIPR Special*  
1661 *Issue*, 20, 119-123.
- 1662 Galy, A., Young, E., Ash, R.D. and O’Nions, R.K. (2000) The formation of chondrules at high gas  
1663 pressures in the solar nebula. *Science*, 290, 1751-1754.

- 1664 Ghiorso, M.S., and Sack, R.O. (1995) Chemical mass transfer in magmatic processes IV. A revised  
1665 and internally consistent thermodynamic model for the interpolation and extrapolation of  
1666 liquid-solid equilibria in magmatic systems at elevated temperatures and  
1667 pressures. *Contributions to Mineralogy and Petrology*, 119, 197-212.
- 1668 Ghiorso, M.S., Hirschmann, M.M., Reiners, P.W., and Kress, V.C. III (2002) The pMELTS: A  
1669 revision of MELTS for improved calculation of phase relations and major element partitioning  
1670 related to partial melting of the mantle to 3 GPa. *Geochemistry Geophysics Geosystems*, 3,  
1671 10.1029/2001GC000217.
- 1672 Gibbs, J.W. (1876-1878) On the equilibrium of heterogeneous substances. *Transactions of the*  
1673 *Connecticut Academy of Arts and Sciences*, 3, 108-248, 343-524.
- 1674 Gilmour, J.D., Crowther, S.A., Busfield, A., Holland, G., and Whitby, J.A. (2009) An early I-Xe  
1675 age for CB chondrite chondrule formation, and a re-evaluation of the closure age of Shallowater  
1676 enstatite. *Meteoritics & Planetary Science*, 44, 573-579.
- 1677 Golden, J., McMillan, M., Downs, R.T., Hystad, G., Stein, H.J., Zimmerman, A., Sverjensky, D.A.  
1678 Armstrong, J., and Hazen, R.M. (2013) Rhenium variations in molybdenite (MoS<sub>2</sub>): Evidence  
1679 for progressive subsurface oxidation. *Earth and Planetary Science Letters*, 366, 1-5.
- 1680 Goldstein, J.I., and Michael, J.R. (2006) The formation of plessite in meteoritic metal. *Meteoritics*  
1681 *& Planetary Science*, 41, 553-570.
- 1682 Gooding, J.L., and Keil, K. (1981) Relative abundance of chondrule primary textural types in  
1683 ordinary chondrites and their bearing on conditions of chondrule formation. *Meteoritics*, 16,  
1684 17-43.
- 1685 Gounelle, M., Young, E.D., Shahar, A., Tonui, E., and Kearsley, A. (2007) Magnesium isotopic  
1686 constraints on the origin of CB<sub>b</sub> chondrites. *Earth and Planetary Science Letters*, 256, 521–533.

- 1687 Greshake, A. (1997) The primitive matrix components of the unique carbonaceous chondrite Acfer  
1688 094: A TEM study. *Geochimica et Cosmochimica Acta*, 61, 437-452.
- 1689 Grossman, J.N., and Brearley, A.J. (2005) The onset of metamorphism in ordinary and  
1690 carbonaceous chondrites. *Meteoritics and Planetary Science*, 40, 87–122.
- 1691 Grossman, J.N., Rubin, A.E., Rambaldi, E.R., Rajan, R.S., and Wasson, J.T. (1985) Chondrules in  
1692 the Qingzhen type-3 enstatite chondrite: Possible precursor components and components and  
1693 comparison to ordinary chondrite chondrules. *Geochimica et Cosmochimica Acta*, 49, 1781-  
1694 1795.
- 1695 Grossman, J.N., Rubin, A.E., and MacPherson, G.J. (1988) ALH 85085: A unique volatile-poor  
1696 carbonaceous chondrite with implications for nebular fractionation processes. *Earth and  
1697 Planetary Science Letters*, 91, 33-54.
- 1698 Grossman, L., and Steele, I.M. (1976) Amoeboid olivine aggregates in the Allende meteorite.  
1699 *Geochimica et Cosmochimica Acta*, 40, 149-155.
- 1700 Haggerty, S.E., and McMahon, B.M. (1979) Magnetite-sulfide-metal complexes in the Allende  
1701 meteorite. *Proceedings of the Lunar and Planetary Science Conference*, 10, 851-870.
- 1702 Hashimoto, A. (1983) Evaporation metamorphism in the early solar nebula—evaporation  
1703 experiments on the melt FeO-MgO-SiO<sub>2</sub>-CaO-Al<sub>2</sub>O<sub>3</sub> and chemical fractionations of primitive  
1704 materials. *Geochemical Journal*, 17, 111-145.
- 1705 Hazen, R.M. (2014) Data-driven abductive discovery in mineralogy. *American Mineralogist*, 99,  
1706 2165-2170.
- 1707 Hazen, R.M. (2019) An evolutionary system of mineralogy: Proposal for a classification based on  
1708 natural kind clustering. *American Mineralogist*, 104, 810-816.

- 1709 Hazen, R.M., and Ferry, J.M. (2010) Mineral evolution: Mineralogy in the fourth dimension.  
1710 Elements, 6, #1, 9-12.
- 1711 Hazen, R.M., and Morrison, S.M. (2020) An evolutionary system of mineralogy, part I: stellar  
1712 mineralogy (>13 to 4.6 Ga). American Mineralogist, 105, in press.
- 1713 Hazen, R.M., Papineau, D., Bleeker, W., Downs, R.T., Ferry, J.M., McCoy, T.L., Sverjensky,  
1714 D.A., and Yang, H. (2008) Mineral evolution. American Mineralogist, 93, 1693-1720.
- 1715 Hazen, R.M., Bekker, A., Bish, D.L., Bleeker, W., Downs, R.T., Farquhar, J., Ferry, J.M., Grew,  
1716 E.S., Knoll, A.H., Papineau, D., Ralph, J.P., Sverjensky, D.A., and Valley, J.W. (2011) Needs  
1717 and opportunities in mineral evolution research. American Mineralogist, 96, 953-963.
- 1718 Hazen, R.M., Sverjensky, D.A., Azzolini, D., Bish, D.L., Elmore, S.C., Hinnov, L., and Milliken,  
1719 R.E. (2013) Clay mineral evolution. American Mineralogist, 98, 2007-2029.
- 1720 Hazen, R.M., Bromberg, Y., Downs, R.T., Eleish, A., Falkowski, P.G., Fox, P., Giovannelli, D.,  
1721 Hummer, D.R., Hystad, G., Golden, J.J., Knoll, A.H., Li, C., Liu, C., Moore, E.K., Morrison,  
1722 S.M., Muscente, A.D., Prabhu, A., Ralph, J., Rucker, M.Y., Runyon, S.E., Warden, L.A.,  
1723 Zhong, H. (2019a) Deep carbon through deep time: Data-driven insights. In B. Orcutt, I.  
1724 Danielle, R. Dasgupta, Eds., Deep Carbon: Past to Present, pp.320-352. Cambridge University  
1725 Press.
- 1726 Hazen, R.M., Downs, R.T., Eleish, A., Fox, P., Gagné, O., Golden, J.J., Grew, E.S., Hummer,  
1727 D.R., Hystad, G., Krivovichev, S.V., Li, C., Liu, C., ma, X., Morrison, S.M., Pan, F., Pires,  
1728 A.J., Prabhu, A., Ralph, J., Runyon, S.E., and Zhong, H. (2019b) Data-driven discovery in  
1729 mineralogy: Recent advances in data resources, analysis, and visualization. China Engineering,  
1730 5, 397-405.

- 1731 Heck, P.R., Greer, J., Kööp, L., Trappitsch, R., Gyngard, F., Busemann, H., Maden, C., Ávila,  
1732 J.N., Davis, A.M., and Wieler, R. (2020) Lifetimes of interstellar dust from cosmic ray exposure  
1733 ages of presolar grains. Proceedings of the National Academy of Sciences USA, Jan. 13, 2020,  
1734 DOI: 10.1073/pnas.1904573117
- 1735 Herndon, J.M., and Rudee, M.L. (1978) Thermal history of the Abee enstatite chondrite. Earth and  
1736 Planetary Science Letters, 41, 101-106.
- 1737 Herndon, J.M., Rowe, M.W., Larson, E.E., and Watson, D.E. (1975) Origin of magnetite and  
1738 pyrrhotite in carbonaceous chondrites. Nature, 253, 516-518.
- 1739 Hewins, R.H., and Zanda, B. (2012) Chondrules: Precursors and interactions with the nebular gas.  
1740 Meteoritics & Planetary Science, 47, 1120-1138.
- 1741 Hewins, R.H., Jones, R.H., and Scott, E.R.D. [Eds.] (1996) Chondrules and the Protoplanetary  
1742 Disk. Cambridge, UK: Cambridge University Press.
- 1743 Hewins, R.H., Connolly, H.C. Jr., Lofgren, G.E., and Libourel, G. (2005) Experimental  
1744 constraints on chondrule formation. Astronomical Society of the Pacific Conference Series,  
1745 341. 286–316.
- 1746 Hezel, D.C., Palme, H., Nasdala, L., and Brenker, F.E. (2006) Origin of SiO<sub>2</sub>-rich components in  
1747 ordinary chondrites. Geochimica et Cosmochimica Acta, 70, 1548-1564.
- 1748 Hezel, D.C., Bland, P.A., Palme, H., Jacquet, E., and Bigolski, J. (2018) Composition of  
1749 chondrules and matrix and their complementary relationship in chondrites. In S.A. Russell, H.C.  
1750 Connolly Jr., and A.N. Krot, Eds., Chondrules: Records of Protoplanetary Disk Processes, pp.  
1751 91-121. Cambridge University Press.

- 1752 Hobart, K.K., Crapster-Pregont, E.J., and Ebel, D.S. (2015) Decoding the history of a layered  
1753 chondrule through olivine grain orientation measurements using EBSD. Proceedings of the  
1754 Lunar and Planetary Science Conference, 46, Abstract #1978.
- 1755 Holland, T.J.B., and Powell, R. (1998) An internally consistent thermodynamic data set for phases  
1756 of petrological interest. *Journal of Metamorphic Petrology*, 16, 309–343.
- 1757 Holst, J.C., Olsen, M.B., Paton, C., Nagashima, K., Schiller, M., Wielandt, D., Larsen, K.K.,  
1758 Connelly, J.N., Jørgensen, J.K., Krot, A.N., Nordlund, Å., and Bizzarro, M. (2013)  $^{182}\text{Hf}$ - $^{182}\text{W}$   
1759 age dating of a  $^{26}\text{Al}$ -poor inclusion and implications for the origin of short-lived radioisotopes  
1760 in the early solar system. *Proceedings of the National Academy of Sciences USA*, 110, 8819-  
1761 8823.
- 1762 Hood, L.L., and Weidenschilling, S.J. (2012) The planetesimal bow shock model of chondrule  
1763 formation: A more quantitative assessment of the standard (fixed Jupiter) case. *Meteoritics &*  
1764 *Planetary Science*, 47. 1715-1727.
- 1765 Howes, L.M., Casey, A.R., Asplund, M., Keller, S.C., Yong, D., Nataf, D.M., Poleski, R., Lind,  
1766 K., Kobayashi, C.; Owen, C.I., Ness, M., Bessell, M.S., Da Costa, G.S., Schmidt, B.P.,  
1767 Tisserand, P., Udalski, A., Szymański, M.K., Soszyński, I., Pietrzyński, G., Ulaczyk, K.,  
1768 Wyrzykowski, L., Pietrukowicz, P., Skowron, J., Kozłowski, S., and Mróz, P. (2015) Extremely  
1769 metal-poor stars from the cosmic dawn in the bulge of the Milky Way. *Nature*, 527, 484-487.
- 1770 Hua, X., and Buseck, P.R. (1995) Fayalite in Kaba and Mokoia carbonaceous chondrites.  
1771 *Geochimica et Cosmochimica Acta*, 59, 563-578.
- 1772 Hua, X., Adam, J., Palme, H., and El Goresy, A. (1988) Fayalite-rich rims, veins, and halos around  
1773 and in forsteritic olivines in CAIs and chondrules in carbonaceous chondrites: Types,

- 1774 compositional profiles and constraints on their formation. *Geochimica et Cosmochimica Acta*,  
1775 52, 1389-1408.
- 1776 Hubbard, A., and Ebel, D.S. (2014) Protoplanetary dust porosity and FU Orionis outbursts: Solving  
1777 the mystery of Earth's missing volatiles. *Icarus*, 237, 84–96.
- 1778 Hubbard, A., and Ebel D.S. (2015) Semarkona: Lessons for chondrule and chondrite formation.  
1779 *Icarus*, 245, 32-37.
- 1780 Hubbard, A., and Ebel, D.S. (2018) Evaluating non-shock, non-collisional models for chondrule  
1781 formation. In S.A. Russell, H.C. Connolly Jr., and A.N. Krot, Eds., *Chondrules: Records of*  
1782 *Protoplanetary Disk Processes*, pp. 400-427. Cambridge University Press.
- 1783 Hutchison, R. (2004) *Meteorites: A Petrologic, Chemical and Isotopic Synthesis*. Cambridge  
1784 University Press.
- 1785 Iida, A., Nakamoto, T., Susa, H, and Nakagawa, Y. (2001) A shock model for chondrule formation  
1786 in a protoplanetary disk. *Icarus*, 153, 430-450.
- 1787 Ikeda, Y. (1980) Petrology of the Allan Hills-764 chondrite (LL3). *Memoirs of the NIPR Special*  
1788 *Issue*, 17, 50-82.
- 1789 Ikeda, Y. (1982) Petrology of the ALH-77003 chondrite (C3). *Memoirs of the NIPR Special Issue*,  
1790 25, 34-65.
- 1791 Ikeda, Y. (1983) Alteration of chondrules and matrices in the four Antarctic carbonaceous  
1792 chondrites ALH 77307 (C3), Y-790123 (C2), Y-75293 (C2), and Y-74662 (C2). *Memoirs of*  
1793 *the NIPR Special Issue*, 30, 93-108.
- 1794 Ikeda, Y. (1988a) Petrochemical study of the Yamato-691 enstatite chondrite (E3) I: Major  
1795 element chemical compositions of chondrules and inclusions. *Proceedings of the NIPR*  
1796 *Symposium on Antarctic Meteorites*, 1, 3-13.

- 1797 Ikeda, Y. (1988b) Petrochemical study of the Yamato-691 enstatite chondrite (E3) II: Descriptions  
1798 and mineral compositions of unusual silicate-inclusions. Proceedings of the NIPR Symposium  
1799 on Antarctic Meteorites, 1, 14-37.
- 1800 Ikeda, Y. (1989a) Petrochemical study of the Yamato-691 enstatite chondrite (E3) IV: Description  
1801 and mineral chemistry of opaque nodules. Proceedings of the NIPR Symposium on Antarctic  
1802 Meteorites, 2, 109-146.
- 1803 Ikeda, Y. (1989b) Petrochemical study of the Yamato-691 enstatite chondrite (E3) III: Description  
1804 and mineral compositions of chondrules. Proceedings of the NIPR Symposium on Antarctic  
1805 Meteorites, 2, 75-108.
- 1806 Ikeda, Y., and Kimura, M. (1995) Anhydrous alteration of Allende chondrules in the solar nebula  
1807 I. Description and alteration of chondrules with known oxygen-isotope compositions.  
1808 Proceedings of the NIPR Symposium on Antarctic Meteorites, 8, 97-122.
- 1809 Ivanov, I., MacPherson, G.J., Zolensky, M.E., Kononkova, N.N., and Migdisova, L.F. (1996) The  
1810 Kaidun meteorite: Composition and origin of inclusions in the metal of an enstatite chondrite  
1811 clast. Meteoritics & Planetary Science, 31, 621-626.
- 1812 Ivanov A.V., Zolensky M.E., Saito A., Ohsumi K., Yang V., Kononkova N.N., and Mikouchi T.  
1813 (2000) Florenskyite, FeTiP, a new phosphide from the Kaidun meteorite. American  
1814 Mineralogist, 85, 1082-1086.
- 1815 Ivanova, M.A., Kononkova, N.N., Krot, A.N., Greenwood, R.C., Franchi, I.A., Verchovsky, A.B.,  
1816 Trieloff, M., Korochantseva, E.V., and Brandstätter, F. (2008) The Isheyevo meteorite:  
1817 Mineralogy, petrology, bulk chemistry, oxygen, nitrogen, carbon isotopic compositions, and  
1818  $^{40}\text{Ar}$ - $^{39}\text{Ar}$  ages. Meteoritics & Planetary Science, 43, 915-940.

- 1819 Izawa, M.R.M., King, P.L., Flemming, R.L., Peterson, R.C., and McCausland, P.J.A. (2010)  
1820 Mineralogical and spectroscopic investigation of enstatite chondrites by X-ray diffraction and  
1821 infrared reflectance spectroscopy. *Journal of Geophysical Research Planets*, 115, E7, E07008  
1822 (18 pp.).
- 1823 Jacquet, E., Piani, L., and Weisberg, M.K. (2018) Chondrules in enstatite chondrites. In S.A.  
1824 Russell, H.C. Connolly Jr., and A.N. Krot, Eds., *Chondrules: Records of Protoplanetary Disk*  
1825 *Processes*, pp. 175-195. Cambridge University Press.
- 1826 Johansen, A., Blum, J., Tanaka, H., et al. (2014) The multifaceted planetesimal formation process.  
1827 In H. Beuther, R.S. Klesson, C.P. Dullemond, and T. Henning, Eds., *Protostars and Planets VI*,  
1828 pp. 547-570. University of Arizona Press.
- 1829 Johnson, B.C., Minton, D.A., Melosh, H.J., and Zuber, M.T. (2012) Impact jetting as the origin of  
1830 chondrules. *Nature*, 517, 339-341.
- 1831 Johnson, B.C. Bowling, T.J., and Melosh, H.J. (2014) Jetting during vertical impacts of spherical  
1832 projectiles. *Icarus*, 238, 13-22.
- 1833 Johnson, B.C., Ciesla, F.J., Dullemond, C.P., and Melosh, H.J. (2018) Formation of chondrules by  
1834 planetesimal collisions. In S.A. Russell, H.C. Connolly Jr., and A.N. Krot, Eds., *Chondrules:*  
1835 *Records of Protoplanetary Disk Processes*, pp. 343-360. Cambridge University Press.
- 1836 Johnson, C.A., and Prinz, M. (1991) Chromite and olivine in type II chondrules in carbonaceous  
1837 and ordinary chondrites: Implications for aqueous alteration. *Geochimica et Cosmochimica*  
1838 *Acta*, 55, 893-904.
- 1839 Jones, R.H. (1990) Petrology and mineralogy of type II, FeO-rich, chondrules in Semarkona  
1840 (LL3.0): Origin by closed-system fractional crystallization, with evidence for supercooling.  
1841 *Geochimica et Cosmochimica Acta*, 54, 1785-1802.

- 1842 Jones, R.H. (1994) Petrology of FeO-poor, porphyritic pyroxene chondrules in the Semarkona  
1843 chondrite. *Geochimica et Cosmochimica Acta*, 58, 5325-5340.
- 1844 Jones, R.H. (1996) FeO-rich, porphyritic olivine chondrules in unequilibrated ordinary chondrites.  
1845 *Geochimica et Cosmochimica Acta*, 60, 3115-3138.
- 1846 Jones, R.H. (1997) Alteration of plagioclase-rich chondrules in CO3 chondrites: Evidence for late-  
1847 stage sodium and iron metasomatism in a nebular environment. In M.E. Zolensky, A.N. Krot,  
1848 and E.R.D. Scott, Eds., *Workshop on Parent-body and Nebular Modification of Chondritic*  
1849 *Materials*, pp. 30-31. Lunar and Planetary Institute.
- 1850 Jones, R.H. (2012) Petrographic constraints on the diversity of chondrule reservoirs in the  
1851 protoplanetary disk. *Meteoritics & Planetary Science*, 47, 1176–1190.
- 1852 Jones, R.H., and Scott, E.R.D. (1989) Petrology and thermal history of type IA chondrules in the  
1853 Semarkona (LL3.0) chondrite. *Proceedings of the Lunar and Planetary Science Conference*, 19,  
1854 523-536.
- 1855 Jones, R.H., McCubbin, F.M., Dreeland, L., Guan, Y., Burger, P.V., and Shearer, C.K. (2014)  
1856 Phosphate minerals in LL chondrites: A record of the action of fluids during metamorphism on  
1857 ordinary chondrite parent bodies. *Geochimica et Cosmochimica Acta*, 132, 120–140.
- 1858 Jones, R.H., Villeneuve, J., and Libourel, G. (2018) Thermal histories of chondrules: Petrologic  
1859 observations and experimental constraints. In S.A. Russell, H.C. Connolly Jr., and A.N. Krot,  
1860 Eds., *Chondrules: Records of Protoplanetary Disk Processes*, pp. 57-90. Cambridge University  
1861 Press.
- 1862 Kawasaki, N., Kato, C., Itoh, S., Wakaki, S., Ito, M., and Yurimoto, H. (2015)  $^{26}\text{Al}$ - $^{26}\text{Mg}$   
1863 chronology and oxygen isotope distributions of multiple melting for a Type C CAI from  
1864 Allende. *Geochimica et Cosmochimica Acta*, 169, 99-114.

- 1865 Keil, K. (1968) Mineralogical and chemical relationships among enstatite chondrites. Journal of  
1866 Geophysical Research, 73, 6945-6976.
- 1867 Keil, K., and Snetsinger, K.G. (1967) Niningerite: A new meteoritic sulfide. Science, 155, 451-  
1868 453.
- 1869 Kerridge, J.F., and Matthews, M.S. (1988) Meteorites and the Early Solar System. University of  
1870 Arizona Press.
- 1871 Kimura, M., and Ikeda, Y. (1992) Mineralogy and petrology of an unusual Belgica-7904  
1872 carbonaceous chondrite. Proceedings of the NIPR Symposium on Antarctic Meteorites, 5, 74-  
1873 119.
- 1874 Kimura, M., Weisberg, M.K., Lin, Y., Suzuki, A., Ohtani, E., and Okazaki, R. (2005) Thermal  
1875 history of the enstatite chondrites from silica polymorphs. Meteoritics & Planetary Science, 40,  
1876 855-868.
- 1877 Kimura, M., Mikouchi, T., Suzuki, A., Miyahara, M., Ohtani, E., and El Goresy, A. (2009)  
1878 Kushiroite,  $\text{CaAlAlSiO}_6$ : A new mineral of the pyroxene group from the ALH 85085 CH  
1879 chondrite, and its genetic significance in refractory inclusions. American Mineralogist, 94,  
1880 1479–1482.
- 1881 Kimura, M., Barrat, J.A., Weisberg, M.K., Imae, N., Yamaguchi, A., and Kojima, H. (2014)  
1882 Petrology and bulk chemistry of Yamato-82094, a new type of carbonaceous chondrite.  
1883 Meteoritics & Planetary Science, 49, 346-357.
- 1884 King, A.R., and Pringle, J.E. (2010). The accretion disc dynamo in the solar nebula. Monthly  
1885 Notices of the Royal Astronomical Society, 404, 1903-1909.
- 1886 King, E.A. [Ed.] (1983) Chondrules and their Origins. Lunar and Planetary Institute.

- 1887 Kita, N.T., and Ushikubo, T. (2012) Evolution of protoplanetary disk inferred from  $^{26}\text{Al}$   
1888 chronology of individual chondrules. *Meteoritics & Planetary Science*, 47, 1108-1119.
- 1889 Kita, N.T., Yin, Q-Z., MacPherson, G.J., Ushikubo, T., Jacobsen, B., Nagashima, K., Kurahashi,  
1890 E., Krot, A.N., and Jacobsen, S.B. (2013)  $^{26}\text{Al}$ - $^{26}\text{Mg}$  isotope systematics of the first solids in  
1891 the early solar system. *Meteoritics & Planetary Science*, 48, 1383-1400.
- 1892 Kita, N.T., Tenner, T.J., Ushikubo, T., Bouvier, A., Wadhwa, M., Bullock, E.S., and MacPherson,  
1893 G.J. (2015) Why do U-Pb ages of chondrules and CAIs have more spread than their  $^{26}\text{Al}$  ages?  
1894 78th Annual Meteoritic Society Meeting, p. 5360.
- 1895 Kitamura, M., Watanabe, S., Isobe, H., and Morimoto, N. (1987) Diopside in chondrules of  
1896 Yamato-691 (EH3). *Memoirs of the NIPR Special Issue*, 46, 2113-122.
- 1897 Kitamura, M., Isobe, H., and Watanabe, S. (1988) Relict minerals and their assemblages in  
1898 Yamato-691 (EH3). *Proceedings of the NIPR Symposium on Antarctic Meteorites*, 1, 38-50.
- 1899 Kleine, T., Budde, G., Hellman, J. L., Kruijer, T.S., and Burkhardt, C. (2018) Tungsten isotopes  
1900 and the origin of chondrules and chondrites. In S.A. Russell, H.C. Connolly Jr., and A.N. Krot,  
1901 Eds., *Chondrules: Records of Protoplanetary Disk Processes*, pp. 276-299. Cambridge  
1902 University Press.
- 1903 Kööp, L., Nakashima, D., Heck, P.R., Kita, N.T., Tenner, T.J., Krot, A.N., Nagashima, K., Park,  
1904 C., and Davis, A.M. (2016a) New constraints on the relationship between  $^{26}\text{Al}$  and oxygen,  
1905 calcium, and titanium isotopic variation in the early solar system from a multielement isotopic  
1906 study of spinel-hibonite inclusions. *Geochimica et Cosmochimica Acta*, 184, 151-172.
- 1907 Kööp, L., Davis, A.M., Nakashima, D., Park, C., Krot, A.N., Nagashima, K., Tenner, T.J., Heck,  
1908 P.R., and Kita, N.T. (2016b) A link between oxygen, calcium and titanium isotopes in  $^{26}\text{Al}$ -

- 1909 poor hibonite-rich CAIs from Murchison and implications for the heterogeneity of dust  
1910 reservoirs in the solar nebula. *Geochimica et Cosmochimica Acta*, 189, 70-95.
- 1911 Kööp, L., Heck, P.R., Busemann, H., Davis, A.M., Greer, J., Maden, C., Meier, M.M.M., and  
1912 Wieler, R. (2018) High early solar activity inferred from helium and neon excess in the oldest  
1913 meteorite inclusions. *Nature Astronomy*, 2, 709-713.
- 1914 Krivovichev, S.V. (2012) Topological complexity of crystal structures: quantitative approach.  
1915 *Acta Crystallographica*, A68, 393-398.
- 1916 Krivovichev, S.V. (2013) Structural complexity of minerals: information storage and processing  
1917 in the mineral world. *Mineralogical Magazine*, 77, 275-326.
- 1918 Krot, A.N. (2019) Refractory inclusions in carbonaceous chondrites: Records of early solar  
1919 systems processes. *Meteoritics & Planetary Science*, 54, 1647-1691.
- 1920 Krot, A.N., and Rubin, A.E. (1994) Glass-rich chondrules in ordinary chondrites. *Meteoritics*, 29,  
1921 697-707.
- 1922 Krot, A.N., and Rubin, A.E. (1996) Microchondrule-bearing chondrule rims: Constraints on  
1923 chondrule formation. In R.H. Hewins, R.H. Jones, and E.R.D. Scott, Eds., *Chondrules and the*  
1924 *Protoplanetary Disk.*, pp. 181-184. Cambridge University Press.
- 1925 Krot, A.E., and Wasson, J.T. (1994) Silica-merrillite/roedderite-bearing chondrules and clasts  
1926 in ordinary chondrites: New occurrences and possible origin. *Meteoritics*, 29, 707-718.
- 1927 Krot, A.N., Ivanova, M.A., and Wasson, J.T. (1993) The origin of chromitic chondrules and the  
1928 volatility of Cr under a range of nebular conditions. *Earth and Planetary Science Letters*, 119,  
1929 569–584.
- 1930 Krot, A.N., Scott, E.R.D., and Zolensky, M.E. (1995) Mineralogical and chemical modification of  
1931 components in CV3 chondrites: Nebular or asteroidal processing? *Meteoritics*, 30, 748-775.

- 1932 Krot, A.N., Rubin, A.E., Keil, K., and Wasson, J.T. (1997a) Microchondrules in ordinary  
1933 chondrites: Implications for chondrule formation. *Geochimica et Cosmochimica Acta*, 61, 463-  
1934 473.
- 1935 Krot, A.N., Zolensky, M.E., Wasson, J.T., Scott, E.R.D., Keil, K., and Ohsumi, K. (1997b) Carbide  
1936 magnetite assemblages in type 3 ordinary chondrites. *Geochimica et Cosmochimica Acta*, 61,  
1937 219-237.
- 1938 Krot, A.N., Ulyanov, A.A., Meibom, A., and Keil, K. (2001a) Forsterite-rich accretionary rims  
1939 around Ca, Al-rich inclusions from the reduced CV3 chondrite Efremovka. *Meteoritics &*  
1940 *Planetary Science*, 36, 611–628.
- 1941 Krot, A.N., Meibom, A., Russell, S.S., Alexander, C.M.O'D., Jeffries, T.E., and Keil, K. (2001b)  
1942 A new astrophysical setting for chondrule formation. *Science*, 291, 1776–1779.
- 1943 Krot, A.N., Petaev, M.I., Russell, S.S., Itoh, S., Fagan, T.J., Yurimoto, H., Chizmadia, L.,  
1944 Weisberg, M.K., Komatsu, M., Ulyanov, A.A., and Keil, K. (2004a) Amoeboid olivine  
1945 aggregates and related objects in carbonaceous chondrites: records of nebular and asteroid  
1946 processes. *Chemie der Erde Geochemistry*, 64, 185-239.
- 1947 Krot, A.N., Libourel, G., Goodrich, C.A., and Petaev, M.I. (2004b) Silica-rich igneous rims around  
1948 magnesian chondrules in CR carbonaceous chondrites: Evidence for fractional condensation  
1949 during chondrule formation. *Meteoritics & Planetary Science*, 39, 1931-1955.
- 1950 Krot, A.N., Amelin, Y., Cassen, P., and Meibom, A. (2005) Young chondrules in CB chondrites  
1951 from a giant impact in the early Solar System. *Nature*, 436, 989-992.
- 1952 Krot, A.N., Nagashima, K., Bizzarro, M., Huss, G.R., Davis, A.M., McKeegan, K.D., Meyer, B.S.,  
1953 and Ulyanov, A.A. (2008) Multiple generations of refractory inclusions in the metal-rich

- 1954 carbonaceous chondrites Acfer 182/214 and Isheyev. *The Astrophysical Journal*, 672, 713–  
1955 721.
- 1956 Krot, A.N., Makide, K., Nagashima, K., Huss, G.R., Oglione, R.C., Ciesla, F.J., Yang, L.,  
1957 Hellebrand, E., and Gaidos, E. (2012) Heterogeneous distribution of  $^{26}\text{Al}$  at the birth of the  
1958 solar system: Evidence from refractory grains and inclusions. *Meteoritics & Planetary Science*,  
1959 47, 1948–1979.
- 1960 Krot, A.N., Keil, K., Scott, E.R.D., Goodrich, C.A., and Weisberg, M.K. (2014) Classification of  
1961 meteorites and their genetic relationships. *Treatise on Geochemistry*, 2nd edition, 1, 2-63.
- 1962 Krot, A.N., Nagashima, K., van Kooten, E.M.M., and Bizzarro, M. (2017) Calcium-aluminum-  
1963 rich inclusions recycled during formation of porphyritic chondrules from CH carbonaceous  
1964 chondrites. *Geochimica et Cosmochimica Acta*, 201, 185–223.
- 1965 Krot, A.N., Nagashima, K., Libourel, G., and Miller, K.E. (2018) Multiple mechanisms of transient  
1966 heating events in the protoplanetary disk. In S.A. Russell, H.C. Connolly Jr., and A.N. Krot,  
1967 Eds., *Chondrules: Records of Protoplanetary Disk Processes*, pp. 11-56. Cambridge University  
1968 Press.
- 1969 Krot, A.N., Ma, C., Nagashima, K., Davis, A.M., Beckett, J.R., Simon, S.B., Komatsu, M., Fagan,  
1970 T.J., Brenker, F., Ivanova, M.A., and Bischoff, A. (2019) Mineralogy, petrology, and oxygen  
1971 isotopic compositions of ultra-refractory inclusions from carbonaceous chondrites.  
1972 *Geochemistry*, 79, 125519 (29 pp.).
- 1973 Kruijer, T.S., Touboul, M., Fischer-Godde, M., Bermingham, K.R., and Kleine, T. (2014)  
1974 Protracted core formation and rapid accretion of protoplanets. *Science*, 344, 1150-1154.

- 1975 Kruijer, T.S., Burkhardt, C., Budde, G., and Kleine, T. (2017) Age of Jupiter from the distinct  
1976 genetics and formation times of meteorites. *Proceedings of the National Academy of Sciences*  
1977 USA. Doi: 10.1073/pnas.1704461114
- 1978 Kuebler, K.E., McSween, H.Y. Jr., Carlson, W.D., and Hirsch, D. (1999) Sizes and masses of  
1979 chondrules and metal-troilite grains in ordinary chondrites: Possible implications for nebular  
1980 sorting. *Icarus*, 141, 96–106.
- 1981 Kurahashi, E., Kita, N.T., Nagahara, H., and Morishita, Y. (2008)  $^{26}\text{Al}$ - $^{26}\text{Mg}$  systematics of  
1982 chondrules in a primitive CO chondrite. *Geochimica et Cosmochimica Acta*, 72, 3865–3882.
- 1983 Lambrechts, M., Johansen, A., and Morbidelli, A. (2014) Separating gas-giant and ice-giant  
1984 planets by halting pebble accretion. *Astronomy & Astrophysics*, 572, A35.
- 1985 Larsen, K., Trinquier, A., Paton, C., Schiller, M., Wielandt, D., Ivanova, M., Connelly, J.N.,  
1986 Nordlund, A., Krot, A.N., and Bizzarro, M. (2011) Evidence for magnesium-isotope  
1987 heterogeneity in the solar protoplanetary disk. *The Astrophysical Journal*, 735, L37–L40.
- 1988 Lauretta, D.S., Kremser, D.T., and Fegley, B.J. (1996) A comparative study of experimental and  
1989 meteoritic metal-sulfide assemblages. *Proceedings of the NIPR Symposium on Antarctic*  
1990 *Meteorites*, 9, 97-110.
- 1991 Lehner, S.W., Buseck, P.R., and McDonough, W.F. (2010) Origin of kamacite, schreibersite, and  
1992 perryite in metal-sulfide nodules of the enstatite chondrite Sahara 97072 (EH3). *Meteoritics &*  
1993 *Planetary Science*, 45, 289–303.
- 1994 Lehnert, K.A., Su, Y., Langmuir, C.H., Sarbas, B., and Nohl, U. (2000) A global geochemical  
1995 database structure for rocks. *Geochemistry Geophysics Geosystems*, 1.
- 1996 Lehnert, K.A., Walker, D., and Sarbas, B. (2007) EarthChem: A geochemistry data network.  
1997 *Geochimica et Cosmochimica Acta*, 71, A559.

- 1998 Leitch, C.A., and Smith, J.V. (1980) Petrography, mineral chemistry and origin of Type I enstatite  
1999 chondrites. *Geochimica et Cosmochimica Acta*, 46, 2083-2097.
- 2000 Lewis, J.A., and Jones, R.H. (2016) Phosphate and feldspar mineralogy of equilibrated L  
2001 chondrites: The record of metasomatism during metamorphism in ordinary chondrite parent  
2002 bodies. *Meteoritics & Planetary Science*, 51, 1886-1913.
- 2003 Lewis, J.A., and Jones, R.H. (2019) Primary feldspar in the Semarkona LL3.00 chondrite:  
2004 Constraints on chondrule formation and secondary alteration. *Meteoritics & Planetary Science*,  
2005 54, 72-89.
- 2006 Libourel, G., Krot, A.N., and Tissandier, L. (2006) Role of gas-melt interaction during chondrule  
2007 formation. *Earth and Planetary Science Letters*, 251, 232-240.
- 2008 Lin, Y., El Goresy, A., Boyer, M., Feng, L., Zhang, J. and Hao, J. (2011) Earliest solid condensates  
2009 consisting of the assemblage oldhamite, sinoite, graphite and excess  $^{36}\text{S}$  in lawrencite from  
2010 Almahata Sitta MS-17 EL3 chondrite. Workshop on Formation of the First Solids in the Solar  
2011 System, Abstract #9040.
- 2012 Luck, J.-M., Ben Othman, D., and Albarède, F. (2005) Zn and Cu isotopic variations in chondrites  
2013 and iron meteorites: Early solar nebula reservoirs and parent-body processes. *Geochimica et*  
2014 *Cosmochimica Acta*, 69, 5351-5363.
- 2015 Lusby, D., Scott, E.R.D., and Keil, K. (1987) Ubiquitous high-Fe silicates in enstatite chondrites.  
2016 Proceedings of the Lunar and Planetary Science Conference (Journal of Geophysical Research),  
2017 17, E679-E695.
- 2018 Luu, T.-H., Hin, R.C., Coath, C.D., and Elliott, T. (2016) High precision Mg-isotope  
2019 measurements of bulk chondrites and the homogeneity of  $^{26}\text{Al}$  in the solar nebula. 79th Annual  
2020 Meteoritical Society Meeting, #6485.

- 2021 Ma, C., and Rossman, G.R. (2009) Grossmanite,  $\text{CaTi}^{3+}\text{AlSiO}_6$ , a new pyroxene from the Allende  
2022 meteorite. *American Mineralogist*, 94, 1491–1494.
- 2023 Ma, C., and Rubin, A.E. (2019) Edscottite,  $\text{Fe}_5\text{C}_2$ , a new iron carbide mineral from the Ni-rich  
2024 Wedderburn IAB iron meteorite. *American Mineralogist*, 104, 1351–1355.
- 2025 MacPherson, G.J. (2014) Calcium-aluminum-rich inclusions in chondritic meteorites. In A.M.  
2026 Davis, H.D. Holland, and K.K. Turekian, Eds., *Treatise on Geochemistry, Vol. 1: Meteorites,*  
2027 *Comets, and Planets, Second Edition.* pp.139-179. Elsevier-Pergamon.
- 2028 MacPherson, G.J., Bullock, E.S., Janney, P.E., Kita, N., Ushikubo, T., Davis, A.M., Wadhwa, M.,  
2029 and Krot, A.N. (2010) Early solar nebula condensates do not have supracanonical initial  
2030  $^{26}\text{Al}/^{27}\text{Al}$ . *The Astrophysical Journal*, 711, L117–L121.
- 2031 MacPherson, G.J., Kita, N.T., Ushikubo, T., Bullock, E.S., and Davis, A.M. (2012) Well-resolved  
2032 variations in the formation ages for Ca-Al-rich inclusions in the early solar system. *Earth and*  
2033 *Planetary Science Letters*, 331, 43–54.
- 2034 Mai, C., Desch, S.J., and Boley, A.C., and Weiss, B.P. (2018) Magnetic fields recorded by  
2035 chondrules formed in nebular shocks. *The Astrophysical Journal*, 857, 96 (13 pp.).
- 2036 Mann, C.R., Boley, A.C., and Morris, M.A. (2016) Planetary embryo bow shocks as a mechanism  
2037 for chondrule formation. *The Astrophysical Journal*, 818, 103-123.
- 2038 Marrocchi, Y., Euverte, R., Villeneuve, J., Batanova, V., Welsch, B., Ferrière, L., and Jacquet, E.  
2039 (2019) Formation of CV chondrules by recycling of amoeboid olivine aggregate-like  
2040 precursors. *Geochimica et Cosmochimica Acta*, 247, 121-141.
- 2041 Mason, B. (1966) The enstatite chondrites. *Geochimica et Cosmochimica Acta*, 30, 23-39.
- 2042 Massalski, T.B., Park, F.R., and Vassalmillet, L.F. (1966) Speculations about plessite. *Geochimica*  
2043 *et Cosmochimica Acta*, 30, 649-662.

- 2044 McCoy, T.J., Pun, A., and Keil, K. (1991a) Spinel-bearing, Al-rich chondrules in two chondrite  
2045 finds from Roosevelt County, New Mexico: Indicators of nebular and parent-body processes.  
2046 *Meteoritics*, 26, 301-309.
- 2047 McCoy, T.J., Scott, E.R.D., Jones, R.H., Keil, K., and Taylor, G.J. (1991b) Composition of  
2048 chondrule silicates in LL3-5 chondrites and implications for their nebular history and parent  
2049 body metamorphism. *Geochimica et Cosmochimica Acta*, 55, 601-619.
- 2050 McNally, C.P., Hubbard, A., Yang, C-C., and Mac Low, M-M. (2014) Temperature fluctuations  
2051 driven by magnetorotational instability in protoplanetary disks. *The Astrophysical Journal*, 791,  
2052 62 (15pp).
- 2053 McSween, H.Y. Jr (1977a) Carbonaceous chondrites of the Ormans type: A metamorphic  
2054 sequence. *Geochimica et Cosmochimica Acta*, 44, 477-491.
- 2055 McSween, H.Y. Jr (1977b) On the nature and origin of isolated olivine grains in carbonaceous  
2056 chondrites. *Geochimica et Cosmochimica Acta*, 411-418.
- 2057 Mendybaev, R.A., Beckett, J.R., Grossman, L., Cooper, R.F., and Bradley, J.P. (2002)  
2058 Volatilization kinetics of silicon carbide in reducing gases: An experimental study with  
2059 application to the survival of presolar grains in the solar nebula. *Geochimica et Cosmochimica*  
2060 *Acta*, 66, 661-682.
- 2061 Mills, S.J., Hatert, F., Nickel, E.H., and Ferrais, G. (2009) The standardization of mineral group  
2062 hierarchies: Application to recent nomenclature proposals. *European Journal of Mineralogy*,  
2063 21, 1073-1080.
- 2064 Miura, Y., and Tomisaka, T. (1984) Composition and structural substitution of meteoritic  
2065 plagioclases (I). *Memoirs of the NIPR Special Issue*, 9, 210-225.

- 2066 Miyamoto, M., Mikouchi, T., and Jones, R.H. (2009) Cooling rates of porphyritic olivine  
2067 chondrules in the Semarkona (LL3.00) ordinary chondrite: A model for diffusional  
2068 equilibration of olivine during fractional crystallization. *Meteoritics & Planetary Science*, 44,  
2069 521-530.
- 2070 Morbidelli, A., Bitsch, B., Crida, A., Gounelle, M., Guillot, T., Jacobson, S.A., Johansen, A.,  
2071 Lambrechts, M., and Lega, E. (2016) Fossilized condensation lines in the Solar System  
2072 protoplanetary disk. *Icarus*, 267, 368–376.
- 2073 Morimoto, N., Fabries, J., Ferguson, A.K., Ginzburg, I.V., Ross, M., Seifert, F.A., Zussman, J.,  
2074 Aoki, K., and Gottardi, G. (1988) Nomenclature of pyroxenes. *American Mineralogist*, 73,  
2075 1123–1133.
- 2076 Morlok, A., Sutton, Y.C., Braithwaite, N.St.J., and Grady, M.M. (2012) Chondrules born in  
2077 plasma? Simulation of gas-grain interaction using plasma arcs with applications to chondrule  
2078 and cosmic spherule formation. *Meteoritics & Planetary Science*, 47, 2269-2280.
- 2079 Morris, M.A., and Boley, A.C. (2018) Formation of chondrules by shock waves. In S.A. Russell,  
2080 H.C. Connolly Jr., and A.N. Krot [Eds]. *Chondrules: Records of Protoplanetary Disk Processes*.  
2081 Cambridge, UK: Cambridge University Press, pp. 375-399.
- 2082 Morrison, S.M., and Hazen, R.M. (2020) An evolutionary system of mineralogy, part II:  
2083 interstellar and solar nebula primary condensation mineralogy (> 4.565 Ga). *American*  
2084 *Mineralogist*, in revision.
- 2085 Morrison, S.M., Liu, C., Eleish, A., Prabhu, A., Li, C., Ralph, J., Downs, R.T., Golden, J.J., Fox,  
2086 P., Hummer, D.R., Meyer, M.B., and Hazen, R.M. (2017) Network analysis of mineralogical  
2087 systems. *American Mineralogist*, 102, 1588-1596.

- 2088 Morrison, S.M., Downs, R.T., Eleish, A., Fox, P., Hummer, D.R., Hystad, G., Golden, J.J., Liu,  
2089 C., Prabhu, A., Zahirovic, S., and Hazen, R.M. (2020) Visualizing carbon minerals: Recent  
2090 advances in C mineral evolution, mineral ecology, and network analysis. *Frontiers in Earth*  
2091 *Sciences*, in press.
- 2092 Moynier, F., Dauphas, N., and Podosek, F.A. (2009) Search for  $^{70}\text{Zn}$  anomalies in meteorites. *The*  
2093 *Astrophysical Journal Letters*, 700, L92-L95.
- 2094 Mueller, G. (1962) Interpretation of micro-structures in carbonaceous meteorites. *Nature*, 196,  
2095 929–932.
- 2096 Müller, W.F., Kurat, G., and Kracher, A. (1979) Chemical and crystallographic study of  
2097 cronstedtite in the matrix of the Cochabamba (CM2) carbonaceous chondrite. *Tschermaks*  
2098 *Mineralogie und Petrographische Mitteilungen*, 26, 293-304.
- 2099 Müller, W.F., Weinbruch, S., Walter, R., and Müller-Beneke, G. (1995) Transmission electron  
2100 microscopy of chondrule minerals in the Allende meteorite: Constraints on the thermal and  
2101 deformational history of granular olivine-pyroxene chondrules. *Planetary and Space Science*,  
2102 43, 469-483.
- 2103 Murakami, T., and Ikeda, Y. (1994) Petrology and mineralogy of the Yamato-86751 CV3  
2104 chondrite. *Meteoritics*, 29, 397-409.
- 2105 Nagahara, H. (1982) Ni-Fe metals in Type 3 ordinary chondrites. *Memoirs of the NIPR Special*  
2106 *Issue*, 25, 86-96.
- 2107 Nagahara, H., and Kushiro, I. (1982) Petrology of chondrules, inclusions and isolated olivine  
2108 grains in ALH-77307 (CO3) chondrite. *Memoirs of the NIPR Special Issue*, 25, 66-77.

- 2109 Nagashima, K., Kita, N.T., and Luu, T.-H. (2018)  $^{26}\text{Al}$ - $^{26}\text{Mg}$  systematics of chondrules. In S.A.  
2110 Russell, H.C. Connolly Jr., and A.N. Krot, Eds., Chondrules: Records of Protoplanetary Disk  
2111 Processes, pp. 247-275. Cambridge University Press.
- 2112 Nakamura-Messenger, K., Clemett, S.J., Rubin, A.E., Choi, B.-G., Zhang, S., Rahman, Z.,  
2113 Oikawa, K., and Keller, L.P. (2012) Wassonite: A new titanium monosulfide mineral in the  
2114 Yamato 691 enstatite chondrite. American Mineralogist, 97, 807-815.
- 2115 Newton, J., Bischoff, A., Arden, J.W., Franchi, I.A., Geiger, T., Greshake, A., and Pillinger, C.T.  
2116 (1995) Acfer 094, a uniquely primitive carbonaceous chondrite from the Sahara. Meteoritics,  
2117 30, 47-56.
- 2118 Noguchi, T. (1989) Texture and chemical composition of pyroxenes in chondrules in carbonaceous  
2119 and unequilibrated ordinary chondrites. Proceedings of the NIPR Symposium on Antarctic  
2120 Meteorites, 2, 169-199.
- 2121 Noguchi, T. (1995) Petrology and mineralogy of the PCA 91082 chondrite and its comparison  
2122 with the Yamato-793495 (CR) chondrite. Proceedings of the NIPR Symposium on Antarctic  
2123 Meteorites, 8, 33-62.
- 2124 Olsen, E.J. (1983)  $\text{SiO}_2$ -bearing chondrules in the Murchison (C2) meteorite. In E.A. King, Ed.,  
2125 Chondrules and their Origins, pp. 223-234. Lunar and Planetary Institute.
- 2126 Oulton, J., Humayun, M., Fedkin, A. and Grossman, L. (2016) Chemical evidence for  
2127 differentiation, evaporation and recondensation from silicate clasts in Gujba. Geochimica et  
2128 Cosmochimica Acta, 177, 254-274.
- 2129 Pederson T.P. (1999) Schwertmannite and awaruite as alteration products in iron meteorites.  
2130 Meteoritics, 62, 5117.

- 2131 Pollack, J.B., Hubickyj, O., Bodenheimer, P., Lisauer, J.J., Podolak, M., and Greenzweig, Y.  
2132 (1996) Formation of the giant planets by concurrent accretion of solids and gas. *Icarus*, 124,  
2133 62-85.
- 2134 Pratesi, G., Caporali, S., Greenwood, R.C., Moggi Cecchi, V., and Franchi, I.A. (2019) A detailed  
2135 mineralogical, petrographic, and geochemical study of the highly reduced chondrite, Acfer 370.  
2136 *Meteoritics & Planetary Science*, 54, 2996-3017.
- 2137 Prinz, M., Weisberg, M.K., and Nehru, C.E. (1988) Gunlock, a new type 3 ordinary chondrite with  
2138 a golfball-sized chondrule. *Meteoritics*, 23, 297.
- 2139 Rambaldi, E.R., and Wasson, J.T. (1984) Metal and associated phases in Krymka and Chainpur:  
2140 Nebular formational processes. *Geochimica et Cosmochimica Acta*, 48, 1885-1897.
- 2141 Rambaldi, E.R., Rajan, R.S., and Housley, R.M. (1986) Roedderite in the Qingzhen (EH3)  
2142 chondrite. *Meteoritics*, 21, 141-149.
- 2143 Ramdohr, P. (1967) Chromite and chromite chondrules in meteorites. *Geochimica et*  
2144 *Cosmochimica Acta*, 31, 1961-1967.
- 2145 Reed, S.J.B. (1968) Perryite in the Kota-Kota and South Oman enstatite chondrites. *Mineralogical*  
2146 *Magazine*, 36, 850-854.
- 2147 Richter, F.M., Mendybaev, R.A., Christensen, J.N., Ebel, D., and Gaffney, A. (2011) Laboratory  
2148 experiments bearing on the origin and evolution of olivine-rich chondrules. *Meteoritics &*  
2149 *Planetary Science*, 46, 1152-1178.
- 2150 Robertson, B.E., Ellis, R.S., Furlanetto, S.R., and Dunlop, J.S. (2015) Cosmic reionization and  
2151 early star-forming galaxies: A joint analysis of new constraints from Planck and the Hubble  
2152 Space Telescope. *The Astrophysical Journal*, 802, L19-L23.

- 2153 Rubin, A.E. (1983) The Adhi Kot breccia and implications for the origins of chondrites and silica-  
2154 rich clasts in enstatite chondrites. *Earth and Planetary Science Letters*, 64, 201-212.
- 2155 Rubin, A.E. (1984) The Blithfield meteorite and the origin of sulfide-rich, metal-poor clasts and  
2156 inclusions in brecciated enstatite chondrites. *Earth and Planetary Science Letters*, 67, 273-283.
- 2157 Rubin, A.E. (1989) An olivine-microchondrule-bearing clast in the Krymka meteorite.  
2158 *Meteoritics*, 24,191–192.
- 2159 Rubin, A.E. (1990) Kamacite and olivine in ordinary chondrites: Intergroup and intragroup  
2160 relationships. *Geochimica et Cosmochimica Acta*, 54, 1217-1232.
- 2161 Rubin, A.E. (1991) Euhedral awaruite in the Allende meteorite: Implications for the origin of  
2162 awaruite- and magnetite-bearing nodules in CV3 chondrites. *American Mineralogist*, 76, 1356-  
2163 1362.
- 2164 Rubin, A.E. (1994a) Metallic copper in ordinary chondrites. *Meteoritics*, 29, 93-98.
- 2165 Rubin, A.E. (1994b) Euhedral tetrataenite in the Jelica meteorite. *Mineralogical Magazine*, 58,  
2166 215-221.
- 2167 Rubin, A.E. (1997a) Igneous graphite in enstatite chondrites. *Mineralogical Magazine*, 61, 699-  
2168 703.
- 2169 Rubin, A.E. (1997b) Sinoite ( $\text{Si}_2\text{N}_2\text{O}$ ): Crystallization from EL chondrite impact melts. *American*  
2170 *Mineralogist*, 82, 1001-1006.
- 2171 Rubin, A.E. (2000) Petrologic, geochemical and experimental constraints on models of chondrule  
2172 formation. *Earth-Science Reviews*, 50, 3–27.
- 2173 Rubin, A.E. (1984) Coarse-grained chondrule rims in type 3 chondrites. *Geochimica et*  
2174 *Cosmochimica Acta*, 48, 1779-1789.

- 2175 Rubin, A.E. (2006) A relict-grain-bearing porphyritic olivine compound chondrule from LL3.0  
2176 Semarkona that experienced limited remelting. *Meteoritics & Planetary Science*, 41, 1027-  
2177 1038.
- 2178 Rubin, A.E. (2010) Physical properties of chondrules in different chondrite groups: Implications  
2179 for multiple melting events in dusty environments. *Geochimica et Cosmochimica Acta*, 74,  
2180 4807-4828.
- 2181 Rubin, A.E. (2011) Origin of the differences in refractory-lithophile-element abundances among  
2182 chondrite groups. *Icarus*, 213, 547-558.
- 2183 Rubin, A.E. (2018) Evaluation of petrologic evidence for high partial pressures of SiO<sub>(g)</sub> in the  
2184 solar nebula. *Meteoritics & Planetary Science*, 53, 2596-2607.
- 2185 Rubin, A.E., and Grossman, J.N. (1985) Phosphate-sulfide assemblages and Al/Ca ratios in type  
2186 3 chondrites. *Meteoritics*, 20, 479-489.
- 2187 Rubin, A.E., and Kallemeyn, G.W. (1989) Carlisle Lakes and Allan Hills 85151: Members of a  
2188 new chondrite grouplet. *Geochimica et Cosmochimica Acta*, 53, 3035-3044.
- 2189 Rubin, A.E., and Kallemeyn, G.W. (1994) Pecora Escarpment 91002: A member of the new  
2190 Rumuruti (R) chondrite group. *Meteoritics*, 29, 255-264.
- 2191 Rubin, A.E., and Ma, C. (2017) Meteoritic minerals and their origins. *Chemie der Erde*, 77, 325-  
2192 385.
- 2193 Rubin, A.E., and Ma, C. (2020) *Meteorite Mineralogy*. Cambridge, UK: Cambridge University  
2194 Press, in press.
- 2195 Rubin, A.E., and Scott, E.R.D. (1997) Abee and related EH chondrite impact-melt breccias.  
2196 *Geochimica et Cosmochimica Acta*, 61, 425-435.

- 2197 Rubin, A.E., and Wasson, J.T. (1987) Chondrules, matrix and coarse-grained chondrule rims in  
2198 the Allende meteorite. *Geochimica et Cosmochimica Acta*, 52, 425-432.
- 2199 Rubin, A.E., and Wasson, J.T. (1988) Chondrules and matrix in the Ornans CO3 meteorite:  
2200 Possible precursor components. *Geochimica et Cosmochimica Acta*, 52, 425-432.
- 2201 Rubin, A.E., Scott, E.R.D., and Keil, K. (1982) Microchondrule-bearing clast in the Piancaldoli  
2202 LL3 meteorite: A new type 3 chondrite and its relevance to the history of chondrules.  
2203 *Geochimica et Cosmochimica Acta*, 46, 1763-1776.
- 2204 Rubin, A.E., James, J.A., Keck, B.D., Weeks, K.S., Sears, D.W.G., and Jarosewich, E. (1985) The  
2205 Colony meteorite and variations in CO3 chondrite properties. *Meteoritics*, 20, 175-196.
- 2206 Rubin, A.E., Wang, D., Kallemeyn, G.W., and Wasson, J.T. (1988) The Ningqiang meteorite:  
2207 Classification and petrology of an anomalous CV chondrite. *Meteoritics*, 23, 13-23.
- 2208 Rubin, A.E., Sailer, A.L., and Wasson, J.T. (1999) Troilite in the chondrules of type-3 ordinary  
2209 chondrites: Implications for chondrule formation. *Geochimica et Cosmochimica Acta*, 63,  
2210 2281-2298.
- 2211 Rubin, A.E., Kallemeyn, G.W., Wasson, J.T., Clayton, R.N., Mayeda, T.K., Grady, M.,  
2212 Verchovsky, A.B., Eugster, O., and Lorenzetti, S. (2003) Formation of metal and silicate  
2213 nodules in Gujba: A new Bencubbin-like meteorite fall. *Geochimica et Cosmochimica Acta*,  
2214 67, 3283-3298.
- 2215 Russell, S.A., Connolly, H.C. Jr., and Krot, A.N. [Eds]. (2018) Chondrules: Records of  
2216 Protoplanetary Disk Processes. Cambridge University Press.
- 2217 Russel, S.S., Lee, M.R., Arden, J.W., and Pillinger, C.T. (1995) The isotopic composition and  
2218 origins of silicon nitride in the ordinary and enstatite chondrites. *Meteoritics*, 30, 399-404.

- 2219 Ruzicka, A. (1990) Deformation and thermal histories of chondrules in the Chainpur (LL3.4)  
2220 chondrite. *Meteoritics*, 25, 101-114.
- 2221 Ruzicka, A. (2012) Chondrule formation by repeated evaporative melting and condensation in  
2222 collisional debris clouds around planetesimals. *Meteoritics & Planetary Science*, 47, 2218-  
2223 2236.
- 2224 Sack, R.O., and Ghiorso, M.S. (2017) Ti<sup>3+</sup>- and Ti<sup>4+</sup>-rich fassaites at the birth of the solar system:  
2225 Thermodynamics and applications. *American Journal of Science*, 317, 807-845.
- 2226 Sanders, I.S., and Scott, E.R.D. (2012) The origin of chondrules and chondrites: Debris from low-  
2227 velocity impacts between molten planetesimals? *Meteoritics & Planetary Science*, 47, 2170-  
2228 2192.
- 2229 Sanders, I.S., and Scott, E.R.D. (2018) Making chondrules by splashing molten planetesimals: The  
2230 dirty impact plume model. In S.A. Russell, H.C. Connolly Jr., and A.N. Krot, Eds., *Chondrules:  
2231 Records of Protoplanetary Disk Processes*, pp. 361-374. Cambridge University Press.
- 2232 Schatz, H. (2010) The evolution of elements and isotopes. *Elements*, 6, 13-17.
- 2233 Schertl, H.-P., Mills, S.J., and Maresch, W.V. (2018) A Compendium of IMA-Approved Mineral  
2234 Nomenclature. International Mineralogical Association.
- 2235 Schrader, D.L., Nagashima, K., Krot, A.N., Ogliore, R.C., Yin, Q.-Z., Amelin, Y., Stirling, C.H.,  
2236 and Kaltenbach, A. (2017) Distribution of <sup>26</sup>Al in the CR chondrite chondrule-forming region  
2237 of the protoplanetary disk. *Geochimica et Cosmochimica Acta*, 201, 275–302.
- 2238 Schulze, H., Bischoff, A., Palme, H., Spettel, B., Dreibus, G., and Otto, J. (1994) Mineralogy and  
2239 chemistry of Rumuruti: The first meteorite fall of the new R chondrite group. *Meteoritics*, 29,  
2240 275-286.

- 2241 Scott, E.R.D. (1988) A new kind of primitive chondrite, Allan Hills 85085. Earth and Planetary  
2242 Science Letters, 91, 1-18.
- 2243 Scott, E.R.D., and Clarke, R.S. Jr. (1979) Identification of clear taenite in meteorites as ordered  
2244 FeNi. Nature, 281, 113-124.
- 2245 Scott, E.R.D., and Jones, R.H. (1990) Disentangling nebular and asteroidal features of CO<sub>3</sub> of  
2246 carbonaceous chondrites. Geochimica et Cosmochimica Acta, 54, 2485-2502.
- 2247 Scott, E.R.D., and Krot, A.N. (2014) Chondrites and their components. In A.M. Davis,  
2248 H.D.Holland, and K.K.Turekian, Eds., Treatise on Geochemistry, Vol. 1: Meteorites, Comets,  
2249 and Planets, Second Edition, pp. 65-137. Elsevier-Pergamon.
- 2250 Scott, E.R.D., and Rajan, S. (1981) metallic minerals, thermal histories, and parent bodies of some  
2251 xenolithic ordinary chondrites. Geochimica et Cosmochimica Acta, 45, 53-67.
- 2252 Scott, E.R.D., and Taylor, G.J. (1983) Chondrules and other components in C, O, and E chondrites:  
2253 Similarities in their properties and origins. Journal of Geophysical Research, 88, B275-B286.
- 2254 Scott, E.R.D., Taylor, G.J., and Maggiore, P. (1982) A new LL3 chondrite, Allan Hills 79003, and  
2255 observations on matrices in ordinary chondrites. Meteoritics, 17, 19-31.
- 2256 Scott, E.R.D., Jones, R.H., and Rubin, A.E. (1994) Classification, metamorphic history, and pre-  
2257 metamorphic composition of chondrules. Geochimica et Cosmochimica Acta, 58, 1203-1209.
- 2258 Sears, D.W.G., and Hasan, F.A. (1987) The type three ordinary chondrites: A review. Surveys in  
2259 Geophysics, 9, 43-97.
- 2260 Sears, D.W.G., Kallemeyn, G.W., and Wasson, J.T. (1982) The compositional classification of  
2261 chondrites. II. The enstatite chondrite groups. Geochimica et Cosmochimica Acta, 46, 597-  
2262 608.

- 2263 Sears, D.W.G., Lu, J., Benoit, P.H., DeHart, J.M., and Lofgren, G.E. (1992) A compositional  
2264 classification scheme for meteoritic chondrules. *Nature*, 357, 207-210.
- 2265 Sears, D.W.G., Morse, A.D., Hutchison, R., Guimon, R.K., Lu, J., Alexander, C.M.O'D., Benoit,  
2266 P.H., Wright, I., Pillinger, C., Xie, T., and Lipschutz, M.E. (1995) Metamorphism and aqueous  
2267 alteration in low petrographic type ordinary chondrites. *Meteoritics*, 30, 169-181.
- 2268 Sheng, Y.J., Hutcheon, I.D., and Wasserburg, G.J. (1991a) Origin of plagioclase-olivine inclusions  
2269 in carbonaceous chondrites. *Geochimica et Cosmochimica Acta*, 55, 581-599.
- 2270 Sheng, Y.J., Beckett, J.R., Hutcheon, I.D., and Wasserberg, G.J. (1991b) Experimental constraints  
2271 on the origin of plagioclase-olivine inclusions and CA chondrules. Abstracts of the Lunar and  
2272 Planetary Science Conference, 22, 1231.
- 2273 Shibata, Y. (1996) Opaque minerals in Antarctic CO3 carbonaceous chondrites. Yamato-74135,  
2274 -790992, -79717, -81020, -81025, -82050, and Allan Hills 77307. Proceedings of the NIPR  
2275 Symposium on Antarctic Meteorites, 9, 79-96.
- 2276 Shimizu, M., Yoshida, H., and Mandarino, J.A. (2002) The new mineral species keilite, (Fe,Mg)S,  
2277 the iron-dominant analogue of niningerite. *Canadian Mineralogist*, 40, 1687-1692.
- 2278 Shu, F.H., Shang, H., and Lee, T. (1996) Toward an astrophysical theory of chondrites. *Science*,  
2279 271, 1545-1552.
- 2280 Simon, S.B., and Haggerty, S.E. (1980) Bulk compositions of chondrules in the Allende meteorite.  
2281 Proceedings of the Lunar and Planetary Science Conference, 11, 901-927.
- 2282 Simon, S.B., Grossman, L., Podosek, F.A., Zinner, E., and Prombo, C.A. (1994) Petrography,  
2283 composition, and origin of large chromian spinels from the Murchison meteorite. *Geochimica*  
2284 *et Cosmochimica Acta*, 58, 1313-1334.

- 2285 Simon, S.B., Grossman, L., Casanova, I., Symes, S., Benoit, P., Sears, D.W.G., and Wacker, J.F.  
2286 (1995) Axtell, a new CV3 chondrite from Texas. *Meteoritics*, 30, 42-46.
- 2287 Singerling, S.A., and Brearley, A.J. (2018) Primary iron sulfides in CM and CR carbonaceous  
2288 chondrites: Insights into nebular processes. *Meteoritics & Planetary Science*, 53, 2078-2106.
- 2289 Smith, D.G.W., Miura, Y., and Launspach, S. (1993) Fe, Ni, and Co variations in the metals from  
2290 some Antarctic chondrites. *Earth and Planetary Science Letters*, 120, 487-498.
- 2291 Sorrell, W. (1995) Nebular lightning and the chondrule factory. *Comments of Astrophysics*, 18,  
2292 151-159.
- 2293 Stöffler, D., Keil, K., and Scott, E.R.D. (1991) Shock metamorphism of ordinary chondrite  
2294 meteorites. *Geochimica et Cosmochimica Acta*, 55, 3845-3867.
- 2295 Tachibana, S., and Huss, G.R. (2005) Sulfur isotopic composition of putative primary troilite in  
2296 chondrules from Bishunpur and Semarkona. *Geochimica et Cosmochimica Acta*, 69, 3075-  
2297 3097.
- 2298 Taylor, G.J., and Heymann, D. (1971) Postshock thermal histories of reheated chondrites. *Journal*  
2299 *of Geophysical Research*, 76, 1879-1893.
- 2300 Taylor, G.J., Okada, A., Scott, E.R.D., Rubin, A.E., Huss, G.R., and Keil, K. (1981) The  
2301 occurrence and implications of carbide-magnetite assemblages in unequilibrated ordinary  
2302 chondrites. *Proceedings of the Lunar and Planetary Science Conference*, 12, 1076-1078.
- 2303 Teitler, S.A., Paque, J.M., Cuzzi, J.N., and Hogan, R.C. (2010) Statistical tests of chondrule  
2304 sorting. *Meteoritics & Planetary Science*, 45, 1124-1135.
- 2305 Tomeoka, K., and Buseck, P.R. (1990) Phyllosilicates in the Mokoia CV carbonaceous chondrite:  
2306 Evidence for aqueous alteration in an oxidizing condition. *Geochimica et Cosmochimica Acta*,  
2307 54, 1787-1796.

- 2308 Töpel-Schadt, J., and Müller, W.F. (1985) The submicroscopic structure of the unequilibrated  
2309 ordinary chondrites, Chainpur, Mezö-Madaras, and Tieschitz. *Meteoritics*, 27, 136-143.
- 2310 Trieloff, M., Storck, J.-C., Mostefaoui, S., El Goresy, A., Hopp, J., Ludwig, T., and Altherr, R.  
2311 (2013) A precise  $^{53}\text{Mn}$ - $^{53}\text{Cr}$  age of sphalerites from the primitive EH3 chondrite Sahara 97158.  
2312 *Meteoritics & Planetary Science Supplement*, 76, 5251.
- 2313 Trinquier, A., Birck, J., and Allegre, C.J. (2007) Widespread  $^{54}\text{Cr}$  heterogeneity in the inner solar  
2314 system. *The Astrophysical Journal*, 655, 1179-1185.
- 2315 Trinquier, A., Elliott, T., Ulfbeck, D., Coath, C., Krot, A.N., and Bizzarro, M. (2009) Origin of  
2316 nucleosynthetic isotope heterogeneity in the solar protoplanetary disk. *Science*, 324, 374-376.
- 2317 Van Schmus, W.R., and Wood, J.A. (1967) A chemical-petrologic classification for the chondrite  
2318 meteorites. *Geochimica et Cosmochimica Acta*, 31, 747-754.
- 2319 Wang, Y., and Hsu, W. (2009) Petrology and mineralogy of the Ningqiang carbonaceous  
2320 chondrite. *Meteoritics & Planetary Science*, 44, 763-780.
- 2321 Wang, Y., Hsu, W., Li, X., Li, Q., Liu, Y., and Tang, G. (2016) Petrology, mineralogy, and oxygen  
2322 isotope compositions of aluminum-rich chondrules from CV3 chondrites. *Meteoritics &*  
2323 *Planetary Science*, 51, 116-137.
- 2324 Warren, P. (2011) Stable-isotopic anomalies and the accretionary assemblage of the Earth and  
2325 Mars: A subordinate role for carbonaceous chondrites. *Earth and Planetary Science Letters*,  
2326 311, 93-100.
- 2327 Wasserburg, G.J., Wimpenny, J., and Yin, Q.-Z. (2012) Mg isotopic heterogeneity, Al-Mg  
2328 isochrons, and canonical  $^{26}\text{Al}/^{27}\text{Al}$  in the early solar system. *Meteoritics & Planetary Science*,  
2329 47, 1980–1997.

- 2330 Wasson, J.T., and Krot, A.N. (1994) Fayalite-silica association in unequilibrated ordinary  
2331 chondrites: Evidence for aqueous alteration on a parent body. *Earth and Planetary Science*  
2332 *Letters*, 122, 403-416.
- 2333 Wasson, J.T., and Rubin, A.E. (2003) Ubiquitous low-FeO relict grains in type-II chondrules and  
2334 limited overgrowths on relicts and high-FeO phenocrysts following the final melting event.  
2335 *Geochimica et Cosmochimica Acta*, 67, 2239-2250.
- 2336 Wasson, J.T., and Wai, C.M. (1970) Composition of the metal, schreibersite and perryite of  
2337 enstatite achondrites and the origin of enstatite chondrites and achondrites. *Geochimica et*  
2338 *Cosmochimica Acta*, 34, 169-184.
- 2339 Wasson, J.T., Krot, A.N., Lee, M.S., and Rubin, A.E. (1995) Compound chondrules. *Geochimica*  
2340 *et Cosmochimica Acta*, 59, 1847-1869.
- 2341 Watanabe, S., Kitamura, M., and Morimoto, N. (1986) Oscillatory zoning of pyroxenes in ALH-  
2342 77214 (L3). *Symposium on Antarctic Meteorites*, 11, 74-75.
- 2343 Weber, D., and Bischoff, A. (1997) Refractory inclusions in the CR chondrite Acler 059-El Djouf  
2344 001: Petrology, chemical composition, and relationship to inclusion populations in other types  
2345 of carbonaceous chondrites. *Chemie der Erde*, 57, 1-24.
- 2346 Weinbruch, S., Palme, H., Müller, W.F., and El Goresy, A. (1990) FeO-rich rims and veins in  
2347 Allende forsterite: Evidence for high-temperature condensation at oxidizing conditions.  
2348 *Meteoritics*, 25, 115-125.
- 2349 Weinbruch, S., Armstrong, J.T., and Palme, H. (1994) Constraints on the thermal history of the  
2350 Allende parent body as derived from olivine-spinel thermometry and Fe/Mg interdiffusion in  
2351 olivine. *Geochimica et Cosmochimica Acta*, 58, 1019-1030.

- 2352 Weinbruch, S., Palme, H., and Spettel, B. (2000) Refractory forsterite in primitive meteorites:  
2353       Condensates from the solar nebula? *Meteoritics and Planetary Science*, 35, 161–171.
- 2354 Weisberg, M.K., and Kimura, M. (2012) The unequilibrated enstatite chondrites. *Chemie der Erde*,  
2355       72, 101-115.
- 2356 Weisberg, M.K., Prinz, M., and Nehru, C.E. (1988) Petrology of ALH85085: A chondrite with  
2357       unique characteristics. *Earth and Planetary Science Letters*, 91, 19-32.
- 2358 Weisberg, M.K., McCoy, T., and Krot, A.N. (2006) Systematics and evaluation of meteorite  
2359       classification. In D. Lauretta and H. McSween, Eds., *Meteorites and the Early Solar System II*,  
2360       pp. 19-52. University of Arizona Press.
- 2361 Weyrauch, M., and Bischoff, A. (2012) Macrochondrules in chondrites – Formation by melting of  
2362       mega-sized dust aggregates and/or by rapid collisions at high temperatures? *Meteoritics &*  
2363       *Planetary Science*, 47, 2237-2250.
- 2364 Weyrauch, M., Horstmann, M., and Bischoff, A. (2018) Chemical variations of sulfides and metal  
2365       in enstatite chondrites – Introduction of a new classification scheme. *Meteoritics & Planetary*  
2366       *Science*, 53, 394-415.
- 2367 Whitby, J.A., Gilmour, J.D., Turner, G., Prinz, M., and Ash, R.D. (2002) Iodine-xenon dating of  
2368       chondrules from the Qingzhen and Kota Kota enstatite chondrites. *Geochimica et*  
2369       *Cosmochimica Acta*, 66, 347-359.
- 2370 Wlotzka, F. (1993) A weathering scale for the ordinary chondrites (abstract). *Meteoritics*, 28, 460.
- 2371 Wombacher, F., Rehkämper, M., Mezger, K., Bischoff, A., and Münker, C. (2008) Cadmium  
2372       stable isotope cosmochemistry. *Geochimica et Cosmochimica Acta*, 72, 646-667.
- 2373 Wood, J.A. (1967) Chondrules: their metallic minerals, thermal histories, and parent planets.  
2374       *Icarus*, 6, 1-49.

- 2375 Wood, J.A. (1996a) Processing of chondritic and planetary material in spiral density waves in the  
2376 nebula. *Meteoritics*, 31, 641-645.
- 2377 Wood, J.A. (1996b) Unresolved issues in the formation of chondrules and chondrites. In R.  
2378 Hewins, R.H. Jones, and E.R.D. Scott, Eds., *Chondrules and the Protoplanetary Disk*, pp. 55-  
2379 70. Cambridge University Press.
- 2380 Wood, J.A., and Hashimoto, A. (1993) Mineral equilibrium in fractionated nebular systems.  
2381 *Geochimica et Cosmochimica Acta*, 57, 2377-2388.
- 2382 Wood, J.A., and Holmberg, B.B. (1994) Constraints placed on chondrule-forming process by  
2383 merrihueite in the Mezo-Madaras chondrite. *Icarus*, 108, 309-324.
- 2384 Zanda, B., Bouret-Denise, M., Peron, C., and Hewins, R.H. (1994) Origin and metamorphic  
2385 redistribution of silicon, chromium, and phosphorus in the metal of chondrites. *Science*, 265,  
2386 1846-1849.
- 2387 Zhang, A., and Hsu, W. (2009) Refractory inclusions and aluminum-rich chondrules in Sayh al  
2388 Uhaymir 290 CH chondrite: Petrography and mineralogy. *Meteoritics & Planetary Science*, 44,  
2389 787-804.
- 2390 Zhang, Y., Huang, S., Schneider, D., Benoit, P.H., and Sears, D.W.G. (1996) Pyroxene structures,  
2391 cathodoluminescence and thermal history of the enstatite chondrites. *Meteoritics and Planetary  
2392 Science*, 31, 87-96.
- 2393 Zhdankin, V., Boldryev, S., and Mason, J. (2017) Influence of a large-scale field on energy  
2394 dissipation in magnetohydrodynamic turbulence. *Monthly Notices of the Royal Astronomical  
2395 Society*, 468, 4025-4029.

- 2396 Zolensky, M., Gounelle, M.U., Mikouchi, T., Ohsumi, K., Le, L., Hagiya, K., and Tachikawa, O.  
2397 (2008) Andreyivanovite: A second new phosphide from the Kaidun meteorite. American  
2398 Mineralogist, 93, 1295-1299.  
2399

2400 **Table 1.** Chronology of nebular processes that affect mineral evolution. “Part” refers to the multi-part evolutionary system of mineralogy.

2401

2402	<b>Object</b>	<b>Earliest Age</b>	<b>Latest Age</b>	<b>Description</b>	<b>Part</b>	<b>Reference*</b>
2403	Stardust	~13 Ga	4.58 Ga	Presolar grains are distinguished by their extreme isotopic anomalies.	I	1-3
2404						
2405	URIs	4567.3 Ma	<4567.0 Ma	Though usually grouped with CAIs, ultra-refractory inclusions display extreme	II	4-7
2406				(x 1000) enrichment in Sc, Zr, Ti, and other elements that lead to distinctive suites		
2407				of minerals.		
2408						
2409	CAIs	4567.3 Ma	4567.0 Ma	CAIs formed in a high-temperature, high gas/dust region near the proto-sun. Within	II	8-10
2410				2 million years, most CAIs had migrated to beyond proto-Jupiter’s orbit under the		
2411				influence of strong solar winds.		
2412						
2413	AOAs	< 4567.3 Ma	4567.0 Ma	Amoeboid olivine aggregates form at lower temperatures than CAIs and URIs,	II	7,11,12
2414				but still in a low-pressure region close to the proto-sun, with high gas/dust.		
2415				Some AOAs incorporate CAIs and thus postdate the first CAIs.		
2416						
2417	Embryos	~4567 Ma		By the time the protoplanetary disk was ~1 million years old, embryonic Jupiter	III	13-16
2418				(mass > 20 Earth mass) created a gravitational barrier between the inner and outer		
2419				solar system. Isotopic studies of iron meteorites suggest that their parent bodies		
2420				must have reached diameters of 10 to 100 km within the first 500,000 years.		
2421						
2422	Chondrules**	~4566 Ma	~4561 Ma	Chondrules vary widely in their physical and chemical characteristics, but most	III	9,17-19
2423				(if not all) chondrules significantly postdate CAIs. Chondrules represent igneous		
2424				processing of nebular material at high temperatures in regions with high dust/gas.		
2425						
2426	CO	4565.6	4564.7			20

2427				
2428	CV	4565.1 +/- 0.8		21,22
2429		4565.6 +/- 1.0		23
2430		4564.5 +/- 0.5		24
2431		4564.3 +/- 0.8		25
2432				
2433	CR	4563.7 +/- 0.6		26
2434		4563.6 +/- 0.6		27
2435				
2436	CB	4562.5 +/- 0.2		28
2437		4562.7 +/- 0.5		29
2438		4562.3 +/- 0.4		30
2439				
2440	EH	4564	4561	31
2441		4562.7 +/- 0.5		
2442				

---

2443 \* 1. Davis (2011); 2. Heck et al. (2020); 3. Hazen & Morrison (2020); 4. El Goresy et al. (2002); 5. Rubin & Ma (2017); 6. Krot et al. (2019); 7. Morrison & Hazen  
2444 (2020); 8. Connelly et al. (2012); 9. Kita et al. (2013); 10. Krot (2019); 11. Grossman & Steele (1976); 12. Krot et al. (2004); 13. Kruijer et al. (2014); 14.  
2445 Lambrechts et al. (2014); 15. Morbidelli et al. (2015); 16. Kruijer et al. (2017); 17. Bollard et al. 2017; 18. Nagashima et al. (2018); 19. Connelly & Bizzarro  
2446 (2018); 20. Kurahashi et al. (2008); 21. Budde et al. (2015); 22. Kleine et al. (2018); 23. Amelin & Krot (2007); 24. Connelly et al. (2008); 25. Connelly & Bizzarro  
2447 (2009); 26. Kleine et al. (2018); 27. Schrader et al. (2017); 28. Bollard et al. (2015); 29. Krot et al. (2005); 30. Gilmour et al. (2009); 31. Whitby et al. (2002); 32.  
2448 Tieloff et al. (2013)

2449  
2450 \*\* Alternative Pb-Pb age measurements of unequilibrated chondrites suggest that the earliest chondrules formed contemporaneously with CAIs at 4567.30 +/- 0.16  
2451 Ma, and extending to 4564.7 +/- 0.3 Ma. According to this model, most chondrules were produced within the first 1 million years of the protoplanetary disk  
2452 (Connelly et al. 2012; Bollard et al. 2017; Connelly & Bizzarro 2018; Krot 2019).

---

2453

2454 **Table 2. 43 primary mineral phases in chondrules.**

2455

2456	<b>Group</b>	<b>Species (Formula)</b>	<b>Natural Kind</b>	<b>Characteristics</b>	<b>References</b>
2457	<b>NATIVE ELEMENTS</b>				
2458					
2459		<b>Iron (Fe,Ni) [“kamacite”]</b>	<i>PC iron</i>	Occurs as a primary phase with up to 10 wt. % Ni	1-3
2460					
2461		<b>Taenite (Fe,Ni)</b>	<i>PC taenite</i>	Typically 10 to 50 wt. % Ni	1,4-7
2462					
2463		<b>Tetrataenite (Fe,Ni)</b>	<i>PC tetrataenite</i>	Typically ~50 wt. % Ni	1,5,6,8,9
2464					
2465		<b>Awaruite (Ni<sub>2</sub>Fe to Ni<sub>3</sub>Fe)</b>	<i>PC awaruite</i>	Typically 65 to 75 wt. % Ni	1,10,11
2466					
2467		<b>Graphite (C)</b>	<i>PC graphite</i>	A common minor phase in enstatite chondrites	1,12,13
2468					
2469	<b>CARBIDES</b>				
2470					
2471		<b>Cohenite [(Fe,Ni)<sub>3</sub>C]</b>	<i>PC cohenite</i>	Associated with haxonite and magnetite	1,3,10,14-18
2472					
2473		<b>Haxonite [(Fe,Ni)<sub>23</sub>C<sub>6</sub>]</b>	<i>PC haxonite</i>	Associated with cohenite and magnetite	3,15,17,18
2474					
2475	<b>NITRIDES</b>				
2476					
2477		<b>Sinoite (Si<sub>2</sub>N<sub>2</sub>O):</b>	<i>PC sinoite</i>	Micron-scale needles in metal nodules from an EL3 clast	19,20
2478					
2479	<b>PHOSPHIDES</b>				
2480					
2481		<b>Schreibersite [(Fe,Ni)<sub>3</sub>P]</b>	<i>PC schreibersite</i>	Occurs as exsolution from P-rich Fe-Ni alloys	1,21-23
2482					
2483	<b>SILICIDES</b>				
2484					
2485		<b>Perryite [(Ni,Fe)<sub>8</sub>(Si,P)<sub>3</sub>]</b>	<i>PC perryite</i>	A minor phase in enstatite chondrites	12,24,25
2486					
2487					

2488	<b>SULFIDES</b>			
2489				
2490	<b>Troilite (FeS)</b>	<i>PC troilite</i>	The most common primary chondrule sulfide	1-3,26-31
2491				
2492	<b>Pentlandite [(Fe,Ni)<sub>9</sub>S<sub>8</sub>]</b>	<i>PC pentlandite</i>	Occurs in unequilibrated OC and CC meteorites	1,27,32-34
2493				
2494	<b>Alabandite (MnS)</b>	<i>PC alabandite</i>	Occurs with other reduced sulfides in EL chondrites	1-3,35-38
2495				
2496	<b>Caswellsilverite (NaCrS<sub>2</sub>)</b>	<i>PC caswellsilverite</i>	Occurs with other reduced sulfides in enstatite chondrites	1-3,35-38
2497				
2498	<b>Daubréelite (FeCr<sub>2</sub>S<sub>4</sub>)</b>	<i>PC daubréelite</i>	Occurs with other reduced sulfides in enstatite chondrites	1-3,35-38
2499				
2500	<b>Ninningerite (MgS)</b>	<i>PC niningerite</i>	Occurs with other reduced sulfides in EH chondrites	1-3,35-38
2501				
2502	<b>Oldhamite (CaS)</b>	<i>PC oldhamite</i>	Occurs with other reduced sulfides in enstatite chondrites	1-3,35-38
2503				
2504	<b>Sphalerite (ZnS)</b>	<i>PC sphalerite</i>	A rare primary phase in EH enstatite chondrite Y-691	39
2505				
2506	<b>Wassonite (TiS)</b>	<i>PC wassonite</i>	A rare primary phase in EH enstatite chondrite Y-691	40
2507				
2508	<b>OXIDES</b>			
2509				
2510	<b>Spinel (MgAl<sub>2</sub>O<sub>4</sub>)</b>	<i>PC spinel</i>	Spinel is a common, if minor, primary OC chondrule phase	1,41-48
2511				
2512	<b>Chromite (Fe<sup>2+</sup>Cr<sub>2</sub>O<sub>4</sub>)</b>	<i>PC chromite</i>	A common oxide phase in UC and CC chondrules	1,49-52
2513				
2514	<b>Magnetite (Fe<sup>2+</sup>Fe<sup>3+</sup><sub>2</sub>O<sub>4</sub>)</b>	<i>PC magnetite</i>	In carbide-magnetite assemblages; with Fe-Ni alloys	1,27,34,53-56
2515				
2516	<b>Rutile (TiO<sub>2</sub>)</b>	<i>PC rutile</i>	A minor phase in plagioclase-olivine inclusions	47
2517				
2518	<b>Ilmenite (FeTiO<sub>3</sub>)</b>	<i>PC ilmenite</i>	In Na-Al-rich chondrules; plagioclase-olivine inclusions	47,57
2519				

2520	<b>Armalcolite</b> [(Mg,Fe <sup>2+</sup> )Ti <sub>2</sub> O <sub>5</sub> ]	<i>PC armalcolite</i>	A minor phase in plagioclase-olivine inclusions	47
2521				
2522	<b>Ferropseudobrookite</b> (Fe <sup>2+</sup> Ti <sub>2</sub> O <sub>5</sub> )	<i>PC ferropseudobrookite</i>	Euhedral crystals in Allan Hills 77015 (EL3)	58,59
2523				
2524	<b>Perovskite</b> (CaTiO <sub>3</sub> )	<i>PC perovskite</i>	A minor phase in plagioclase-olivine inclusions	47
2525				
2526	<b>Zirconolite</b> (CaZrTi <sub>2</sub> O <sub>7</sub> )	<i>PC zirconolite</i>	A minor phase in plagioclase-olivine inclusions	47
2527				
2528	<b>PHOSPHATES</b>			
2529				
2530	<b>Merrillite</b> [Ca <sub>9</sub> NaMg(PO <sub>4</sub> ) <sub>7</sub> ]	<i>PC merrillite</i>	Minor phase in glass-rich and silica-pyroxene chondrules	48,60,61
2531				
2532	<b>SILICATES</b>			
2533	<b>Cristobalite</b> (SiO <sub>2</sub> )	<i>PC cristobalite</i>	Occurs in silica-rich chondrules in OC and EC chondrites	18,61-63
2534				
2535	<b>Tridymite</b> (SiO <sub>2</sub> )	<i>PC tridymite</i>	Occurs in silica-rich chondrules in OC and EC chondrites	61-64
2536				
2537	<b>Silica Glass</b> (SiO <sub>2</sub> )	<i>PC silica glass</i>	In silica-rich chondrules from both NC and CC chondrites	61,63,65,66
2538				
2539	<b>Olivine</b> [(Mg,Fe) <sub>2</sub> SiO <sub>4</sub> ]	<i>PC olivine</i>	A common primary chondrule phase in all chondrite types	1-3,67
2540				
2541	<b>Orthoenstatite</b> [(Mg,Fe)SiO <sub>3</sub> ]	<i>PC orthoenstatite</i>	Less common than clinoenstatite; in OC, EC, and CC	1-3,33,68-71
2542				
2543	<b>Clinoenstatite</b> [(Mg,Fe)SiO <sub>3</sub> ]	<i>PC clinoenstatite</i>	A common primary chondrule phase in all chondrite types	1-3,70,72
2544				
2545	<b>Pigeonite</b> [(Mg,Fe,Ca)SiO <sub>3</sub> ]	<i>PC pigeonite</i>	As crystals and as layers coating clinoenstatite	1,64,70,73-74
2546				
2547	<b>Augite</b> [(Ca,Mg,Fe)(Mg,Fe,±Al,±Ti <sup>3+</sup> )(±Al,±Ti <sup>4+</sup> ,Si)SiO <sub>6</sub> ]			
2548		<i>PC augite</i>	A common primary chondrule phase	1,57,70,74-76
2549				

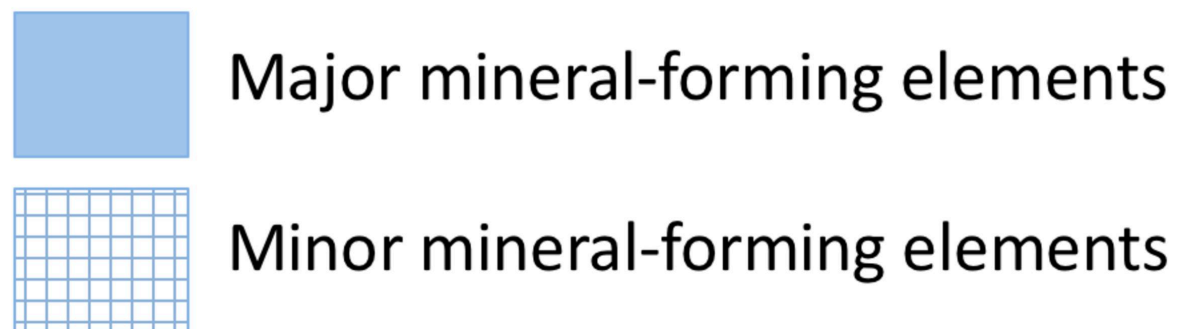
2550	<b>Anorthite</b> [(Ca,Na)(Al,Si) <sub>2</sub> Si <sub>2</sub> O <sub>8</sub> ]	<i>PC anorthite</i>	A common primary phase; notable in Al-rich chondrules	1,64,77-82
2551				
2552	<b>Albite</b> (NaAlSi <sub>3</sub> O <sub>8</sub> )	<i>PC albite</i>	Occurs with ferropseudobrookite in Allan Hills 77015 (EL3)	58,59
2553				
2554	<b>Nepheline</b> [Na <sub>3</sub> K(Al <sub>4</sub> Si <sub>4</sub> O <sub>16</sub> )]	<i>PC nepheline</i>	Epitaxial intergrowths with anorthite; Al-rich chondrules	1,68,74,77
2555				
2556	<b>Sapphirine</b> [Mg <sub>4</sub> (Mg <sub>3</sub> Al <sub>9</sub> )O <sub>4</sub> (Si <sub>3</sub> Al <sub>9</sub> O <sub>36</sub> )]	<i>PC sapphirine</i>	A minor phase in plagioclase-olivine inclusions	47,74
2557				
2558	<b>Roedderite</b> [(Na,K) <sub>2</sub> Mg <sub>5</sub> Si <sub>12</sub> O <sub>30</sub> ]	<i>PC roedderite</i>	A minor phase in silica-rich chondrules	83-86
2559				
2560	<b>Silicate Glass</b> (Ca,Mg,Al,Si,O)	<i>PC silicate glass</i>	Common in chondrule mesostasis	60
2561				
2562				

---

2563 **References:** 1. Brearley & Jones (1998); 2. Rubin & Ma (2017); 3. Rubin & Ma (2020); 4. Afiattalab & Wasson (1980); 5. Scott & Rajan  
2564 (1981); 6. Nagahara (1982); 7. Wood (1967); 8. Bevan & Axon (1980); 9. Rubin (1994b); 10. Taylor et al. (1981); 11. Smith et al. (1993); 12.  
2565 Keil (1968); 13. Leitch & Smith (1980); 14. Scott et al. (1982); 15. Scott & Jones (1982); 16. Herndon & Rudee (1978); 17. Shibata (1996); 18.  
2566 Rubin (1983); 19. Lin et al. (2011); 20. El Goresy et al. (2011); 21. Wasson & Wei (1970); 22. Rambaldi & Wasson (1984); 23. Zanda et al.  
2567 (1994); 24. Reed (1968); 25. Lehner et al. (2010); 26. Rubin et al. (1999); 27. Krot et al. (1997b); 28. Lauretta et al. (1996); 29. Singerling &  
2568 Brearley (2018); 30. El Goresy et al. (1988); 31. Ikeda (1989a); 32. Jones & Scott (1989); 33. Jones (1996); 34. Barth et al. (2018); 35. Buseck  
2569 & Holdsworth (1972); 36. Fogel (1997); 37. Avril et al. (2013); 38. Weyrauch et al. (2018); 39. El Goresy & Ehlers (1989); 40. Nakamura-  
2570 Messenger et al. (2012); 41. Bischoff & Keil (1983); 42. Ikeda (1980); 43. McCoy et al. (1991a); 44. Wang et al. (2016); 45. McSween  
2571 (1977b); 46. Simon et al. (1994); 47. Sheng et al. (1991b); 48. Krot et al. (1993); 49. Bunch et al. (1967); 50. Davy et al. (1978); 51. Johnson &  
2572 Prinz (1991); 52. Weinbruch et al. (1994); 53. Taylor et al. (1981); 54. Haggerty & McMahan (1979); 55. Ikeda (1983); 56. Scott & Jones  
2573 (1990); 57. Bischoff & Keil (1984); 58. Fujimaki et al. (1981a); 59. Fujimaki et al. (1981b); 60. Krot & Rubin (1994); 61. Brigham et al.  
2574 (1986); 62. Bridges et al. (1995); 63. Kimura et al. (2005); 64. Ikeda (1989b); 65. Wasson & Krot (1994); 66. Olsen (1983); 67. Scott & Krot  
2575 (2014); 68. Ikeda (1982); 69. Watanabe et al. (1986); 70. Noguchi (1989); 71. Zhang et al. (1996); 72. Müller et al. (1995); 73. Kitamura et al.  
2576 (1987); 74. Sheng et al. (1991a); 75. Wang et al. (2016); 76. Noguchi (1995); 77. Jones (1997); 78. Greshake (1997); 79. Bischoff et al. (1985);  
2577 80. Noguchi (1994); 81. Murakami & Ikeda (1994); 82. Ikeda & Kimura (1995); 83. Dodd et al. (1965); 84. Rambaldi et al. (1986); 85. Krot &  
2578 Wasson (1994); 86. Wood & Holmberg (1994)

---

# PRIMARY MINERAL-FORMING ELEMENTS IN CHONDRULES



1 H																	2 He				
3 Li	4 Be															5 B	6 C	7 N	8 O	9 F	10 Ne
11 Na	12 Mg															13 Al	14 Si	15 P	16 S	17 Cl	18 Ar
19 K	20 Ca	21 Sc	22 Ti	23 V	24 Cr	25 Mn	26 Fe	27 Co	28 Ni	29 Cu	30 Zn	31 Ga	32 Ge	33 As	34 Se	35 Br	36 Kr				
37 Rb	38 Sr	39 Y	40 Zr	41 Nb	42 Mo	43 Tc	44 Ru	45 Rh	46 Pd	47 Ag	48 Cd	49 In	50 Sn	51 Sb	52 Te	53 I	54 Xe				
55 Cs	56 Ba	57 *La	72 Hf	73 Ta	74 W	75 Re	76 Os	77 Ir	78 Pt	79 Au	80 Hg	81 Tl	82 Pb	83 Bi	84 Po	85 At	86 Rn				
87 Fr	88 Ra	89 #Ac	104 Rf	105 Db	106 Sg	107 Bh	108 Hs	109 Mt	110 Ds	111 Rg	112 Cn	113 Nh	114 Fl	115 Mc	116 Lv	117 Ts	118 Og				

